Engineering and characterization of membrane fusion machinery from Influenza hemagglutinin in a mammalian system

A Dissertation Presented for the
Doctor of Philosophy
Degree
The University of Tennessee, Knoxville

Mauricio Valverde
December 2018

This dissertation is dedicated to my parents, Mauricio and Nidia Valverde, my sister, Nicolle Valverde, and my wife, Sara Valverde

"In his heart a man plans his course, but the Lord determines his steps."

Proverbs 16:9

ACKNOWLEDGEMENTS

First, I would like to thank my lord and savior Jesus Christ for guiding my path and allowing me to accomplish my goals. "Trust in the Lord with all your heart; and do not lean unto your own understanding. In all your ways acknowledge him and he will direct your paths." (Proverbs 3:5-6).

I would like to thank my advisor, Dr. Eric T. Boder, for giving me the opportunity to work in his lab. This project was something that caught my attention even before I decided to attend the University of Tennessee and I am thankful that you allowed me to work on it. Thank you for the tremendous patience you have had with me and I will always be grateful. Thank you for your guidance and challenging me to develop as a scientist. I would like to thank all the lab mates and graduate students who showed interest and helped provide a different perspective on my experiments.

I would like to thank my parents for the sacrifices they made in order to provide me with all the opportunities for success and a better life in this country. I am thankful for importance of education that they instilled in me at a young age. Their constant support throughout my education has encouraged me to complete my Ph.D.

I would like to thank my wife, Sara E. Valverde. Thank you for your love and support for these last couple of years. Without you I don't think I would have ever finished this process. Thank you for putting up with rarely seeing me because cell culture and experiments awaited me. In the time I did have away from the lab you always helped me relax and remember that there was a purpose to all this. Thank you for always encouraging and believing in me.

ABSTRACT

Membrane fusion proteins are expressed by many viruses and play a crucial role in fusing two distinct membranes. Hemagglutinin (HA), the viral fusion protein of influenza, catalyzes fusion of the viral and target membrane by undergoing a conformational change triggered by a lowered pH of the endosome. The rearrangement, which is essential for fusion activity, exposes a highly conserved fusion peptide region. An engineered HA protein, with an altered fusion peptide region, has a high affinity for the fluorescent ligand, FlAsH. Using the engineered sensing HA, which allows real time monitoring of open state, we probe for kinetics of the conformational change.

We report that the engineered sensing HA, with an altered fusion peptide region that was designed to bind FlAsH after activation, shows induction by FlAsH binding at pH 7.0. The engineered HA shows activation of the fusion associated conformational change induced by alternative environmental stimuli compared to the wild-type protein. We suggest a novel alternative pathway to activation through binding the fusion peptide region which could impact the treatment of many enveloped viruses. We demonstrate that the engineered sensing HA co-expressed with fusion capable wild-type HA create modular systems that drive fusion triggered by ligand binding.

We further investigate the role of membrane properties in the activation of HA and the fusion induced by the viral protein. We show that the depletion of cholesterol leads to a significant delay in the kinetics of conformational activation and the extent of fusion. We also examine peptides that alter the membrane and show that disruption leads to the conformational change

required for fusion. These results indicate that further studies of the HA behavior in synthetic membranes with defined phospholipids would be beneficial.

To design new alternative environmental stimuli, we probed the entire HA gene for potential mutagenesis sites. Creating random mutant libraries and screening for desired phenotypes we have assessed the amino acids that can tolerate mutations with the help of next generation sequencing. With a landscape of tolerated mutational positions we can guide future rational design when trying to engineer the conformational change induced by a new exciting environmental stimulus.

TABLE OF CONTENTS

LIST OF FIGURES

CHAPTER 1
INTRODUCTION

Engineering novel phenotypes into existing functional proteins has been made possible by structural information guiding rational designs. Membrane proteins and their role in the transfer of molecules across the membrane, fluidity, and permeability are an interesting set of proteins that lend themselves to nanoscale devices. One set of proteins with an interesting mechanism is fusion proteins found in viruses that catalyze the fusion of two membranes. Creating novel proteins that would respond to certain signals in a specific environment would lend itself to controlled drug or gene delivery. Proteins that respond to biological signals irreversibly have also been used as biosensors. Our goal is to engineer a biological response to ligands, with high sensitivity, and create a novel protein to initiate the fusion of two membranes. Engineering the influenza virus machinery, which enables efficient delivery of genetic material, will provide novel biomaterial that can selectively catalyze fusion.

Our goal is to understand and engineer the process of membrane fusion catalyzed by viral fusion proteins. Fusion proteins facilitate the combining of two membranes in processes such as viral infection, secretion, and phagocytosis. Understanding and engineering the mechanism of viral fusion protein activity will lend insight toward the design of efficient delivery systems for the transport of drugs, genes, or imaging agents across a membrane. Effective delivery of payloads to specific cells could influence therapies of many diseases. Hemagglutinin (HA) is a viral fusion protein that binds receptors on the target cell causing endocytosis of the virosome. Ha then undergoes an irreversible conformational change upon acidification to catalyze the fusion of endosomal and viral membranes during influenza infection. The conformational change of recombinantly-expressed cell surface HA to the fusion active state has been associated with a cell-wide autocatalytic activation (Lee, et al., 2006). Other viral fusion proteins go through similar

rearrangements in order to deliver viral DNA to the host cell. We propose to study the autocatalytic mechanism and the cross-talk of viral fusion proteins in the membrane. With the use of deep sequencing, we furthermore plan to probe for mutation-tolerant residues as well as residues that play a role in the activation of HA. We also suggest that a novel alternative pathway to activation can be created by engineering the fusion peptide region of HA and that a ligand binding to this region can activate the conformational change. This alternative pathway could impact the therapy of many enveloped viruses. Understanding this novel pathway of activation can lend insight to more desirable ligands that could activate HA before it is endocytosed, leaving it unable to infect.

Background

Membrane fusion proteins are expressed by many viruses and play a crucial role in fusing two distinct membranes (Pecheur, et al., 1999). They play a role not only in viral infection but also in secretion, and phagocytosis. Hemagglutinin is the viral fusion protein of influenza, which is a membrane-enveloped virus. This virus, like many others, attaches to receptor proteins on the surface of the target membrane to begin the infection process (Pecheur, et al., 1999). After binding influenza is internalized by endocytosis. In the endosome HA is triggered into an irreversible conformational change by the low pH of the acidified endosome which helps overcome the energy barrier of membrane fusion (Coleman, et al., 2003). The rearrangement, which is essential for fusion activity, exposes a 20 amino acid sequence, the fusion peptide, which was previously buried within the protein's core (Skehel and Wiley, 2000). The fusion peptide is a hydrophobic region

which is highly conserved among the subtypes of HA and other class I viral fusion glycoproteins such as paramyxovirus, human immunodeficiency virus, and human T-cell leukemia virus (Russel, et al., 2004; Wilson et. al., 2005). Models suggest the insertion of the fusion peptide into the endosome is a critical step that disrupts the membrane structure (Jahn, et al., 2003). Full length HA with cleaved fusion peptide region fails to catalyze fusion. Fusion peptides in solution have been shown to interact with membranes via fluorescence resonance energy transfer experiments and also cause lysis of liposomes at high concentrations. Several other dramatic conformational changes such as the protein folding on itself contribute to the proximity of the two distinct membranes (Shangguan et. al., 1998).

Lipid packing contributes to the destabilization of the target membrane making fusion more favorable. The energy released by the conformational change helps catalyze the fusion of the viral membrane and the endosome creating a pathway for the release of its viral RNA into the cytoplasm of the host cell (Chernomordik, et al., 2008). Several other enveloped viruses, like human immunodeficiency virus and Moloney murine leukemia virus, have similar hydrophobic regions that contribute to fusion. They also go through conformational rearrangements in order to catalyze fusion and allow the release of viral genetic material into the cytoplasm of the host cell (Hughson, 1997). This makes enveloped viruses such as influenza very efficient at delivering viral genetic material to hosts cells. Engineering the influenza virus machinery, which enables efficient delivery of genetic material, will provide new mechanistic understanding, and could lead to novel biomaterials that can selectively fuse with cells on demand.

HA is a classic model fusion protein and its role in the fusion of influenza's viral membrane with the endosome is widely studied (Eckert, et al., 2001; Harrison 2008; White 1990). It is a

transmembrane glycoprotein that assembles in a homotrimer made of heterodimer subunits. Each monomer is synthesized as a single polypeptide chain, HA0, which is cleaved by a protease into two subunits, HA1 and HA2, held together by a single disulfide link (Carr and Kim 1993; Skehel and Wiley 2000). The newly formed N-terminus of HA2 contains the fusion peptide in the first 20 amino acids. Following the proteolytic cleavage, the fusion peptide relocates from an exposed loop into a buried cavity inside the trimeric coiled-coil structure (Cross, et al., 2009). Hemagglutinin is induced by either a low pH or an increase in temperature. Some models suggest that protonation of residues in the HA1 head group (Bottcher, et al., 1999; Chen, et al., 1995; Godley et al., 1992; Huang, et al., 2002; Kemble et al., 1992) destabilize the trimer causing HA to go through an irreversible conformational change; other models suggest residues in the fusion peptide and around the cavity where the fusion peptide resides (Cross, et al., 2001; Daniels, et al., 1985; Lin, et al., 1997; Thoennes, et al., 2008) are responsible for this destabilization in response to acidic pH. This conformational change exposes the fusion peptide and removes it from the cavity, relocating it approximately 100 angstroms in the direction away from the viral membrane toward the target membrane. The fusion peptide in the extended intermediate conformation then interacts with the target membrane (Figure1.1, all figures located at the end of each chapter). The extended conformation then collapses bringing the membranes into close proximity. The first intermediates stage of fusion shared by enveloped viruses is the mixing of lipids where the outer leaflets merge together while the outer leaflets remain intact, depicted in Figure 1.1.

Autocatalytic Activation.

The fusion peptide region of HA was epitope tagged by a previous graduate student in the lab to enable simple observation of the conformational state by immunofluorescence. An assay where HA from the fowl plague virus (FPV), an H7N1 antigenic subtype of influenza A (A/FPV/Rostock/34), is expressed on the surface of mammalian cells where the conformational change can be detected by immunofluorescent staining (Lee, et al., 2006). With this assay, it has been demonstrated that the conformational change of HA to the fusion active state is associated with a cell-wide autocatalytic activation as well as aggregations of the HA on the surface of the cell. The mechanism of cell-wide communication of HAs on the surface of a cell would suggest the protein's interaction with the membrane as a key contributor. Perturbing the lipid packing of the membrane structure as well as the membrane tension could provide an environment where the trimers can partially denature and dissociate, which could lead to activation. The aggregation also seen with autocatalytic activation would also support the need for proximity of activated and non-activated trimers. The relative timing of both the aggregation and activation is something that would have to be addressed. Perturbing the membrane environment has been shown to affect the folded stability of OmpA in bacteria (Hong and Tamm, 2004). Hemagglutinin trimers refolding can greatly disrupt the membrane structure and tension, which is consistent with a necessary step in fusion between two membranes. The role that membrane structure and tension has on HA could provide insight into the mechanisms of other viral fusion proteins.

Impacts of Engineered Viral Fusion Proteins.

The use of engineered viral fusion proteins to selectively deliver a payload could provide advances in efficient delivery of drugs, genes, or imaging agents. We propose engineering a protein that would allow for the possibility of controlling membrane fusion in response to different stimuli. Working with the machinery already in place with viral fusion proteins, we envision being able to engineer many possible targets that could trigger fusion. Using the cross-talk seen in autocatalytic activation, we could co-express target sensing proteins, which might not be fusion active, with fusion active proteins. This would make modular systems that add selectivity to the delivery of a payload and would create "smart" containers that could potentially deliver payloads in response to specific markers or specific environments.

In previous work, the fusion peptide region of HA was epitope tagged to enable simple observation of the conformational change by immunofluorescence. The second half of the residues in the fusion peptide were replaced with an epitope, c-myc (the mutant HA named HA3.1), which allows staining and detection of cells expressing HA in a conformationally sensitive manner (Lee, 2007). The fusion peptide is buried within the core of the coiled-coil trimer in its inactive state; this conformation does not allow for the staining of HA3.1 expressing cells. Once the HA is activated, the fusion peptide is exposed, and it acts as a detection flag which can now be easily detected by anti-c-myc antibodies. Only the activated HA can be stained. We can also use a monoclonal antibody, HC58, to stain in a conformationally sensitive manner. Monoclonal antibody HC58 binds only the pre-active state of HA and loses its ability to bind after HA refolds into its active state (Sugrue, et al., 1990). Using both HC58 and anti-c-myc antibodies, we can dual stain and simultaneously probe the conformational state of HAs on transfected cells.

Transfected cells were pH pulsed and incubated at a certain pH to observe conformational state, and pH's in the transition region demonstrated a bimodal response (Lee et. al., 2006). In the transition pH range, 5.2 -5.4, cells had a cell wide response to activation refolding. At intermediate pH's, 5.2 – 5.4, there were no cells with partial levels of c-myc epitope exposure or partial loss of the HC58 binding (Figure 1.2). There was a mixture of cells with either fully refolded active HA or full inactive HA.

Fluorescence microscopy data also agreed with flow cytometry data and demonstrated no single cell with both exposed c-myc tag and ability to bind HC58 (Lee et. al., 2007). Transfected cells expressing HA3.1 were activated at intermediate pH, similar to the flow cytometry data, and dual stained with antibody HC58 and anti-c-myc. Cells were exclusively positive for one or the other antibodies but not both on the same cell (Figure 1.3). Cells that were positive for anti-c-myc, active state, showed aggregation on the cell surface (Figure 1.4). Cells that were positive only for the HC58 antibody, inactive state, had no aggregation on the cell surface. Previous studies have also shown how refolding of HA coincides with aggregation of the trimers (Gutman, et al., 1993; Chernomordik and Kozlov, 2003).

A model that includes a positive feedback mechanism by which activated trimers promote the activation of nonactive trimers has been shown to depend on the fusion peptide region (Lee, 2007). Cells expressing HA3.1 at low levels (16 h post transfection) were incubated at pH 5.0 (pulsed) prior to further culturing to allow synthesis and expression of new trimers (Figure 1.5A & 1.5B). 8 h after the pulse cells showed an increase in HA trimers which were in the activated state even in the absence of a low pH (Figure 1.5A). New HA trimers expressed after the pulse spontaneously refolding to activated stated support the model of positive feedback. Treating the

HA with thermolysin, which cleaves the fusion peptide region, after the pulse prior to further culturing abolishes spontaneous refolding (Figure 1.5B) indicating the importance of the presence of the fusion peptide region for autocatalytic activation. We hypothesize that the fusion peptide, which is exposed after induction, inserts into its own cell membrane altering the tension and curvature. As nonactive HA come into the partially denatured membrane environment it leads to refolding to its active state spontaneously. The idea that membrane environment, modulated by fusion peptide insertion, contributes to the autocatalytic phenomenon motivates an aim of the proposed work.

Our lab previously used directed evolution to introduce both stabilizing and destabilizing mutations into HA. Studies show that the wild-type HA typically is fully refolded by a pH of 5.2 (Daniels et al., 1987; Ilyushina et al., 2007). Novel mutants demonstrating altered activation pH, previously isolated by our lab, were examined and used to make point mutants to assess the impact of individual mutations. Point mutants showed ability to alter pH activation in both stabilizing and destabilizing phenotypes. Point mutants were common in the head group domain indicating the role those residues play in holding the HA trimer together. The data support a model where the separation of head group domains leads to activation.

The use of directed evolution with selection on the conformational change did not depend on maintaining fusion activity or sialic acid receptor binding ability. The receptors on target cells, sialic acid, bind HA which mediates the initial process of internalization of influenza virus (Sauer et al., 2014; Leung et al., 2012; Wilks et al., 2012). Sialic acid is a sugar with a nine-carbon backbone that exits in a variety of conformations. Subtypes of HA have shown to have a specificity for certain conformations of sialic acid (Wilks et al., 2012). The clones isolated from directed

evolution had lost their ability to catalyze fusion. It has been shown that co-expressing altered pH mutants with wild-type on the same cell creates a modular system that allows the mutated HA, that activates at a high pH, to function as a trigger to activate a wild-type HA that would normally not activate at a pH > 5.4 (Lee, 2007). This allows us to engineer HA for other bio-sensing capabilities without having to maintain the fusion ability. Co-expressing wild type and altered pH HA can be shown to drive fusion at pH of 5.6 while wild type alone will only drive fusion at a pH < 5.4. The altered HA mutant acts as a trigger activating signal for the wild-type. The autocatalytic phenomenon allows for designing stimulus sensing phenotypes without having to maintain the fusion capability. With the help of directed evolution, we plan to engineer HA mutants that could be ligand activated.

Transient Mammalian Expression.

The study of complex function proteins, such as viral fusion proteins, require the use of eukaryotic cells. Mammalian cell surface display is used in this project for the quantitative functional analysis of HA. The surface display along with immunostaining allows for the analysis of the conformational refolding of the protein which is essential for fusion. This tool for monitoring the conformational change specifically decouples the need to screen for fusion. The advantage is that tools that monitor refolding via fusion often lose critical information of the refolding of HA. This same cell surface display is also a crucial tool used in our directed evolution aim that requires the expression of large libraries and allows us to screen for novel proteins.

In all cases below, unless otherwise stated, HA expression is achieved through the transfection of CHO-K1 cells. Transfected CHO cells are cultured in selective growth medium,

0.85 mg/ml geneticin (Hyclone, Logan, UT), 16 h post-transfection. This allows for a full 24 h after plasmid is introduced to the cells before selection can begin. The selection at 0.85 mg/ml geneticin continues for 48 h. Following this selection expression levels of HA on CHO cells are above 90% 3 days after transfection and around 99% 4 days after (Figure 1.6A). The expression levels were monitored via immunostaining with mAb HC2, which binds HA in any conformational state, for the first 4 days (Figure 1.6A). The high expression levels stay consistent when using 0.25 mg/ml geneticin for the following 10 days. Cells used in assays were always selected for at least 4 days and checked for expression. Expression levels drop by 14 days after the transfection (Figure 1.6B). This allows for the use of the transfected CHO cells for at least a week of analysis experiments.

Appendix

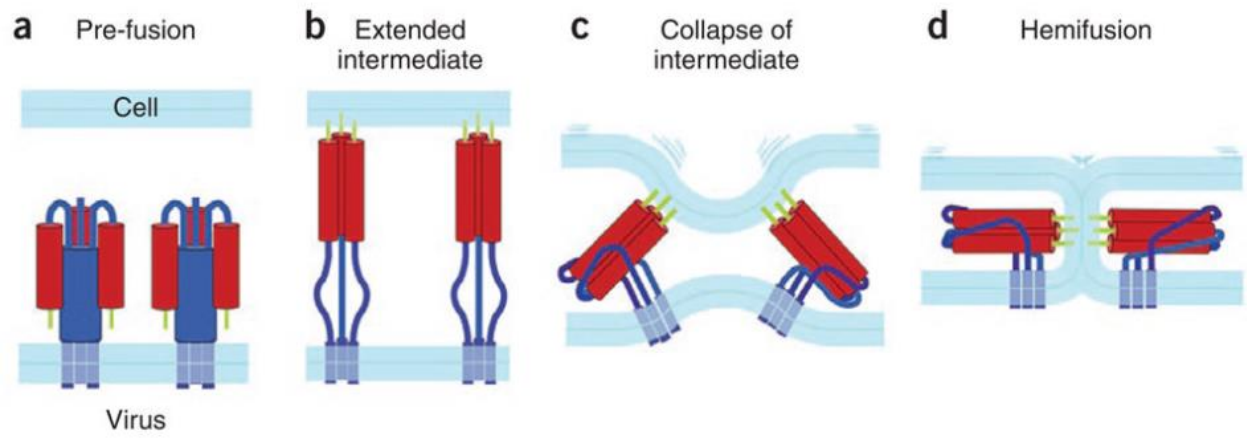

Figure 1.1. Fusion induced by viral fusion proteins. Events of HA refolding that catalyze membrane fusion. (a) Prefusion conformation with the fusion peptide (light green) pointing away from target cell membrane representing inactive state. (b) Extended intermediate. Protein refolds, extending the fusion peptide to interact with the target membrane. (c) Collapse of extended intermediate. C-terminal segment of the protein folds back along the outside of the trimer core. The segments from the three subunits fold back independently, the trimer can bow outward, away from the deforming membrane. (d) Hemifusion. When collapse of the intermediate has proceeded far enough to bring the two bilayers into contact, the apposed, proximal leaflets merge into a hemifusion stalk. Figure reprinted from Harrison, 2008, with permission from Nature publishing group.

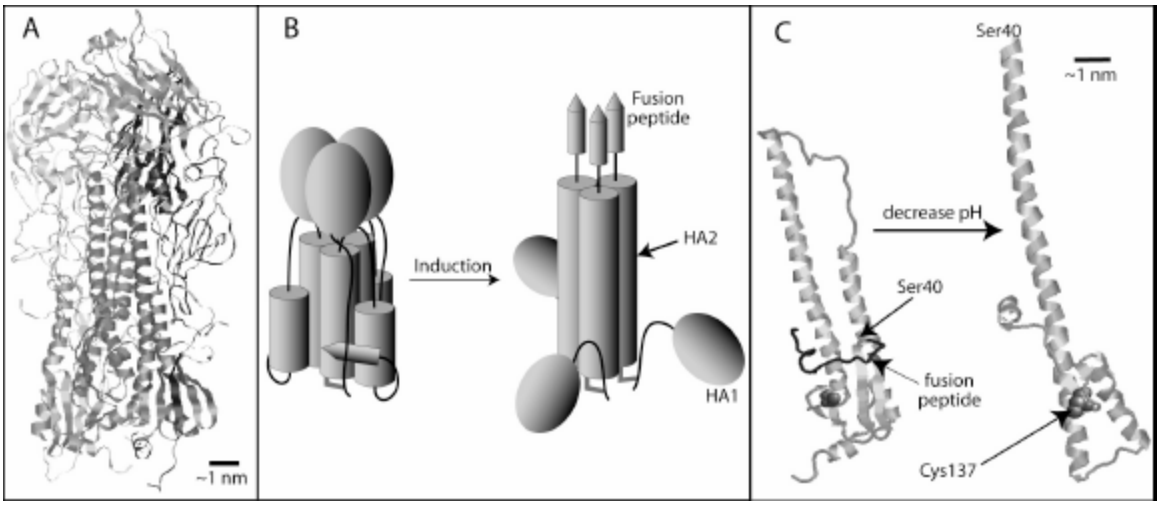

Figure 1.2. **Conformational change of hemagglutinin (HA**). (A) Ribbon diagram of HA metastable conformation before activation. (B) Cartoon diagram of HA refolding triggered by induction step (pH or temperature) (C) Changes in HA2 subunit after induction (HA1 not shown). HA2 residue Cys137 forms the only disulfide bond with a Cys in subunit HA1 to tether the subunits. The 39 residues on the N-terminal are not observed on the structure on the right.

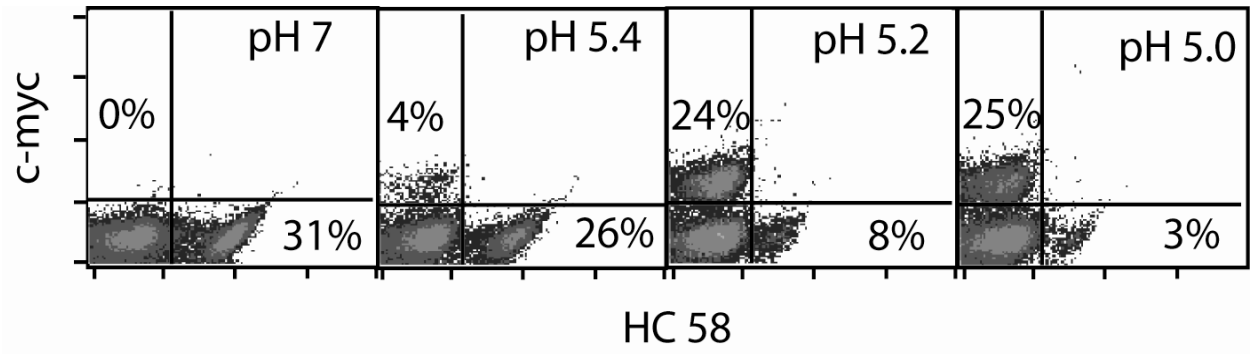

Figure 1.3. **Autocatalytic conformational change**. Cells expressing HA mutant with c-myc epitope were incubated at indicated pH for 5 min. Cells were co-stained with HC58 and anti-c-myc. At intermediate pH's (5.4 and 5.2) cells show staining for only one of the antibodies, demonstrating a fully active or fully inactive HA profile. Figure reprinted from Lee et. al., 2007, with permission from Elsevier publishing.

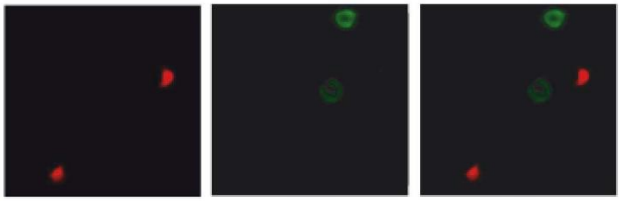

Figure 1.4. Aggregation of activated cells. Cells expressing HA mutant with c-myc epitope was incubated for 5 min at pH 5.4 and co-stained with biotin-HC58/streptavidin-FITC and 9E10/anti-mouse TRITC. Inverted fluorescence microscope at 40x magnification and Image J was used to analyze the images. Figure reprinted from Lee et. al., 2007, with permission from Elsevier publishing.

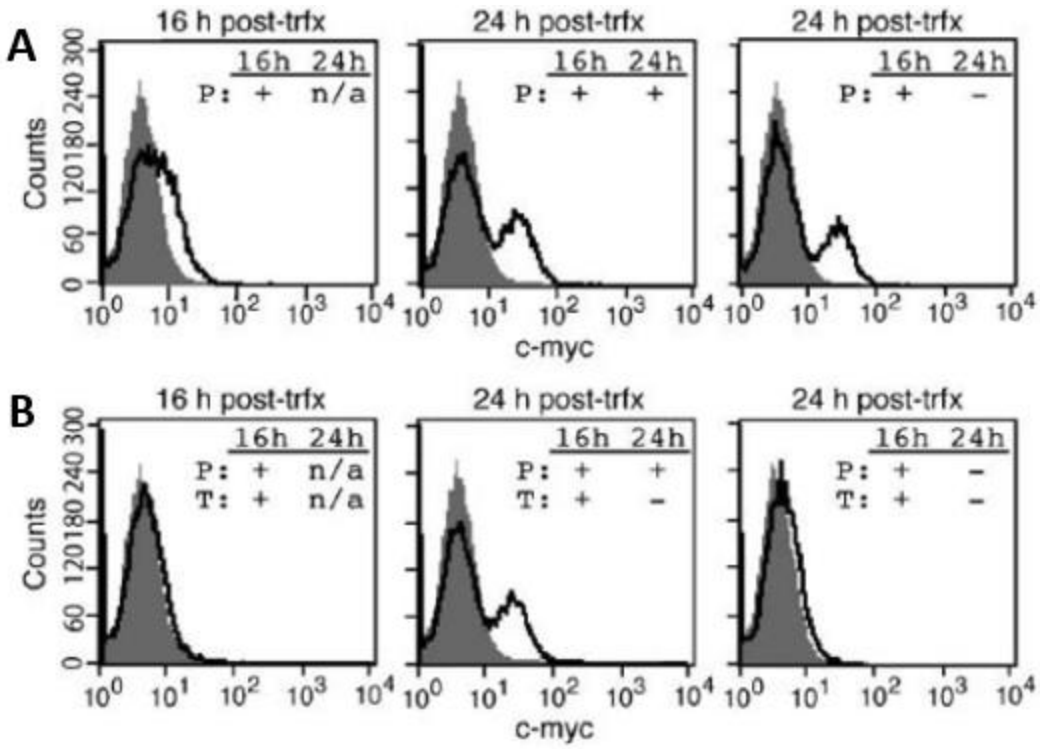

Figure 1.5. Autocatalytic activation dependence on fusion peptide. Cells expressing HA3.1 were analyzed at 16 h and 24 h post transfection. (A) Cells were pulsed at a pH 5.0 and labeled with c-myc. Additional 8 h of culturing and analyzed with (P: +) and without (P: -). (B) Cells were pulsed at a pH 5.0 and labeled with c-myc. Treated with thermolysin to cleave fusion peptide prior to further culturing. Additional 8 h of culturing and analyzed with (P: +) and without (P: -). Figure reprinted from Lee et. al., 2007, with permission from Elsevier publishing.

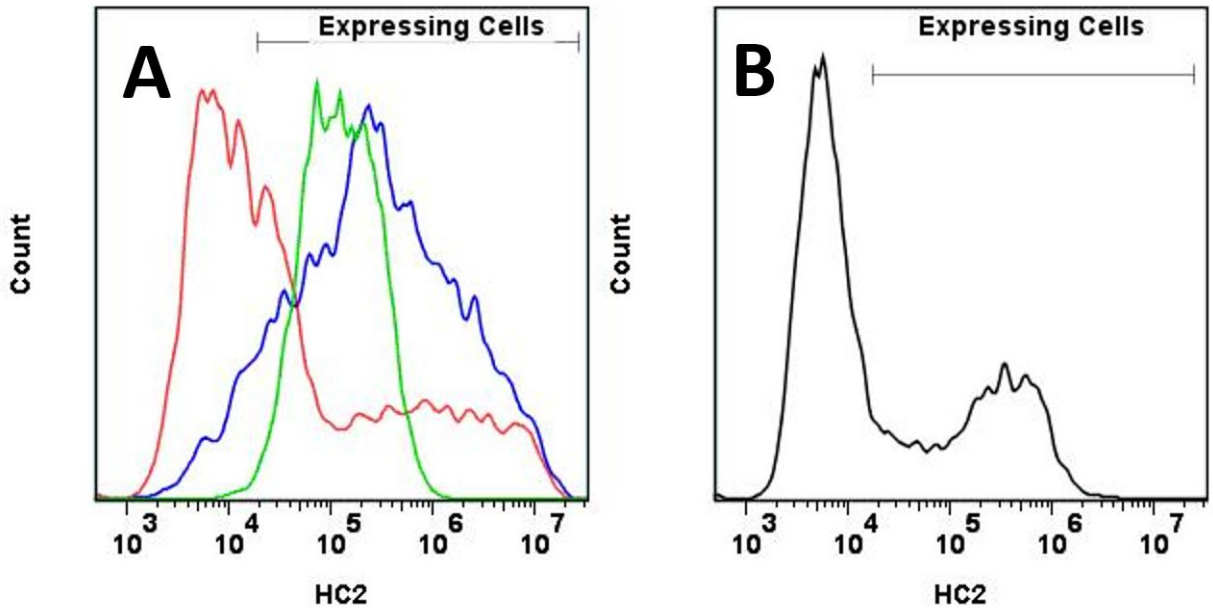

Figure 1.6. Transient transfection selection. CHO cells were transfected with plasmid containing HAcmyc and analyzed for expression using mAb HC2. A gate showing the expressing cell population was drawn based on non-transfected CHO cells as negatives. (A) The expression levels were monitored at 48 h (red), 72 h (blue), and 96 h (green). Cells maintain a high expression level for 10 days after transfection. (B) 14 days after transfection the population of cells expressing HA has dropped.

CHAPTER 2
LIGAND INDUCTION AND MODULAR SYSTEMS

Abstract

Here we report that an engineered sensing HA, bearing an altered fusion peptide region designed to bind to a fluorescent ligand (FlAsH) after activation, shows induction by FlAsH binding at a neutral pH. We suggest a novel alternative pathway to activation through binding the fusion peptide region which could impact the therapy of many enveloped viruses. Furthermore, we demonstrate that the engineered sensing HA loses its fusion function, but co-expression with fusion capable wild-type HA create modular systems that drive fusion triggered by ligand binding. Modular systems can potentially be engineered to drive fusion triggered by a variety of environmental stimuli which can benefit the design of efficient drug or gene delivery.

Methods and Materials

Plasmids.

Fowl plague virus (A/FPV/Rostock/34) HA gene (Lin et al. 2001) was digested with XhoI and NotI and ligated into the retroviral expression vector pLNCX2 (Clontech, Mountain View, CA). Overlap extension PCR was used to replace fusion peptide residues 13-18 (amino acids 355-360) with a tetra-cysteine tag (CCPGCC) and ligated into pLNCX2 (Clontech), herein referred to as HA4xCys or HA4.4. A previously created HA mutant with a c-myc epitope tag sequence (EQKLISEEDL) cloned into the fusion peptide residues 11-20 (amino acids 353 – 362) was also ligated into the pLNCX2 (Clontech) vector (Lee et al. 2006), herein referred to as HAcymc. A T7

bacteriophage promoter was cloned into the promoter region of pMCS-Red Firefly Luc (Pierce, Rockford, IL) plasmid. The red firefly Luciferase gene under the control of the T7 bacteriophage promoter was digested with XhoI and NotI and ligated into the retroviral vector pLNCX2. A mammalian expression vector with a T7 RNA polymerase insert, pCAG-T7pol was used to express the polymerase in the target cells, BHK-21. The plasmid pCAG-T7pol was a gift from Ian Wickersham (Addgene plasmid # 59926). All DNA manipulations were performed in E. coli Top10 or DH5α and cultured in Luria broth (LB; 10 g/L tryptone, 5 g/L yeast extract, 10 g/L NaCl) supplemented with ampicillin at 50 µg/ml.

Cell Culture.

CHO-K1 cells (ATCC CCL-61) and BHK-21 cells (ATCC CCL-10) were cultured in Dulbecco's Modified Eagles Medium: Kaighn's Modification of Ham's F-12 (DMEM:F-12K) and Eagle's Minimum Essential Medium (EMEM), respectively. Both media were supplemented with 10% fetal bovine serum (FBS) (Hyclone, Logan, UT), 100 µg/ml penicillin and 100 µg/ml streptomycin (Life Technologies, Grand Island, NY). CHO-K1 cells were transfected with plasmids using Lipofectamine 2000 Reagent (Invitrogen, Carlsbad, CA) according to manufacturer's protocol. CHO-K1 cells were also used as effector cells in the fusion assay's, they were co-transfected with HA and a luciferase reporter plasmid under the control of T7 bacteriophage promotor. Transfected CHO cells were cultured in selective growth medium, 0.85 mg/ml geneticin (Hyclone, Logan, UT), 16 h post-transfection and selected for 48 h before any assay. After first 48 h selection 0.25 mg/ml geneticin was used to grow cells and maintains ~100% expression for 1 week. All transfections of CHO cells followed the same selection process. CHO-

K1 cells were used to surface express HA wild type and mutants in all assays, except where indicated otherwise. BHK-21 cells were transfected, using Lipofectamine 2000, with T7 RNA polymerase plasmid and used as target cells in fusion assays.

Analysis of Induced HA.

All adherent cells were detached using 0.05% trypsin-EDTA (Hyclone) and aliquoted into 1.5mL microcentrifuge tubes and placed on ice. Cells were washed twice with PBSA and pelleted at 800xg using a benchtop microcentrifuge. The cells were then exposed to a pH induction step using citrate buffer at appropriate pH for 5 min at room temperature or a FlAsH induction step by addition of FlAsH buffer containing 2.5 μM FlAsH-EDT_2 and 0.25 μM 1, 2-ethanedithiol (EDT) in serum free 1:1 DMEM:F-12K media, for 15 min at room temperature. The TC-FlAsH in cell tetra-cysteine tag detection kit (Molecular Probes # T34561, Eugene, OR) was used and optimized according to the manufacturer's recommendations. After the induction step, the cells were immunofluorescently stained and assayed by flow cytometry. Cell surface expression was determined by monoclonal antibody (mAb) HC2 immunofluorescent staining, and HA conformation was determined by pre-activation specific monoclonal antibody HC58 (Sugrue et. al, 1990) staining, along with secondary antibodies of appropriate specificity. A previously shown mutant, HAcmyc, was used to monitor the activated state by staining with mAb 9e10 (Lee et al 2006).

Fusion Assays.

For a qualitative syncytium assay, CHO-K1 cells transfected with HA were used as effector cells. CHO-K1 cells either expressed only wild type HA or only tetra-cysteine HA mutant HA4xCys or co-expressed wild-type HA and HA4xCys due to co-transformation. Un-transfected BHK-21 cells were stained with PKH26 (Sigma-Aldrich, Saint Louis, MO), a membrane labeling dye, according to manufacturer's protocol, and used as the target cells. CHO cells co-expressing different combinations of HA were then mixed at a 1:1 ratio with BHK-21 target cells. The mixture was then exposed to an induction step for 15 min at a neutral pH in FlAsH buffer, 2.5 µM FlAsH-EDT2 and 0.25 µM EDT in serum free DMEM:F-12K media or citrate buffer at appropriate pH for 5 min. Negative FlAsH buffer contains no FlAsH-EDT2 and 0.25 µM EDT in serum free 1:1 DMEM:F-12K media. After the FlAsH incubation, the cells were spun down and re-suspended in full media (DMEM:F-12K supplemented with 10% fetal bovine serum and 100 µg/ml penicillin and 100 µg/ml streptomycin) and then incubated in an Eppendorf tube for 30 minutes to allow for syncytia formation. Syncytia formation was observed using Nikon Eclipse Ti (Nikon, Melville, NY) inverted microscope with an attached camera.

A quantitative cell fusion assay using a luciferase reporter (Byrd-Leotis et. al., 2015) was used to assess HA-mediated membrane fusion. CHO cells were transfected with HA plasmid and a plasmid containing Red Firefly Luciferase gene (Pierce) under the control of a T7 bacteriophage promoter using Lipofectamine 2000 (Invitrogen) according to manufactures protocol to create effector cells. 16 h post-transfection, the effector cells were placed in selective growth medium containing 0.85 mg/ml geneticin (Hyclone) for 48 h. Target BHK-21 cells were transfected with pCAG-T7, a plasmid containing T7 bacteriophage polymerase under the control of a constitutive

promoter, also using Lipofectamine 2000. pCAG-T7 pol was a gift from Ian Wickersham (Addgene plasmid # 59926). 48 - 72 h after transfection of the target cells, the HA-expressing cells were washed with PBS and treated with 0.05% trypsin-EDTA (Hyclone). The CHO effector cells were then overlaid on the target cells and incubated for 1 h at 37 ˚C to allow cells to adhere. Cells were washed once with PBS (Hyclone) and then exposed to appropriate induction buffer for 5 or 15 min. At the end of the induction complete growth medium was added to neutralize the reaction. The cells were incubated for 6 h at 37 ˚C to allow for cell-cell fusion and plasmid transfer leading to expression of luciferase. The cells were then washed once with PBS and lysed with 0.1 ml of lysis buffer (Pierce) and incubated in a 37 ˚C shaker for 15 min. 20 µl of lysate was transferred to a 96-well plate and 50 µl of D-luciferin substrate and 1 µl of Firefly signal enhancer (Pierce) were added to each well. Luciferase-catalyzed luminescence resulting from cell fusion was quantified using a Bio-Tek Synergy 2 multi-mode plate reader (Bio-Tek, Winooski, VT).

Results

Ligand (Flash) Binding.

To build a system allowing us to simultaneously assess the conformational rearrangement and aggregation of HA, we introduced a tetra-cysteine tag in the fusion peptide region. The tetra-cysteine peptide, CCPGCC, was cloned into the fusion peptide region (see Methods) of HA. The tetra-cysteine sequence can bind the fluorescent dye 4’,5’-bis(1,3,2-dithiarsolan-2-yl)fluorescein (FlAsH), which fluoresces only upon binding the 6-amino acid sequence, potentially allowing the

use of real-time microscopy to monitor the kinetics of conformational rearrangement and subcellular localization (including aggregation) of HA upon activation (Griffin et. al., 1998). HAcmyc, which similarly has a c-myc epitope tag in the fusion peptide region of HA, was used as a negative control due to its lack of binding to FlAsH. CHO cells were transfected with either tetra-cysteine or c-myc HA and subjected to selection described in the methods. FlAsH buffer was added to cells expressing the two different HA mutants and analyzed for fluorescence. Microscopy analysis showed dye binding the tetra-cysteine mutant (named HA4xCys), which indicates activation of hemagglutinin, even in the absence of low pH when incubated with FlAsH buffer. Both samples of HA4xCys incubated with FlAsH buffer at pH 5 and neutral pH showed similar fluorescence and the negative control, HAcmyc, showed no significant fluorescence.

To analyze the kinetics of ligand binding, we used CHO cells transfected with either HA4xCys or HAcmyc. We analyzed CHO cells transfected with HA4xCys for ligand binding by inducing with a FlAsH buffer containing FlAsH-EDT2 at different concentrations and 0.25 µM EDT in a HEPES buffered serum free 1:1 DMEM:F-12K media, for 15 min at room temperature. After the induction cells were stained with mAb HC58, which binds only the inactive state of HA, and analyzed via flow cytometry. CHO cells expressing HA4xCys and induced with FlAsH buffer demonstrated the loss of HC58 binding only at 2.5 µM FlAsH (Figure 2.1). The loss of HC58 binding indicates that the HA has gone through the conformational change. Negative FlAsH buffer, which has no ligand but still contains 0.25 µM EDT in serum free 1:1 DMEM:F-12K media, and 0.25 µM FlAsH have a higher HC58 fluorescence than the negative control which indicates the HA is still in the inactive state (Figure 2.1). Kinetic data, analyzed with flow cytometry, shows a delay in fluorescence prior to the induction with FlAsH buffer followed by a rapid increase in

fluorescence after 7 min for HA4xCys (Figure 2.2A, blue), whereas the control HAcmyc (Figure 2.2A, black) shows no increase in fluorescence after 7 min. This suggests that binding of the ligand in the absence of a low pH is potentially causing the conformational change. This data also agrees with microscopy data of the same two samples. CHO cells expressing HA4xCys and negative control CHO cells expressing HAcmyc both had a small increase in fluorescence at 1 min prior to FlAsH incubation but only the HA4xCys cells has a rapid increase after 7 min (Figure 2.3).

Ligand Induced Conformational Change.

To monitor conformational change a previously developed assay using immunofluorescent staining and flow cytometry was used (Lee et al. 2006). Monoclonal antibody (mAb) HC58, which binds only the pre-activation trimer conformation, was used to stain HA (Sugrue et al. 1990). CHO cells transfected with either HA4xCys or HAcmyc were exposed to an induction step, stained with HC58, and analyzed with flow cytometry. Using a mock $FlAsH^-$ buffer induction step (no FlAsH present) at pH 7.0 for 5 min, both samples retained the ability to bind HC58 (Figure 2.2 Column B). An induction step with the $FlAsH^+$ buffer for 15 min caused only the HA4xCys CHO cells to go through the conformational change and lose the ability to bind HC58 (Figure 2.2 Column C). An induction step at pH 5.2 for 5 min, which has been shown by previous assays to cause wild-type H7 HA to undergo a conformational change to its active state, caused both the HA4xCys and HAcmyc (negative control) to lose HC58 binding (Figure 2.2 Column D). Demonstrating that the FlAsH buffer at a neutral pH causes the same reaction in HA4xCys that a low pH would cause in any HA. The fluorescent ligand (FlAsH dye) presumably binds the tetra-Cys tag in the pre-activation state, changes its position, and destabilizes the conformation, allowing the HA timer to

refold to the activated conformation. This novel alternative pathway to activation suggests it may be possible to create fusogenic HA proteins responding to a variety of stimuli, provided they can be engineered for ligand binding to the fusion peptide region.

The ligand binding reaction was buffered to prevent a change in the pH. The organo-arsenics found in FlAsH-EDT2 create a reversible covalent bond with pair of thiols. The design of the tetra-cysteine peptide, CCPGCC, provide a cooperative and favorable reaction for the arsenics (Griffin et al., 1998; Pomorski et al., 2011). A HEPES buffer at a significantly higher concentration was used to preclude the possibility of the reaction producing enough protons to change the pH. We cannot exclude the possibility of a micro-environment of low pH created by FlAsH binding, but the overall pH of the buffer should not be change due to the 15mM HEPES buffer.

Autocatalytic Crosstalk.

The cell-wide autocatalytic activation of HA's conformational change allows us to create modular systems where HA's communicate (crosstalk) with each other (Lee et al. 2006). Modular systems where HA's with sensing capabilities (ligand activating) can activate co-expressed HA's with a fusion phenotype allow us to engineer HA without having to retain fusion function. The HAcmyc mutant, which was shown not bind FlAsH previously, was co-expressed with HA4xCys (sensing HA). Co-expressed cells were exposed to an induction step then stained with mAb 9e10 which binds only the HAcmyc that has gone through a conformational change to the active state. Flow cytometry data shows cells co-expressing tetra-cysteine and c-myc mutants demonstrated full activation of HA trimers in the presence of FlAsH at a neutral pH (Figure 2.4C) and no activation is seen using the mock FlAsH buffer induction (Figure 2.4B). This suggests that trimers

activated by FlAsH can activate c-myc trimers through autocatalytic crosstalk. To further test crosstalk we transfected CHO cells with both HAcmyc and HA4xCys mutants at different plasmid ratios (HAcmyc: HA4xCys) keeping the total amount of plasmid the same. The transfected cells were then exposed to an induction step of either pH 5.2 for 5 min, mock FlAsH buffer at pH 7.0 for 15 min, or FlAsH buffer for 15 min then analyzed by flow cytometry as described above in the methods. This assay suggests that HA4xCys mutants activated by FlAsH binding the fusion peptide region can activate c-myc trimers through autocatalysis. Activated HAcmyc would allow us to monitor the conformational change indicated by c-myc signal, median fluorescence intensity (MFI), via immunofluorescent staining with mAb 9e10 and flow cytometry (Figure 2.5). The median fluorescence intensities were normalized with negative and positive controls as described in Figure 2.11. Ratios 1:2, 2:1, 5:1 show an increase in c-myc MFI and support the idea that trimers made up of only HAcmyc can be activated by autocatalysis (Figure 2.5). At the ratio of 10:1, which doesn't agree with statistical analysis shown in Figure 2.6, we see a drop in the c-myc signal when we expected it to keep increasing along with the sample that was induced with low pH (Figure 2.5). This may be due to the density dependence of HA to undergo its conformational change. The low surface density of HA trimers that are activatable by FlAsH may need a longer induction time to observe a larger signal. The signal that we are observing could be due to the cells that are expressing higher amounts of FlAsH inducible trimers. Statistical analysis suggests that heterotrimers are not solely responsible for the c-myc fluorescence signal (Figure 2.6). The level of c-myc signal is significantly higher, more so than the cells induced with low pH, than what we would expect if only mixed trimers were induced. Theoretically, there are four possible trimer combinations when transfecting with two different HA: all HAcmyc, all HA4.4, or two distinct

heterotrimers (1 HAcmyc:2 HA4.4 and 2 HAcmyc:1 HA4.4). If only heterotrimers, trimers made up of a combination of HA4.4 and HAcmyc, were responsible for our c-myc signal then we would expect a drop-in MFI at the 5:1 ratio which was not observed (Figure 2.5). More experiments are needed to determine the ratio of expression levels of the two mutants. Crosstalk allows us to potentially create systems in which co-expressing HA's engineered for novel sensing functions with fusion capable HA (wild type) could make modular fusogenic systems that are triggered by alternative stimuli.

Syncytia Formation.

To test modular fusogenic systems we co-transfected with HA4xCys and wild- type HA (wtHA) and tested for qualitative syncytium formation via microscopy. A syncytium is a multinucleated cell that forms from multiple cells fusing together. Qualitative syncytia assays have been used to monitor fusion in both influenza and human immunodeficiency viruses (Byrd-Leotis, et al., 2015; Huerta et. al., 2009). The fusion mechanism pathway contains an intermediate stage where the outer contacting lipid leaflets merge while the inner leaflet remains intact, called hemifusion (Chernomordik et al., 2006; Jahn et al., 2006; Podbilewicz et al., 2006; White et al., 2008). The intermediate stage of hemifusion allows for the staining of the membrane and monitoring of the dye transfer to indicate the beginning steps of fusion. CHO cells expressing HA (effector cells) were incubated with target cells, subjected to different induction steps, and analyzed for syncytium formation. Un-transfected BHK-21 cells stained with PKH26 (Sigma-Aldrich), a membrane labeling dye, were used as our target cells. The effector cells were exposed to an induction step of either 15 min at a neutral pH FlAsH buffer or 5 min pH 5.2 citrate buffer.

After the induction step, the cells were spun down and re-suspended in full medium and then incubated in an Eppendorf tube with target cells, PKH26 stained BHK-21 cells, for 30 min to allow for syncytia formation and PKH26 dye transfer which was visualized and photographed using Nikon Eclipse Ti inverted microscope with an attached camera. Syncytia formation and a dispersed PKH26 dye, indicating transfer, was observed at a neutral pH with the FlAsH induction when both tetra-cysteine and wild-type HA are co-expressed (Figure 2.7C). Similarly, effector cells expressing wild-type HA showed both syncytium formation and dye transfer (Figure 2.7B). Effector cells expressing only tetra-cysteine mutant and induced with FlAsH showed ligand binding but showed no syncytium formation or PKH26 dye transfer (Figure 2.7D). This was expected due to the tetra-cysteine peptide being cloned into a conserved fusion peptide region and other studies that show the loss of fusion activity due to single point mutants in this region (Li 05). Even though the FlAsH-sensing HA could undergo the fusion associated conformational change, the tetra-cysteine mutation caused a loss of syncytium formation capability. Co-expressing the tetra-cysteine mutant with a fusion capable wild-type HA allowed for the recovery of syncytium formation triggered by ligand binding in our modular system. The syncytium assay coincides with the flow cytometry data showing activation of non-FlAsH binding HA co-expressed with tetra-cysteine HA in the presence of ligand.

Quantitative Assessment of HA-mediated Fusion.

We also tested the modular system's ability to drive fusion using a quantitative luciferase-based assay. The luciferase assay allows us to obtain a qualitative measurement that corresponds to luciferase activity to monitor fusion. The effector cells, expressing HA and carrying luciferase

plasmid, ability to transfer plasmid encoding firefly luciferase under the control of T7 bacteriophage promoter to target cells expressing T7 bacteriophage polymerase are an indirect measure to indicate fusion (Byrd-Leotis et al. 2015, Figure 2.8). To test the modular systems ability to drive fusion we examined the wild-type HA and 3 mutants (W243S, G237R, and G365C) which all activate at a higher pH than the wild-type (Figure 2.9). The destabilized mutants were isolated from directed evolution work and characterized using immunostaining and flow cytometry done previously in our lab. CHO cells were first transfected with only 1 HA plasmid and plasmid containing Red Firefly Luciferase gene under the control of a T7 bacteriophage promoter using lipofectamine. BHK-21 cells expressing T7 bacteriophage polymerase were used as target cells. The wild-type HA was able to drive fusion at a pH 5.43 (Figure 2.9A) but none of the three mutants were able to drive fusion when expressed alone (Figure 2.9B, 2.9C, 2.9D ▲). The relative luminescence unit was normalized as described in Figure 2.12. CHO cells co-expressing the mutant HA and wild-type (Figure 2.9B, 2.9C, 2.9D ●) were used as effector cells with the same target cells as before. When the mutants were co-expressed with a fusion capable wild-type it showed the ability to drive fusion at a higher pH which correlated with the destabilized mutant's refolding pH. The data was fitted to a dose response curve with variable slope as described in Figure 2.13.

CHO cells (effector cells) were transfected with both HA4xCys and wild-type HA as well as a firefly luciferase gene under the control of a T7 bacteriophage promoter (Pierce, Rockford, IL). Effector cells expressing only HA4xCys mutant was used as a negative control due to its loss of forming syncytia. Target BHK-21 cells were transfected with pCAG-T7, a plasmid to express T7 bacteriophage polymerase but were not subject to any selection. pCAG-T7pol was a gift from

Ian Wickersham (Addgene plasmid # 59926). CHO effector cells were overlaid on BHK-21 target cells then exposed to a FlAsH buffer induction step for 15 min at different concentrations of FlAsH keeping the other buffer concentrations the same (Methods for further detail). After neutralization of the FlAsH buffer, sufficient incubation time was allowed for fusion and plasmid transfer leading to expression of luciferase. Lysates were analyzed for bio-luminescence activity of Luciferase using a Bio-Tek Synergy 2 plate reader. The modular system induced by FlAsH demonstrates fusion comparable to wild-type effector cells induced by pH 5.2 at FlAsH concentrations ≥ 2.5 μM after the data was normalized as described above (Figure 2.10). Fitting a dose response curve with variable slope to our titration data indicates an EC50 of 1.04 μM FlAsH (Figure 2.10 & Figure 2.14). Effector cells expressing only HA4xCys showed no luciferase activity which was expected given that the highly conserved fusion peptide region was mutated (Figure 2.10). The modular system tested with both the luciferase assay and the syncytium assay are in agreement. Taken together, we show the capability of modular systems that are triggered by alternative stimuli to drive fusion even if the sensing HA is unable to induce membrane fusion. Fusogenic modular systems can co-express HA's engineered for a variety of novel sensing functions with HA's that contain an actuating component.

Discussion

A broader understanding of the general mechanisms of fusion can lead to more efficient therapy of many enveloped viruses. The novel alternative pathway that we suggest here of

activation through binding the fusion peptide region provides the potential to target a highly conserved region found in all subtypes of HA. The fusion peptide also has common motifs found in other class I viral fusion glycoproteins such as paramyxovirus, human immunodeficiency virus (HIV), and human T-cell leukemia virus (Russel et al., 2004; Wilson et. al., 2005). There has also been literature that suggests the stability of HA is influenced by the residues in the fusion peptide and the fusion peptide pocket, a cavity where the peptide forms extensive contacts in the pre-activation state (Cross et al., 2001; Ilyushin et al., 2007; Thoennes et al., 2008; White et al., 2016). The FlAsH dye presumably binds the tag in the pre-activation state and destabilizes it, allowing the HA timer to refold to the activated conformation. Potential therapies can be envisioned where activation of HA on the virion by ligand binding prior to endocytosis would render the virus unable to infect. It's been shown that pretreatment of influenza virus before a target cell is present leaves the virus enable to infect (Markovic et al., 2001; Leikina et al., 2002; Gutman et al., 1993). The extent of inactivation has also been observed to depend on the strain and the difference in inactivation attributed to the difference in kinetics (Markovic et al., 2001)

The trimers activated by FlAsH can activate non-ligand binding trimers through an autocatalysis which can potentially arise from effects mediated by locally altered membrane structure and tension. The model for autocatalysis has been proposed and the dependence of this phenomena on the fusion peptide was shown that by treatment with thermolysin which cleaves the fusion peptide (Lee et al., 2006). The initial reversible conformational change of HA upon acidification or ligand binding removes the hydrophobic fusion peptide from the cavity. The mechanism of cell-wide communication of HAs on the surface of a cell would suggest the protein's interaction with the membrane as a key contributor. Previous work has shown how the fusion

peptide can cause perturbations in the membrane (Harrison et al., 2015; Ivanovic et al., 2013). Perturbing the lipid packing of the membrane structure as well as the membrane tension could provide an environment where the trimers can partially denature and dissociate, which could lead to activation. Perturbing the membrane tension has been shown to affect the folded stability of OmpA in bacteria (Hong and Tamm, 2004). Another membrane perturbing peptide, the 42 amino acid fragment of β-Amyloid, has been shown to have antiviral activity with two strains of influenza in vitro presumably by causing viral aggregation or altering the viral membrane (White et al., 2014). Hemagglutinin trimers refolding can greatly disrupt the membrane structure and tension, which is consistent with a necessary step in fusion between two membranes. The role that membrane structure and tension has on FPV HA could provide insight into the mechanisms of other viral fusion proteins which undergo a similar conformational change. Our proposed model for the membrane being a key contributor to crosstalk could potentially be applied to other viral fusion proteins.

The crosstalk of two distinct HA's allows us to create modular systems where sensing HA can refold due to a novel stimulus which would then trigger an HA with an actuating component depicted in Figure 2.11. Potential fusogenic modular systems can provide selectivity to delivery systems. Both of our syncytium and luciferase fusion assays suggests the potential to create these modular fusogenic systems. The sensing mutant, HA4xCys, is triggered by ligand binding to undergo its fusion associated conformational change but is unable to induce fusion when expressed alone. Engineering of the fusion peptide region to bind a variety of stimuli could provide novel sensing functions while not having to retain the fusion capability. The sensing HA co-expressed

with a fusion capable HA, such as wild-type, would create a fusogenic systems that would be induced in specific environments.

Appendix

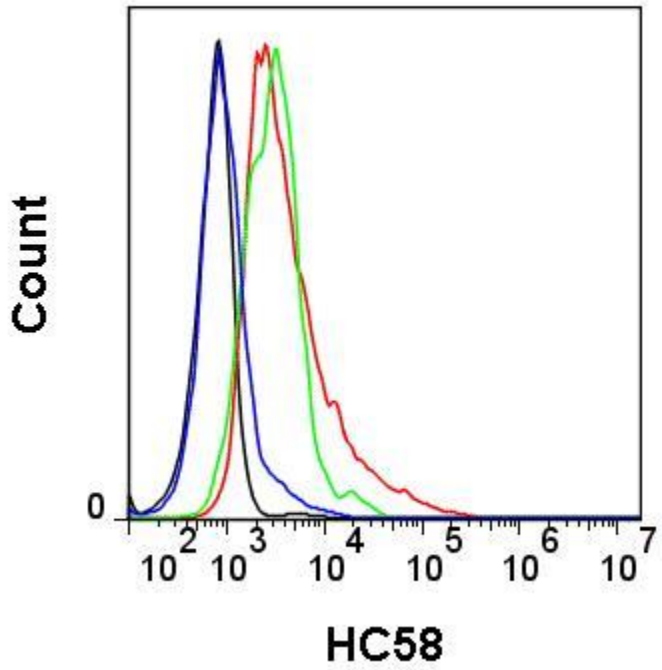

Figure 2.1. Activation of mutant HA with ligand (FlAsH). CHO cells were transfected with HA4xCys plasmid, induced with different concentrations of FlAsH buffer, and analyzed by flow cytometry. The induction step with indicated FlAsH buffer was performed for 15 min (based on microscopy data) and then staines with HC58 (which binds inactive conformation of HA). Black curve on histogram indicate un-transfected CHO cells, green curve are cells induced with mock FlAsH buffer (0 µM FlAsH), red curve are cells induced at 0.25 µM FlAsH, blue curve are cells induced at 2.5 µM FlAsH .

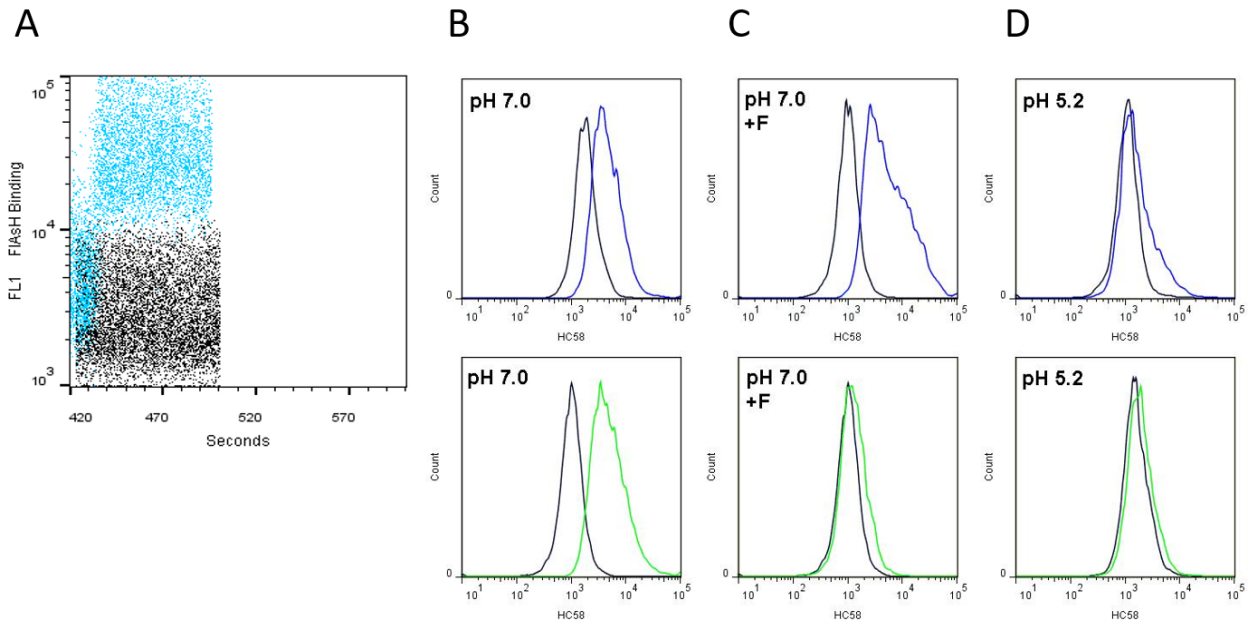

Figure 2.2. Binding and activation of mutant HA with ligand (FlAsH) induction. (A) CHO cells were transfected with HA4xCys (blue) or negative control HAcmyc (black) and analyzed with flow cytometry. Flash buffer at neutral pH was added at t = 0. Multiple samples were tested for ligand binding starting every min. The graph only shows fluorescence of both samples starting at t = 420 s. (B-D) CHO cells were transfected, induced, and analyzed by flow cytometry. Black curves on histograms indicate un-transfected CHO cells, blue curves are CHO cells transfected with HA c-myc, and green curves are CHO cells transfected with HA 4xCys. All staining was performed with mAb HC58 which binds inactive conformation of HA. (Column B) Cells are pulsed at indicated pH for 5 min and stained with HC58. Both top and bottom show fluorescence higher than negative which indicates inactive HA. (Column C) Cells are pulsed at indicated pH with FlAsH buffer for 15 min and stained with HC58. Top shows HA c-myc (negative control) fluorescence is higher than un-transfected CHO cells indicating inactive HA. Bottom shows cells expressing HA 4xCys with similar fluorescence as un-transfected CHO cells which indicates FlAsH induced conformational change. (Column D) Cells are incubated at pH 5.2 for 5 min and stained with HC58. Both top and bottom have similar fluorescence to un-transfected cells which indicates low pH induced both samples.

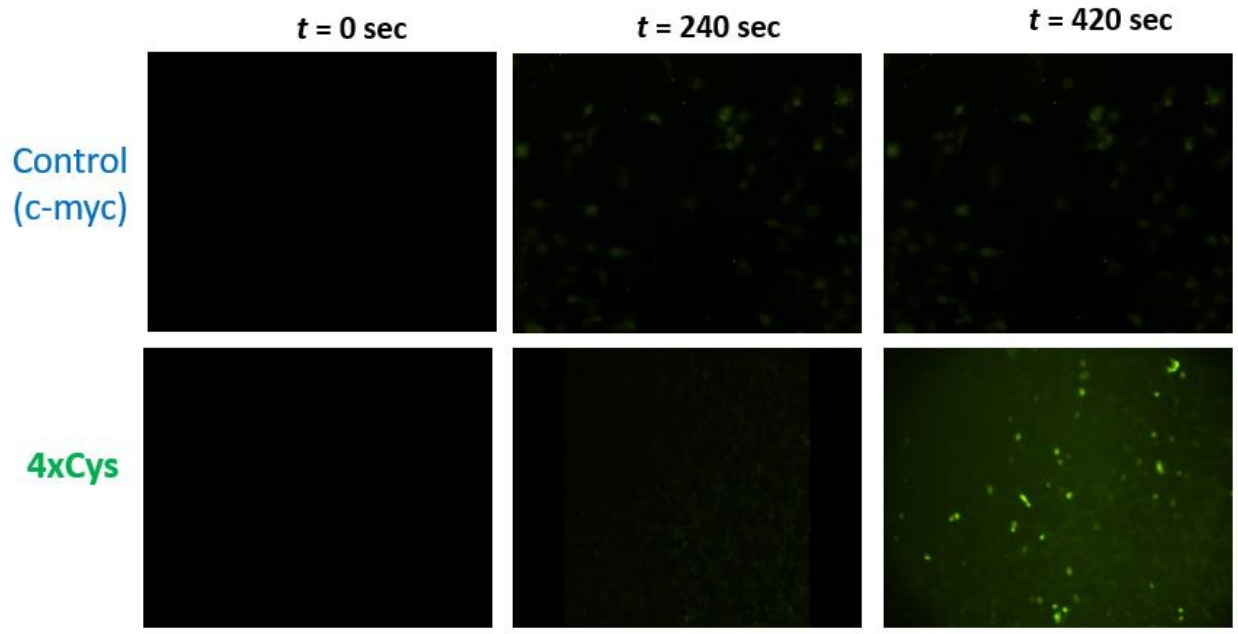

Figure 2.3. Ligand binding kinetics. CHO cells were transfected with HA4xCys and analyzed via microscopy. CHO cells transfected with HAcmyc were used as a negative control. FlAsH buffer was added at t = 0 sec and fluorescence was monitored. A slight increase was seen after 1 min that is also seen in the negatives control which we attribute to background. After 7 min a rapid increase is seen in the CHO cells expressing HA4xCys. The entire assay is done at a neutral pH.

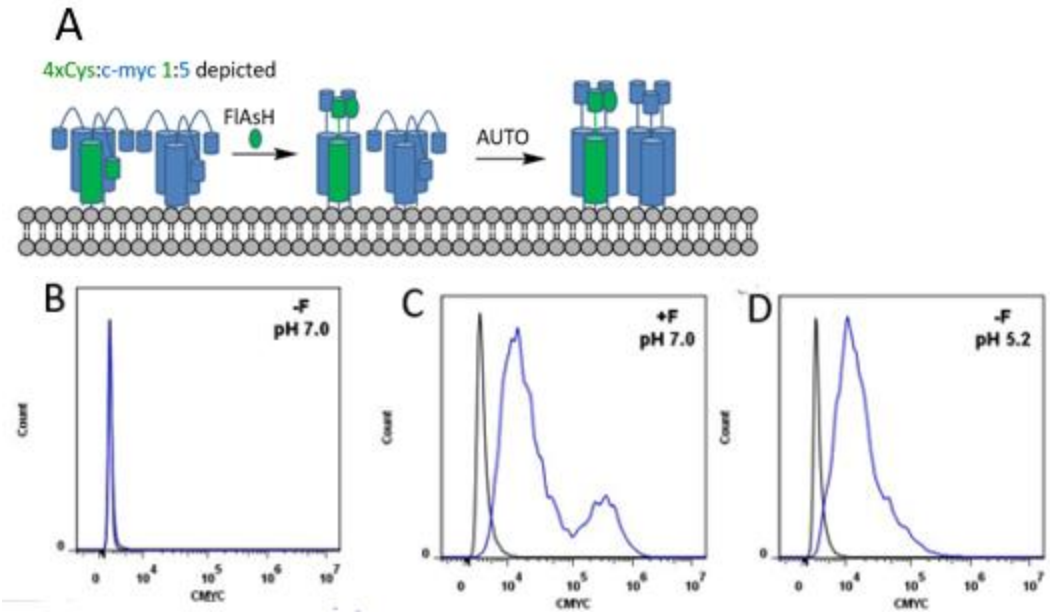

Figure 2.4. Crosstalk between HA trimers. (A) Diagram showing FlAsH dye inducing conformational change of HA 4xCys monomer. Crosstalk between trimers activate non-HA 4xCys monomers. (B-D) Black curves are un-transfected CHO cells and blue curves are CHO cells transfected with both HA 4xCys: HA c-myc at 1:5 ratio. (B) Cells are incubated at indicated pH for 15 min with no FlAsH and stained with anti-c-myc. Blue curve overlaps the negative control indicated no activation. (C) Cells are incubated at indicated pH for 15 min with FlAsH and stained with anti-c-myc. Blue curve shows higher fluorescence than negative indicating that non-4xCys HA monomers were triggered with dye. The graph indicates two populations of expressing cells that are both positive for c-myc signal. The higher intensity population are cells expressing at a higher level which is the smaller peak (D) Cells are incubated at indicated pH for 5 min and stained with anti-c-myc. Blue curve shows higher fluorescence than negative showing that low pH can trigger the conformational change. It is presumed that the higher expressers are lost in this graph due to the low pH being more stressful than the ligand induction and lysing the cells.

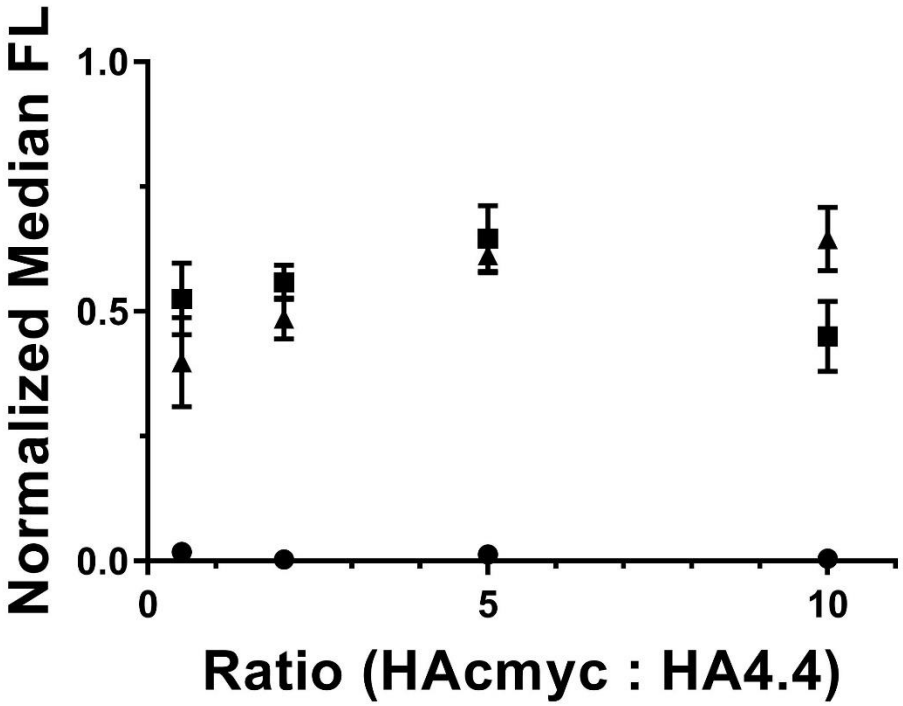

Figure 2.5. Crosstalk of HA3.1 : HA4.4 at different ratios. CHO cells were transfected at 1:2, 2:1, 5:1, and 10:1. The cells were then activated by pH 5.2 (▲), pH 7.0 (●), or FlAsH (■). The c-myc signal was monitored by immunostaining and flow cytometry. Median Fluorescence was calculated for 3 independent experiments with the standard deviation as error bars. Normalized using CHO cells transfected with only HAcmyc plasmid.

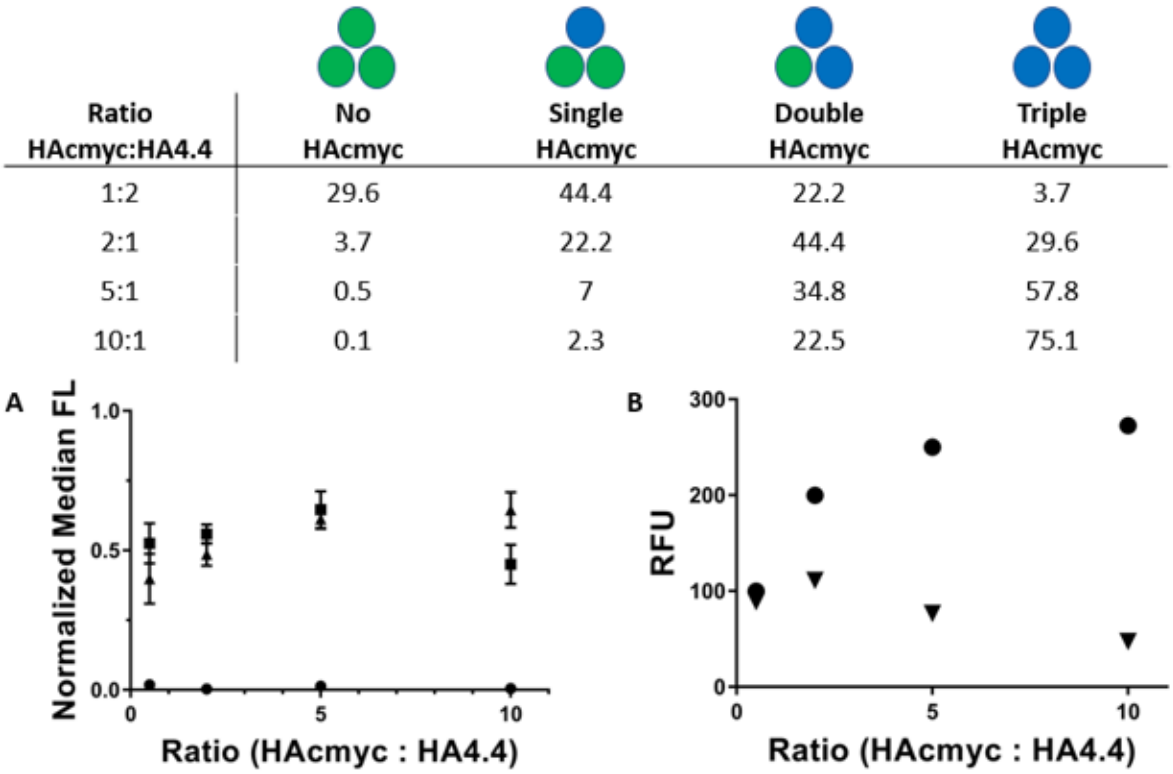

Ratio HAcmyc:HA4.4	No HAcmyc	Single HAcmyc	Double HAcmyc	Triple HAcmyc
1:2	29.6	44.4	22.2	3.7
2:1	3.7	22.2	44.4	29.6
5:1	0.5	7	34.8	57.8
10:1	0.1	2.3	22.5	75.1

Figure 2.6. Probabilistic analysis of heterotrimers. The probability of heterotrimers, trimers made up of a combination of HA4.4 and HAcmyc, are shown in the table. Only HAcmyc monomers (blue circles) would show a fluorescence signal when stained with mAb 9e10. Columns with single, double, and triple HAcmyc monomers were multiplied by 1, 2, or 3 respectively to predict a relative fluorescence. (A) Crosstalk of HA3.1 : HA4xCys at different ratios. CHO cells were transfected at 1:2, 2:1, 5:1, and 10:1. The cells were then activated by pH 5.2 (▲), pH 7.0 (●), or FlAsH (■). The c-myc signal was monitored by immunostaining and flow cytometry. Median Fluorescence was calculated for 3 independent experiments. Normalized to CHO cells transfected with only HAcmyc plasmid. (B) Relative fluorescence predicted by statistical analysis for 1:2, 2:1, 5:1, and 10:1 ratios (HAcmyc : HA4.4). Predicted relative fluorescence for two different scenarios are shown. The two scenarios are if only heterotrimers are activated (▼) and if all trimers (including HAcmyc homotrimers) are activated (●).

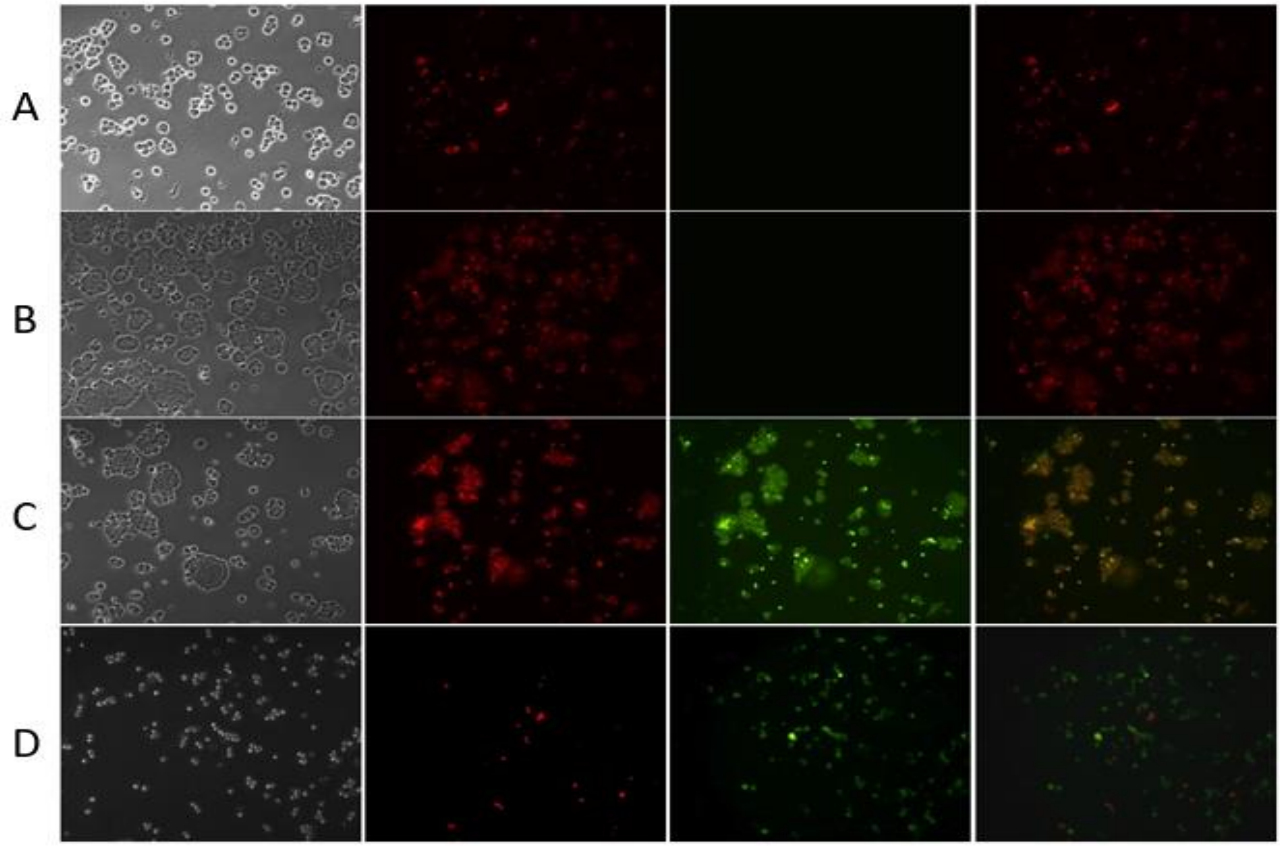

Figure 2.7. Syncytia formation indicating fusion. Column 1 is a bright field image in which we are looking for multicell sized formations to indicate fusion. Column 2 and column 3 are images of PKH26 and FlAsH stains respectively. Column 4 is an overlay of column 2 and 3. In all cases the same BHK-21 stained with PKH26 were used as target cells. (Row A) Un-transfected CHO cells are incubated for 5 min at 5.2 pH then incubated with target cells. No syncytia formation was observed. (Row B) Cells transfected with HA WT and triggered by 5 min incubation at pH 5.2. First box shows syncytia formation. Second box shows a more dispersed PKH26 dye indicating transfer of dye. (Row C) Cells transfected with both HA WT and HA 4xCys at 1:1 and incubated with FlAsH. First box shows syncytia formation. Second and third box show a dispersed stain of both PKH26 and FlAsH. Fourth box is an overlay done with Image J. Overlapping red and green dye indicates coincidences of syncytia formation and dye transfer. (Row D) Cells transfected with HA 4xCys incubated with FlAsH showed no syncytia formation.

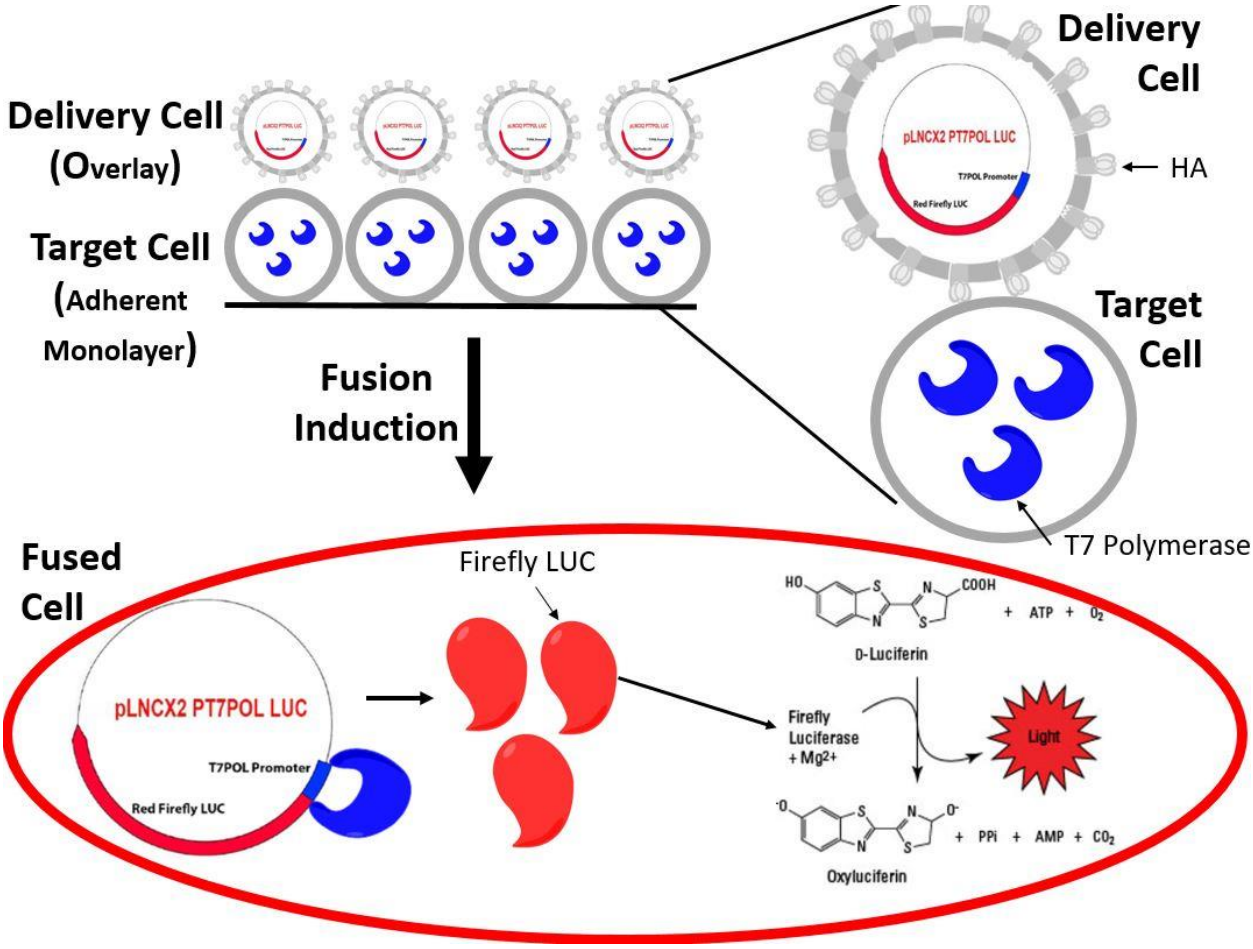

Figure 2.8. Quantitative cell fusion assay. Delivery cells expressing HA and carrying plasmid with red firefly luciferase gene under the control of T7 polymerase are overlaid on target cells. Target cells express the T7 polymerase. An activation step is used to induce fusion. After the activation step the cells are neutralized to non-activating conditions and sufficient time is allowed for fusion of effector and target cells as well as the transfer and expression of the T7 luciferase plasmid for the expression of luciferase protein. The bio-luminescence of the lysates are analyzed for successful fusion. The activity of luciferase when it reacts with D-Luciferin will indirectly indicate fusion.

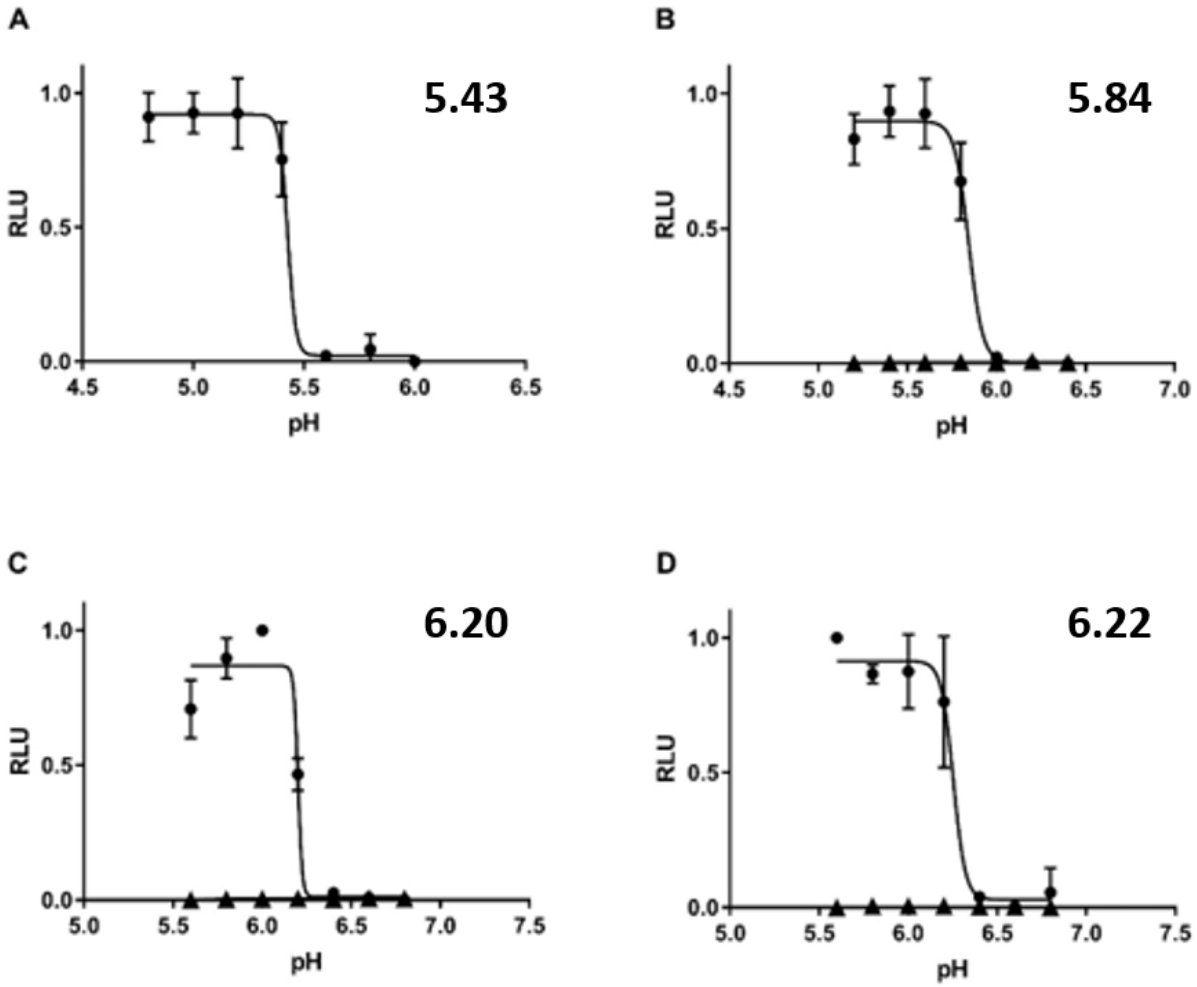

Figure 2.9. Quantitative cell fusion assay of wild-type and mutants. Effector cells contain red firefly luciferase gene under control of T7 polymerase and express either one or two HA proteins. Target BHK-21 cells expressing T7 polymerase. Effector cells are overlaid onto target cells and incubated at specific pH for 5 min. After neutralization 6 h incubation is given to allow fusion and plasmid transfer leading to expression of luciferase. Lysis of the cell mixture is analyzed for luminescence. (A) Wild-type (B) W243S (▲) and W243S + WT (●). (C) G237R (▲) and G237R + WT (●). (D) G365C (▲) and G365C + WT (●). The transition pH obtained from 3 independent experiments are shown in the top right corner of each graph. Error bars are standard deviations.

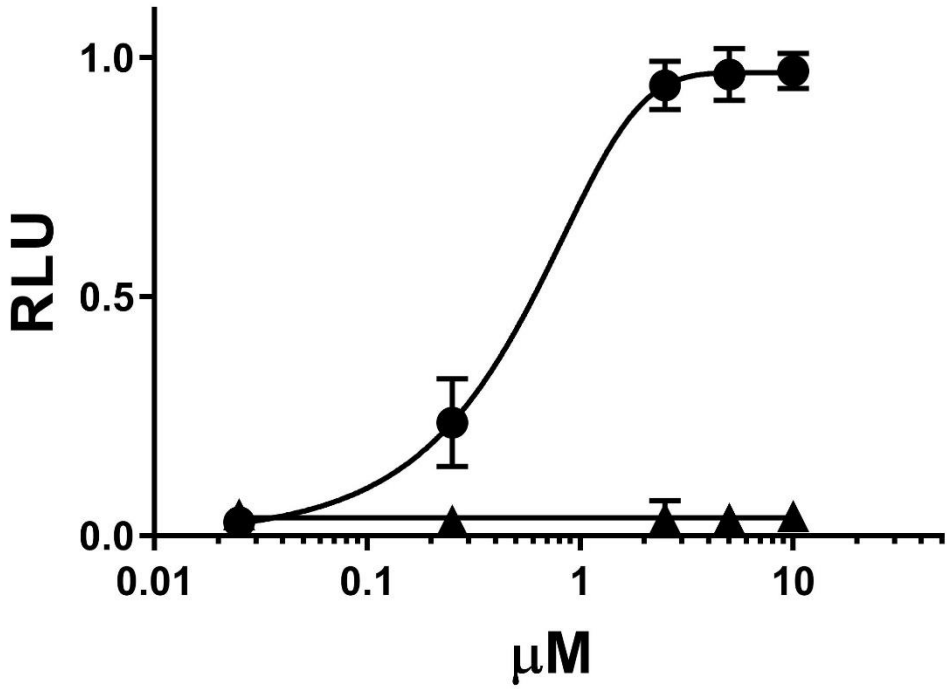

Figure 2.10. Quantitative luciferase-based fusion assay induced by ligand (FlAsH). CHO effector cells are expressing HA and carrying plasmid with red firefly luciferase gene under the control of T7 polymerase are overlaid on target cells. BHK-21 target cells express the T7 polymerase. After FlAsH buffer induction the reaction is neutralized, and sufficient time is allowed for fusion, transfer of luciferase plasmid, and expression of luciferase protein. The bio-luminescence of the lysates are analyzed using Bio-Tek Synergy 2 plate reader. Graph shows luminescence normalized to effector cells expressing wild-type HA. Modular system (●), effector cells expressing both HA4xCys and HAcmyc, show luminescence comparable to wild-type for [FlAsH] ≥ 2.5 μM. Effector cells expressing only HA4.4 (▲) showed no luciferase activity. Dose response with variable slope was fitted to data of three independent experiments with the error bars as the standard deviation produced a EC50 = 1.28 μM.

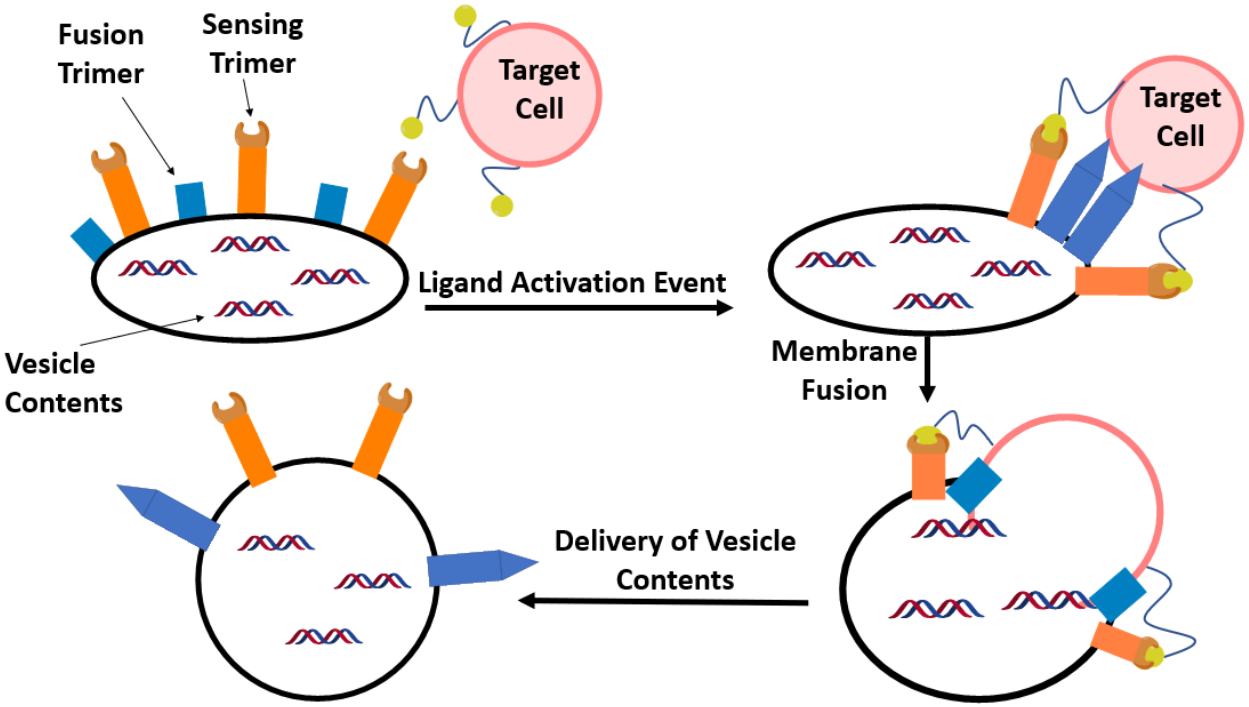

Figure 2.11. Application of modular systems. Diagram depicts a modular system co-expressing a sensing HA and fusion active HA. The sensing trimer would be triggered by a stimulus specific to the target cell. Refolding of the sensing HA along with the autocatalytic activation of the fusion trimer would facilitate the delivery of a cargo to the target cell.

$$NMFI = \frac{MFI_{sample} - MFI_{bkgd}}{MFI_{max} - MFI_{bkgd}}$$

Figure 2.12. Normalized median fluorescence intensity (NMFI). Non-transfected CHO cells (negative) were stained to determine the median fluorescence intensity background (MFI_{bkgd}). Cells transfected with only HAcmyc and stained are used to determine the median fluorescence intensity maximum (MFI_{max}).

$$NRLU = \frac{RLU_{sample} - RLU_{bkgd}}{RLU_{max} - RLU_{bkgd}}$$

Figure 2.13. Normalized relative luminescence unit (NRLU). Non-transfected CHO cells were incubated with target cells and treated in the same way to determine the relative luminescence unit background (RLU_{bkgd}). CHO cells transfected with HA wild type were used to determine the maximum relative luminescence unit (RLU_{max}).

$$Y = Bottom + \frac{Top - Bottom}{(1 + 10^{log(EC50 - x) * slope})}$$

Figure 2.14. Dose response with variable slope. Four variables were fitted to the raw data. The top and bottom being the maximum and base response relatively. A variable slope is fitted to the transition area. The amount of agonist required to get half of the maximum response, EC50, is used to characterize the sample.

CHAPTER 3
MEMBRANE ENVIRONMENT

Abstract

The membrane's role in autocatalytic activation of HA can lend insight into the mechanism of fusion through viral fusion proteins. The suggested interaction of HA fusion peptide with the membrane shows the N-terminal portion of the peptide to embed in the nonpolar membrane core and disrupt lipid structure (Han, et al., 2001; Huang, et.al., 2004; Li et al., 2005; Vaccaro, et al., 2005). The cleavage of the fusion peptide was also shown to have eliminated autocatalytic activation (Lee et al., 2006). Excess amounts of fusion peptide in solution can disrupt the membrane (Vaccaro, et al., 2005) and lead to effects in our immunostaining assay or FlAsH kinetic assay. Here, we present evidence that incubation of CHO cells expressing HA with exogenous fusion peptide causes the conformational change in wild type and mutants. We also present a cholesterol dependence on the kinetics of activation as well as the extent of fusion.

Background

The structures of hemagglutinin in its pre- and post- fusion conformation has been solved for many subtypes and give insight to the key conformational changes that occur during fusion. In the pre-fusion state the HA exists as a trimer on the surface of the viral envelope with the N-terminus containing the fusion peptide and the C-terminus containing the transmembrane domain inserted in the virion. Each monomer contains a A-helix – β-loop – B-helix region that it referred to as the coiled-coil (Wilson et al., 1981; Figure 3.1). The trimer comes together to form a cavity

where the fusion peptide resides before the conformational change (Chen et al., 1999). After acidification the HA1 headgroups dissociate and the major structural changes happen in HA2 subunit. The β-loop in the coiled-coil becomes a α-helix which combines A-helix and B-helix forming a large α-helical rod near the N-terminal which contains the fusion peptide (Qiao et al., 1998; White et al., 2008; White et al., 2016; Harrison et al., 2015). This loop to helix transition extends the fusion peptide toward the target membrane. Another key structural change is a portion of the B-helix becomes a loop which connects the large α-helical rod to a shorter α-helix. This transition allows for the C-terminal region to fold against the N-terminal region which bring the fusion peptide and transmembrane domain in close proximity forming a six-helix bundle (6HB). This post-fusion structure shows how the N-terminal fusion peptide potentially inserts into the target membrane and after folding which facilitates fusion ends up in the same membrane as the C-terminal transmembrane domain.

The composition of the membrane has also been shown to affect fusion mediated by enveloped viruses. Cholesterol, which modulates the membrane environment, can change the fluidity, thickness, and intrinsic curvature. The polar hydroxyl group which aligns with ester carbonyl group of phospholipids creates an ordering effect that reduces the movement of the lipid tails (Heftberger et al., 2015). The order also straightens out the lipid tails causing a thicker membrane (Pan et al., 2008). Cholesterol also causes an intrinsic negative curve is generated due to the small polar head group compared to its apolar region. These highly curved areas created by the intrinsic negative curve have been linked to fusion intermediates (Chernomordik et al., 2008; Aeffner et al., 2012). The preference of cholesterol for longer saturated phospholipids generate lipid rafts (Feigenson et al., 2006; Lingwood et al., 2010). These lipid rafts have been suggested

to transport viral fusion proteins to locations on the cell for infection as well as viral budding (Manes et al., 2003; Scheiffele et al., 1999; Freed, 2015; Yang et al., 2016).

Methods and Materials

Cell Culture.

CHO-K1 cells (ATCC CCL-61) were cultured in Dulbecco's Modified Eagles Medium: Kaighn's Modification of Ham's F-12 (DMEM:F-12K). Medium was supplemented with 10% fetal bovine serum (FBS) (Hyclone, Logan, UT), 100 µg/ml penicillin and 100 µg/ml streptomycin (Life Technologies, Grand Island, NY) to generate full growth medium. CHO-K1 cells were cultured at 37 ˚C and 5% CO_2. BHK-21 cells were cultured as described in chapter two and used as target cells in fusion assays.

Plasmids and Transfections.

The retroviral expression vector pLNCX2 (Clontech, Mountain View, CA) was used with the fowl plague virus (A/FPV/Rostock/34) HA gene (Lin et al. 2001) ligated in-between a XhoI and NotI site. Overlap extension PCR was used to replace the second half of the fusion peptide region, residues 11-20, with a c-myc epitope tag (EQKLISEEDL), herein referred to as HAcmyc. This allowed for specific staining with anti-c-myc antibody for the activated conformation. Overlap extension PCR was used to replace fusion peptide residues 13-18 (amino acids 355-360) with a tetra-cysteine tag (CCPGCC) and ligated into pLNCX2 (Clontech), herein referred to as

HA4xCys. All DNA manipulations were performed in E. Coli DH5α and cultured in Luria broth and supplemented with ampicillin at 50 µg/mL unless otherwise stated. Transfection using Lipofectamine 2000 reagent (Invitrogen, Carlsbad, CA) of CHO-K1 cells were used in all experiments to surface display HA libraries following the manufacturer's recommended procedure. Transfected CHO cells were cultured in selective full growth medium, 0.85 mg/ml geneticin (Hyclone, Logan, UT), 16 h post-transfection and selected for 48 h before any assay. After first 48 h selection 0.25 mg/ml geneticin was used to grow cells and maintains ~100% expression for 1 week.

Membrane Manipulation.

Transfected CHO-K1 cells were grown to ~90% confluency in T-25 flasks (Corning, Corning, NY) before used in any experiments. Adherent cells were detached from flasks using 0.05% trypsin-EDTA (Hyclone) and transferred into 1.5 mL microcentrifuge tubes and placed on ice. The cells were washed twice with PBSA and pelleted using a benchtop microcentrifuge. The cells were then subjected to either a cyclodextrin treatment or FPV fusion peptide treatment. To remove cholesterol from the membrane cells were exposed to methyl-β-cyclodextrin (Sigma-Aldrich, St Louis, MO) at indicated concentration in serum free DMEM:F-12K media for 15 min at room temperature. A synthetic peptide purchased from Genscript that is made up of the first 20 amino acids of HA2 from fowl plague virus HA, herein referred to as FPV-FP (Genscript, Piscataway, NJ), was applied to the cells. The quantity of peptide order was 14 mg at a purity of 95% aliquoted into 5 vials which was diluted in dH_20 to 1 mM for our freeze stocks. Trifluoroacetic acid which is used to cleave synthesized peptides from solid resins was removed and guaranteed

to be < 1 % in all aliquots. Cells were incubated in serum free DMEM:F-12K media buffered with 15 mM HEPES with peptide at indicated concentrations for 30 min at 37˚C. After incubation with cyclodextrin or FPV-FP cells were pelleted at 800xg and resuspended and washed twice with PBSA.

After washes cells that were treated with methyl-β-cyclodextrin (MβC) were aliquoted into tubes at ~ 5 x 10^5 cells. These cells were pelleted in a microcentrifuge and resuspended in FlAsH buffer, containing 2.5 µM FlAsH-EDT2 and 0.25 µM EDT in serum free 1:1 DMEM:F-12K medium. Negative FlAsH buffer contains no FlAsH-EDT2 and 0.25 µM EDT in serum free 1:1 DMEM:F-12K media. Cells resuspended in FlAsH buffer were immediately analyzed by flow cytometry to monitor FlAsH binding kinetics.

After washes cells that were treated with FPV-FP were immunofluorescently stained and assayed by flow cytometry. Cell surface expression was determined by monoclonal antibody (mAb) HC2 and HA conformation was determined by pre-activation specific monoclonal antibody HC58 (Sugrue et. al, 1990). For HAcmyc-expressing cells, activated state was monitored by mAb 9e10 (Lee et al 2006).

Peptide Incubation Followed by pH Pulse.

To determine the effect of low concentrations of FPV-FP a triplicate set of peptide experiments were followed by a low pH incubation. After FPV-FP incubation at a low concentration, 1 µM, and 3 extensive wash steps cells were exposed to a pH induction step, citrate buffer at pH range from 5.0 to 6.0 for 5 min at room temperature. Cell surface expression was determined by monoclonal antibody (mAb) HC2 and HA conformation was determined by pre-

activation specific monoclonal antibody HC58 (Sugrue et. al, 1990). Bi-modal response allowed for the flow cytometry data to be gated based on controls to allow the calculation of fraction of cells induced. The fraction induced represents the number of cells positive for activated HA divided by the number of cells analyzed and expressing HA. A variable slope dose-response curve was fitted to data in order to calculate an EC50 value that characterized the transition pH.

Fusion Assay.

The same fusion assay from Chapter 2 using a luciferase reporter (Byrd-Leotis et. al.) to assess HA-mediated membrane fusion was applied after MβC incubations. Plasmid containing Red Firefly Luciferase gene (Pierce) was cloned into a pLNCX2 plasmid (Clontech). Primers were designed to add the luciferase gene in between a XhoI and Not I site with a T7 polymerase promoter upstream of the gene. CHO cells were transfected with HA plasmid or co-transfected with two distinct HA genes and a plasmid containing Red Firefly Luciferase gene (Pierce) under the control of a T7 bacteriophage promoter using Lipofectamine 2000 (Invitrogen) according to manufactures protocol to create effector cells. 16 h post-transfection, the effector cells were placed in selective growth medium containing 0.85 mg/ml geneticin (Hyclone) for 48 h. Target BHK-21 cells were transfected with pCAG-T7, a plasmid containing T7 bacteriophage polymerase also using Lipofectamine 2000. pCAG-T7 pol was a gift from Ian Wickersham (Addgene plasmid # 59926). 48 - 72 h after transfection of the target cells, the HA-expressing cells were washed with PBS and treated with 0.05% trypsin-EDTA (Hyclone). The CHO effector cells were then overlaid on the target cells and incubated for 1 h at 37 ˚C to allow cells to adhere. Cells were washed once with PBS (Hyclone) and then exposed to appropriate induction buffer for 5 or 15 min. At the end

of the induction complete growth medium was added to neutralize the reaction. The cells were incubated for 6 h at 37 ˚C to allow for cell-cell fusion and plasmid transfer leading to expression of luciferase. The cells were then washed once with PBS and lysed with 0.1 ml of lysis buffer (Pierce) and incubated in a 37 ˚C shaker for 15 min. 20 µl of lysate was transferred to a 96-well plate and 50 µl of D-luciferin substrate and 1 µl of Firefly signal enhancer (Pierce) were added to each well. Luciferase-catalyzed luminescence resulting from cell fusion was quantified using a Bio-Tek Synergy 2 multi-mode plate reader (Bio-Tek, Winooski, VT).

Results

MβC Effect on FlAsH Binding Kinetics.

To test the importance of the cell membrane MβC was used remove cholesterol from the membrane. Cells that were transfected with HA4xCys plasmid were used in FlAsH binding kinetic experiments. Cells expressing HA4xCys were incubated in 10 mM MβC for 15 min at room temperature then resuspended in FlAsH buffer and analyzed via flow cytometry. HA4xCys cells that were treated with MβC (blue) show a delay in FlAsH binding that is not seen in HA4xCys cells with no MβC (black) incubation (Figure 3.2). HA4xCys cells that had no MβC incubation (negative control) showed that FlAsH binding occurred at ~ 420 sec. FlAsH binding was delayed an average of 155 sec over three independent experiments when treated with MβC. This indicates that by reducing the amount of cholesterol in the membrane there is a longer lag time before the

ligand binding that indicates the conformational change. This would indicate that the membrane environment plays a role in the refolding of HA.

Extent of Fusion Reduced by MβC.

We further tested the role cholesterol plays in the fusion catalyzed by HA. We showed previously that the conformational change of HA is delayed with the depletion of cholesterol. The quantitative luciferase fusion assay was used in combination with MβC incubation to determine the effect of cholesterol depletion on the extent of fusion. CHO cells expressing wild type HA were tested using either a 5.2 pH induction or a FlAsH induction. The modular system expressing both a fusion active HA, wild type HA, and a sensing HA, HA4.4, was also tested with the same two induction steps. Prior to inducing the conformational change, the cells expressing the HA's were incubated with non- MβC, 5 mM MβC, 10 mM MβC, or 20 mM MβC buffer for 15 min at room temperature. Following the neutralizing of the MβC buffer the cells were overlaid with target cells, BHK-21 expressing T7 polymerase, and induced by a 5 min pH 5.2 or a 15 min FlAsH buffer incubation. The cells were then treated as explained in the methods and the extent of cell fusion, between HA expressing CHO and target BHK-21 cells, was quantified using a Bio-Tek Synergy 2 multi-mode plate reader. The raw data was normalized using positive and negative controls as described in Figure 2.12. CHO cells expressing only wild type HA produced luciferase signal when induced by low pH but had no luciferase signal when induced with FlAsH ligand. The titration of MβC shows a decrease in the extent of fusion as higher levels of cholesterol is depleted (Figure 3.3). The modular system had a positive luciferase signal for both the low pH and FlAsH ligand

induction steps. Similar to the HA wild type the modular system's extent of fusion was decreased as the amount of cholesterol depleted increased (Figure 3.3).

Taken together, with the longer lag time before activation, the cholesterol in the membrane plays a role in the activation and fusion catalyzed by HA. The link of HA to lipid rafts can potentially contribute to the both the delay in kinetics and the reduction in fusion.

FPV-FP Effect on HA Activation.

To test the role of the membranes interaction with HA we used fusion peptide in solution which mimics the exposed fusion peptide of HA after activation and allows for the interaction of the peptide with a membrane. The fusion peptide of fowl plague virus (A/FPV/Rostock/34) HA is derived from the first 20 amino acids from the N-terminal of HA2 subunit. The sequence of the peptide is GLFGAIAGFIENGWEGLVDG and was synthesized and purified as described in the methods section. Our goal was to mimic an activated HA environment when the fusion peptide is exposed and able to interact with the cell membrane. Fusion peptides have been shown to bury into the target membrane in a kinked α-helical structure and disrupt the lipid packing (Huang, et.al., 2004; Li et al., 2005; Vaccaro, et al., 2005). Cells that were transfected with HA wild type plasmid and gone through selection were used to monitor refolding after incubation with FPV-FP at different concentrations. After the incubation with FPV-FP cells expressing HA wild type were immunofluorescently stained and analyzed via flow cytometry. Using mAb HC58, which is conformation specific to pre-activation state, we observed that median fluorescence intensity for 3 independent experiments dropped when using concentrations of peptide $\geq$ 10 μM (Figure 3.4). As a negative control a myosin light chain kinase (MLCK) peptide, with a sequence of

ARRKWQKGGHAVRAIGRLSS, was used and no concentration of this peptide showed a decrease in fluorescence. The drop in median fluorescence indicates that the HA have gone through the conformational change to the active state. This suggests that the peptide disrupting the membrane packing is sufficient enough to cause the conformational change.

Similarly, CHO cells transfected with HAcmyc, which allows us to monitor the active state of HA, were also used in FPV-FP experiments. Using mAb 9e10 to monitor the active state of HA after incubations with FPV-FP, we observed that concentrations of peptide ≥ 100 μM showed an increase in median fluorescence while the negative control MLCK showed no increase (Figure 3.5). The increase in fluorescence over three independent experiments indicates that the HAcmyc was going through its conformational change to the active state induced only by the peptide. This agreed with the peptide induction seen in the wild type HA monitored by an antibody specific to pre-activation state. The need for a higher amount of peptide induction seen in HAcmyc can be attributed to the mutant HA lacking a complete fusion peptide region. HAcmyc mutant has the second half of the fusion peptide region mutated. Plasticity reports of the fusion peptide region have shown a number of mutations that effect the interaction with the membrane (Li et al., 2005; Vaccaro et al., 2005; Qiao et al., 1999). A single mutation of Gly-1 to Serine allows for lipid mixing (hemifusion) but inhibits fusion and molecular simulations suggests that the peptide interacts with the lipids differently. Whereas, mutation of Gly-1 to Valine blocks both hemifusion and fusion. HAcmyc trimers have eight total mutations with three hydrophobic residues being replaced by charged ones. It's possible that the fusion peptide interacts with the membrane but not as effectively as the wild-type. Due to the coarse-grained titration it is possible that 10 μM FPV-FP might be close to the amount of peptide needed to cause the conformational change in the

mutant HA's. The concentration difference needed to activate HA wild type and mutant HA might be closer than the data suggests. To determine if other HA mutants also required higher concentrations of peptide to induce conformational change HA4xCys was tested as well as HAcmyc using mAb HC58.

CHO cells expressing HA wild type, HAcmyc, and HA4xCys were all incubated with FPV-FP and immune-stained using mAb HC58 to monitor the conformational change. Both mutant HA's, HAcmyc and HA4xCys, required higher concentrations of peptide to induce conformational change when compared to HA wild type (Figure 3.6). The median fluorescence decrease is cause by a loss of HC58 binding, which is indicates the HA has gone through a conformational change. Wild type HA (black) is induced at ≥ 10 μM FPV-FP were as the two mutants, HAcmyc (blue) and HA4xCys (green), are induced at 100 μM FPV-FP. This agrees with the mAb 9E10 stain that also shows that HA's with mutated fusion peptide region require higher concentrations of peptide to induce conformational change.

Low Concentration of FPV-FP Followed by pH Pulse.

To further test the ability of FPV-FP to disrupt the membrane environment and its effect of HA we used a low concentration of peptide followed by a pH pulse. CHO cells expressing HA wild type were first incubated in FPV-FP before being exposed to a low pH pulse. We used 1 μM FPV-FP because at this concentration the peptide was not able to induce the conformational change. A MLCK peptide was used as a negative control. Following the peptide incubation, a pH titration ranging from 5.0 – 6.0 was applied to determine the pH of transition. Staining with mAb HC58 was used to monitor the pre-activation state and analyzed via flow cytometry. Histogram

curves from flow cytometry were used to determine the percentage of cells that had gone through the conformational change. The percent induced was the population of cells that loss the ability to bind mAb HC58. The pH of transition, pH at which 50% of the cells had been induced, for FPV HA wild type has been shown to be at pH 5.4. The pH titration showed that with the incubation of 1 μM FPV-FP (●) before the pH pulse destabilized the HA and the transition pH increased to 5.78 when fitting a dose response variable slope curve (Figure 3.7). The negative control MLCK peptide (▲) showed no effect on the transition pH when compared to the wild type which was calculated to be 5.36 after fitting a dose response curve to the data. These results agree with the previous peptide induction and also indicates that the FPV-FP destabilizes the membrane allowing for the HA to transition at higher pH's.

Discussion

The need to better understand the fascinating phenomenon of autocatalysis seen in the conformational switch of HA can lead to better engineering the modular systems shown in Chapter 2. It could also broaden the understanding of the conformational change necessary for enveloped viral infection. The model of cell-wide communication proposed in Chapter 2 and its dependence on the fusion peptide was the rationale for the experiments done in this chapter. It is speculated that the hydrophobic fusion peptide's initial exposure, displacement from the cavity, and ability to insert into its own membrane resulting in locally altered membrane properties and providing a decrease in activation energy to enable refolding. This model for autocatalysis suggests that the

interaction of HA with the membrane plays a key role in the cell-wide switching behavior which we tested with exogenous peptide and depletion of membrane cholesterol.

Membrane composition was altered by applying methyl-β-cyclodextrin (MβC) to cells to extract cholesterol (Lu, et al., 2012). The cells with depleted amounts of cholesterol showed longer lag time when monitoring the conformational change with HA4xCys mutant. The link of not only HA but various other viral fusion proteins to lipid rafts supports the idea that by disrupting that association and the lateral dissociation of HA results in slower kinetics and decreased fusion activity (Krautkramer et al., 2014; Molotkovsky et al., 2018; Dou et al., 2018; Ohkura et al., 2014; Chang et al., 2012; Takeda et al., 2003). The lipid rafts are cholesterol dependent and cyclodextrin treatment has been shown to deplete percentages of the membrane that exists as rafts. The cells treated with MβC also showed a lower extent of fusion. Cells with lower amount of cholesterol showed a reduction in fusion by about 50%. This leads to questions weather other viral fusion proteins have a cholesterol dependence. The key role that the membrane environment has on viral fusion can impact therapy of many enveloped viruses.

Exogenous fusion peptide from H7 fowl plague virus was used to alter the local membrane environment and it was shown to cause the conformational refolding of HA at a neutral pH of both wild type HA and mutant HA's (HAcmyc and HA4xCys). It was also shown that using lower concentrations of exogenous peptide causes the transition pH of wild type HA to increase which indicates that the fusion peptide destabilizes trimers expressed on the surface of the cell. The suggested interaction of HA fusion peptide with the membrane shows the N-terminal portion of the peptide to embed in the nonpolar membrane core and disrupt lipid structure (Han, et al., 2001; Huang, et.al., 2004; Li et al., 2005; Vaccaro, et al., 2005). The cleavage of the fusion peptide was

also shown to have eliminated autocatalytic activation (Lee, 2007). Excess amounts of fusion peptide in solution disrupt the membrane (Vaccaro, et al., 2005) and lead to refolding of HA trimers. Studies with other membrane altering peptides, such as β-amyloid pathogenic factor in Alzheimer's which causes pores, has been shown to inhibit Influenza A virus (White, et al., 2014). These experiments taken together with the cholesterol depletion experiments suggest that the membrane environment plays a role in the activation of HA and in the fusion catalyzed by the viral protein.

Appendix

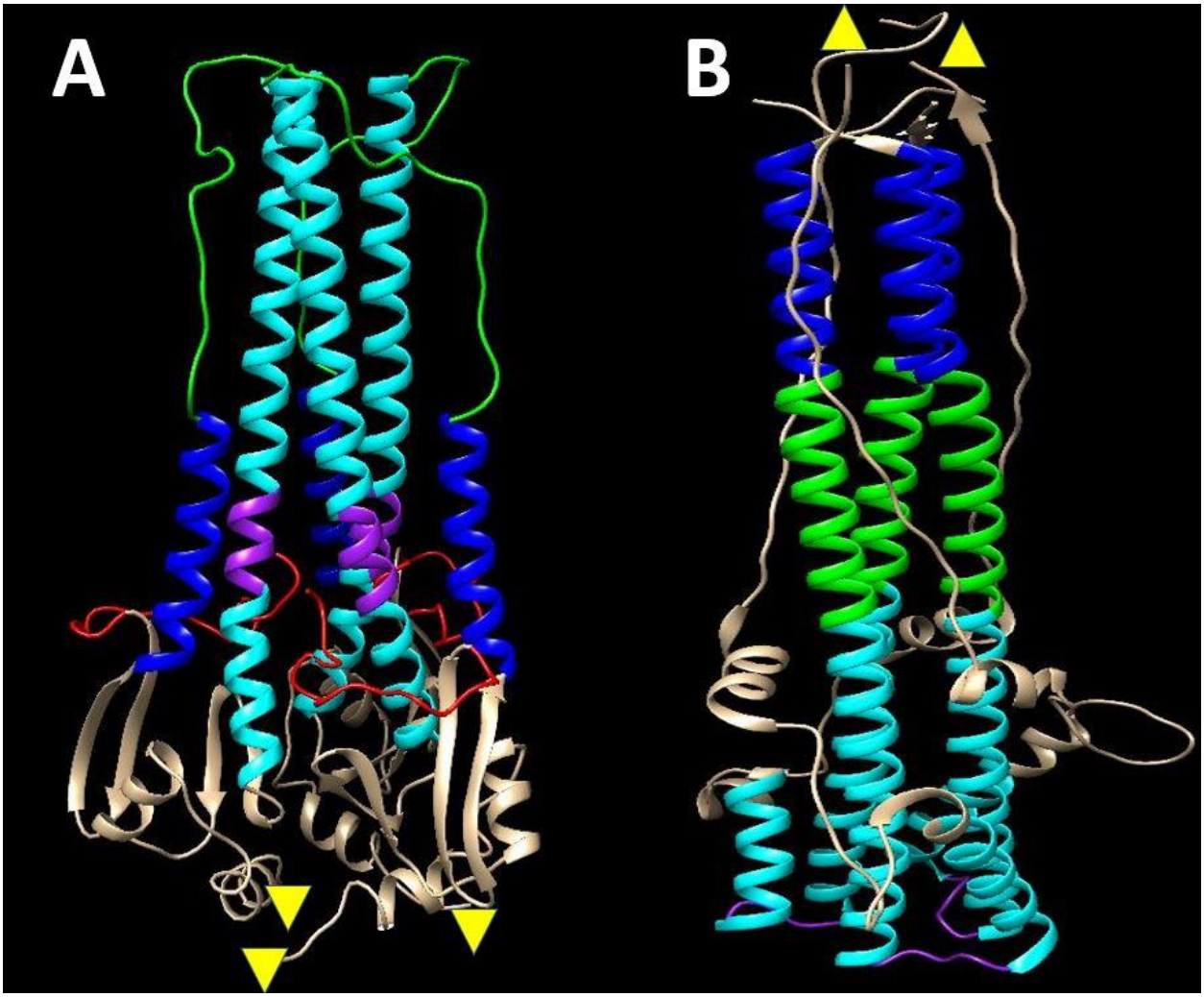

Figure 3.1. Structural rearrangements of HA2. The trimer structures of HA2 fusion subunit are shown here in the pre-fusion (A) and post-fusion (B) state. Yellow triangle indicates where the transmembrane domain would be located. Only the HA2 subunit is shown. The coiled-coil is represented by the A-helix (blue), β-loop (green), and the B-Helix (cyan). The key regions that have conformational changes are the β-loop (green) and helix section of the B-Helix (purple). The fusion peptide (red) is only depicted in the pre-fusion state and is on the N-terminus side of the A-helix (blue). The structures were downloaded from the Protein Data Bank. 2HMG (A) and 1QU1 (B) and rendered on UCSF Chimera not drawn to scale.

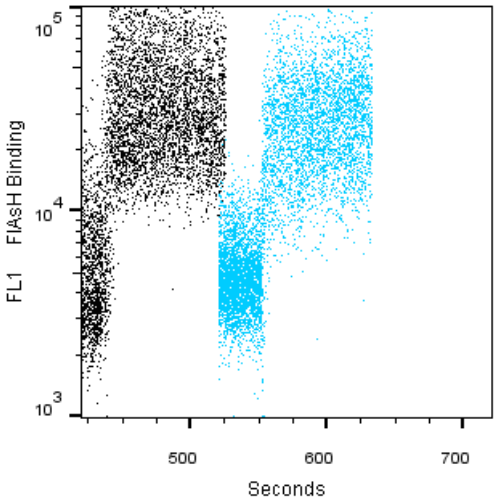

Figure 3.2. Cholesterol depletion causing delayed kinetics. CHO cells were transfected with HA4xCys. Cells expressing HA4xCys were incubated for 15 min at room temperature in 10 mM MβC (blue) or non- MβC buffer (black). The cells treated with MβC showed a longer lag time that is no seen in the negative control. The delay is attributed to the depletion of cholesterol and its role in autocatalysis.

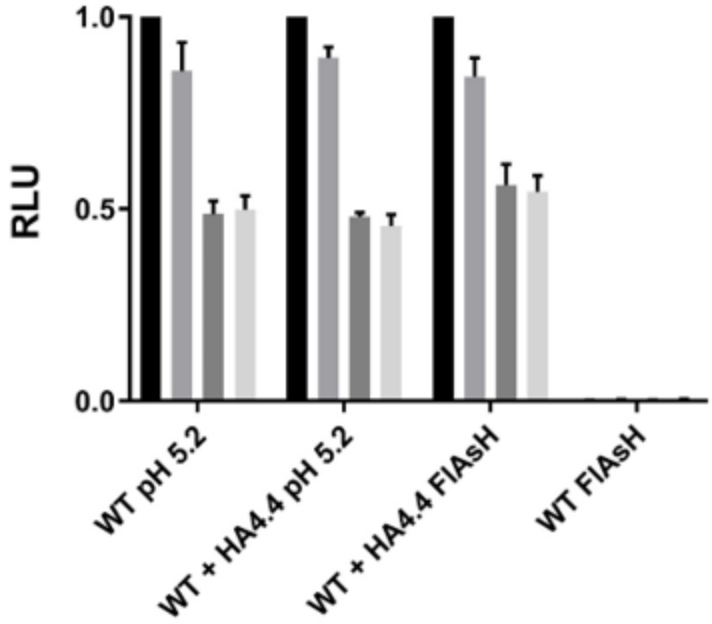

Figure 3.3. Extent of fusion with cholesterol depletion. CHO cells expressing wild type HA and a modular system (HA wild type and HA4.4) were tested for extent of fusion after a MβC incubation. Non- MβC, 5 mM MβC, 10 mM MβC, and 20 mM MβC (shown from left to right grey-scale bars) was used prior to the indicated induction step. Both systems were tested using either a pH 5.2 or a FlAsH ligand induction. Average of 3 independent were normalized and std deviations shown as error bars.

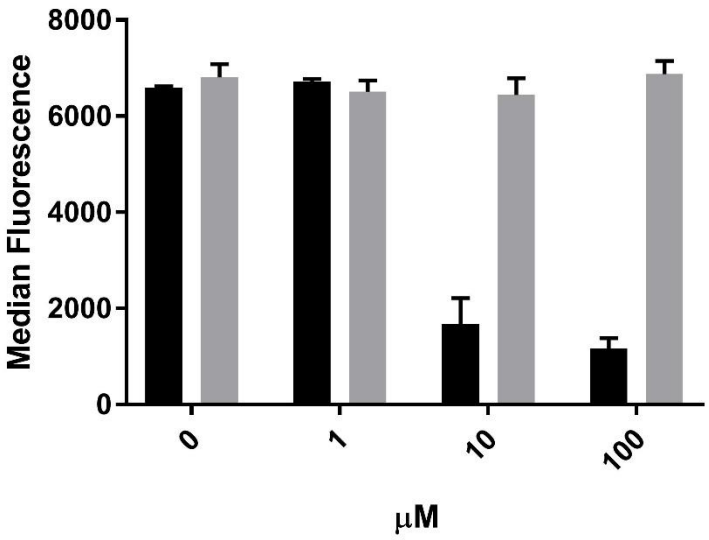

Figure 3.4. FPV-FP wild-type activation. CHO cells expressing wild type HA were incubated with peptide at indicated concentration. FPV-FP (black) or MLCK (grey) peptide was incubated with the cells for 30 min at 37˚C. The cells were stained with, pre-active state specific antibody, mAb HC58. The median fluorescence intensity was averaged for 3 independent experiments with the std deviation shown as error bars.

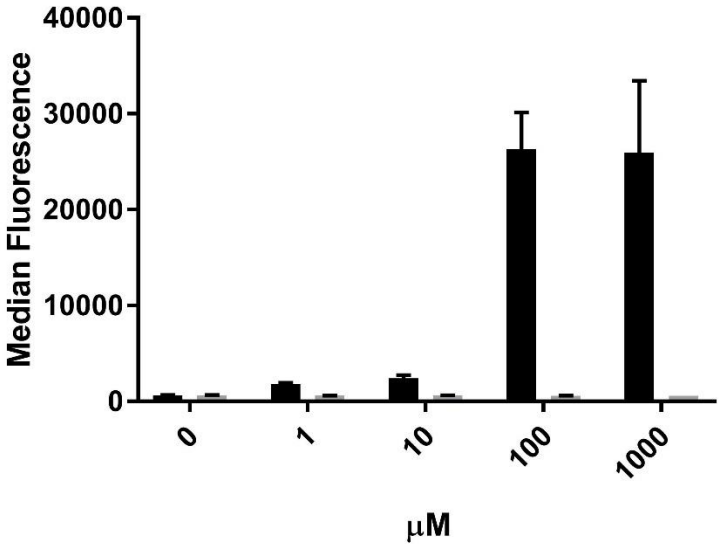

Figure 3.5. FPV-FP HAcmyc activation. CHO cells expressing HAcmyc were incubated with peptide at indicated concentration. FPV-FP (black) or MLCK (grey) peptide was incubated with the cells for 30 min at 37˚C. No significant fluorescence above the negative control (non-transfected cells) was observed for incubations with the MLCK peptide. The cells were stained with, active state specific antibody, mAb 9E10. The median fluorescence intensity was averaged for 3 independent experiments with the std deviation shown as error bars.

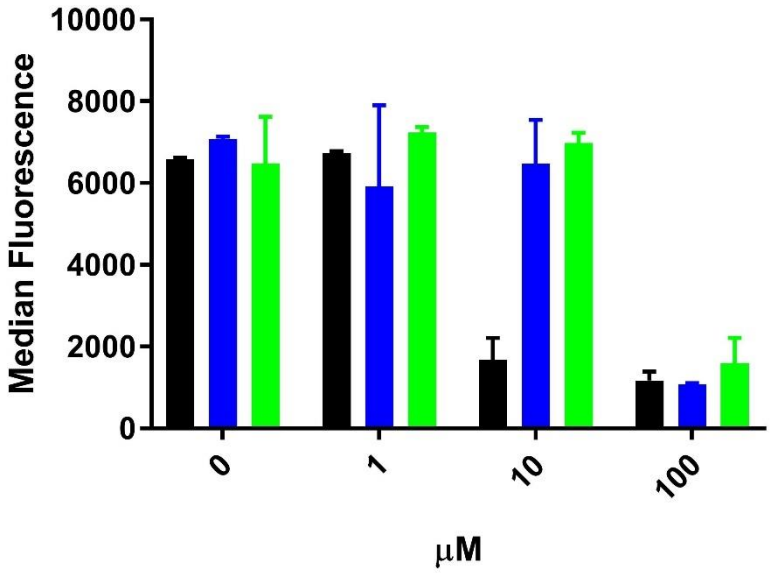

Figure 3.6. FPV-FP induction. CHO cells expressing wild type HA (black), HAcmyc (blue), and HA4xCys (green) were incubated with peptide at indicated concentration. FPV-FP peptide was incubated with the cells for 30 min at 37˚C. The cells were stained with, pre-active state specific antibody, mAb HC58. The median fluorescence intensity was averaged for 3 independent experiments with the std deviation shown as error bars.

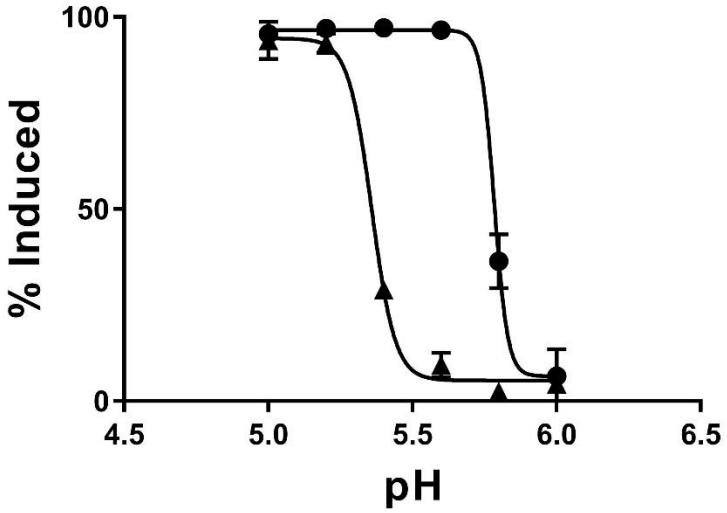

Figure 3.7. Low concentration FPV-FP followed by pH pulse. CHO cells expressing wild type HA were incubated with either FPV-FP or MLCK peptide at 1 μM. FPV-FP (●) or MLCK (▲) peptide was with the cells for 30 min at 37˚C. After the peptide was removed the cells were treated at indicated pH. The cells were stained with, pre-active state specific antibody, mAb HC58. The median fluorescence of a non-transfected CHO cell was used to determine a gate separating active and pre-active states. After subtracting background, the percent induced was determined. The data was averaged for 3 independent experiments with the std deviation shown as error bars.

CHAPTER 4
AUTOCATALYTIC ACTIVATION OF X31 AND CROSSTALK

Abstract

The conformational change of foul plague virus HA expressed on CHO cells were shown to have switching behavior and in Chapter 2 we demonstrate crosstalk between HA mutants of the same subtype (Lee et al., 2006). The proposed model of refolding of FPV HA to the fusion active conformation could potentially be applied to other viral fusion proteins or subtypes of HA. Here we are using the robust cell surface display system as a tool to demonstrate that the autocatalytic phenomena apply to other subtypes of HA and other viral fusion proteins. Here, we present evidence for the ability to activate other viral fusion proteins or other subtypes of HA via autocatalytic activation. Communication between different subtypes and other viral fusion proteins was monitored using a similar immunoassaying via flow cytometry.

Background

In this chapter we will discuss a human influenza virus hemagglutinin (X31-HA) as well as two other viral fusion proteins from vesicular stomatitis virus (VSV-G) and human immunodeficiency virus type 1 (gp-160). All three viral fusion proteins are found on the viral envelope and mediate fusion with the target membrane. They share a common pathway through fusion with similar intermediates. The two subtypes of HA, H3 and H7, differ in sequence but the overall structure is very similar. X31-HA is still made up of a receptor binding domain, HA1, and a fusion domain, HA2, that is proteolytically cleaved. The HA1 subunit's of H7 and H3 share a

sequence identity of 39.3% while the HA2 subunits share a 68.6% similarity (Russel et al., 2004). The overall conformational change and process of fusion remains the same between the subtypes.

The viral fusion proteins from different viruses differ not only in sequence but the structures are diverse (Figure 4.8). Even with the difference in sequence the three proteins studied here share common themes. In each case the protein exits as a trimer on the viral membrane before it is triggered to undergo its conformational change that forms an extended trimer intermediate, which brings the fusion peptide region toward the target membrane (Harrison, 2015; Baquero et al., 2015). The pre- and post-fusion structures indicate that the extended intermediate folds on itself bringing the two membranes into close contact, presumably initiating lipid-mixing, much like what is shown for H7 HA in Figure 3.1 forming 6-helix bundles (Roche et al., 2006; Roche et al., 2007; Gallo et al., 2003; Moore et al., 2003).

Vesicular stomatitis virus viral fusion protein (VSV-G) exists as trimers on the surface of the viral membrane but has also been observed to exists as a monomer in some cases (Roche et al., 2006; Albertini et al., 2012). The viral fusion protein is made up of a combination of α-helices and β-sheets which differs from hemagglutinin which is mainly helices. In its prefusion state the VSV-G fusion peptide loops are completely exposed unlike both HA and gp-120/gp-41 complex and are found between 3 β-sheets. Each monomer contains two fusion loops that are extended toward the target membrane after acidification. VSV-G is triggered into its conformational change in the early endosome at pH ~ 6.1 and requires no other proteins to drive fusion (Kim et al., 2017; Roche et al., 2008; Stanifer et al., 2011). The reversibility of VSV-G is unique to this viral fusion protein compared to HA. The viral fusion protein exists in a dynamic equilibrium that HA does not exits in until the pH has already dropped. HA's metastable state does not allow for any partially

activated trimers unless there is a pH drop. The pH change in VSV-G shifts the equilibrium of the proteins conformational state. Ultimately the final fusion state after the extended intermediate folds back is also a 6-helix bundle that brings the two apposing membranes in close proximity (Roche et al., 2007).

Human immunodeficiency virus type 1 viral fusion protein (gp-160) is proteolytically cleaved to a trimer consisting of three gp-120/gp-41 heterodimers where it exists in its metastable state much like hemagglutinin. The triggering is mediated by gp-120 receptor binding domain that is shed after binding CD4, but the full activation of viral fusion protein requires a second coreceptor, CXC4R OR CCR5 of the chemokine family of receptors, (Moore et al., 1990; Harrison, 2015; Gallo et al., 2003; White et al., 2008). The binding of the coreceptor has been shown to enhance the refolding and is some cases seen to be required for complete activation (Mkrtchyan et al., 2005; Platt et al., 2007). The fusion peptide of gp-41 is found on the N-terminus of the fusion subunit similar to HA. After the triggering the fusion peptide is extended toward the target membrane and the final post fusion states also resembles the 6-helix bundle.

Methods and Materials

Plasmids.

Fowl plague virus (A/FPV/Rostock/34) HA gene (Lin et al. 2001) was digested with XhoI and NotI and ligated into the retroviral expression vector pLNCX2 (Clontech, Mountain View, CA). A previously created HA mutant with a c-myc epitope tag sequence (EQKLISEEDL) cloned

into the fusion peptide residues 11-20 (amino acids 353 – 362) was also ligated into the pLNCX2 (Clontech) vector (Lee et al. 2006), herein referred to as HAcymc. In a similar cloning step human influenza virus (A/Aichi/68/X31) HA, H3 subtype, was mutated with c-myc epitope tag sequence into the fusion peptide region at residues 11 – 20. The c-myc epitope tagged H3 HA was digested and ligated into pLNCX2 (Clontech), herein referred to as X31-HAcmyc. Oligonucleotides were designed to isolate the fusion protein, protein G, from vesicular stomatitis virus (VSV) from pVSV-G plasmid (Clontech). The resulting PCR product was digested with Xho-I and Not-I and ligated into pLNCX2 (Clontech), herein referred to as VSV-G. The mammalian expression plasmid containing gp-160, p96ZM651gp160-opt, was obtained from the NIH Aids Reagent Program. The gp-160 gene is inserted into a pcDNA3.1(-) plasmid with a CMV promotor and geneticin resistance. All DNA manipulation were performed in E. coli Top10 or DH5α and cultured in Luria broth (LB; 10 g/L tryptone, 5 g/L yeast extract, 10 g/L NaCl) supplemented with ampicillin at 50 µg/ml.

Cell Culture.

CHO-K1 cells (ATCC CCL-61) were cultured in Dulbecco's Modified Eagles Medium: Kaighn's Modification of Ham's F-12 (DMEM:F-12K). The medium was supplemented with 10% fetal bovine serum (FBS) (Hyclone, Logan, UT), 100 µg/ml penicillin and 100 µg/ml streptomycin (Life Technologies, Grand Island, NY). CHO-K1 cells were transfected with plasmids using Lipofectamine 2000 Reagent (Invitrogen, Carlsbad, CA) according to manufacturer's protocol. Transfected CHO cells were cultured in selective growth medium, 0.85 mg/ml geneticin (Hyclone, Logan, UT), 16 h post-transfection and selected for 48 h before any assay. After first 48 h selection

0.25 mg/ml geneticin was used to grow cells and maintains ~100% expression for 1 week. All transfections of CHO cells followed the same selection process unless stated otherwise. CHO-K1 cells were used to surface express HA wild type, HA mutants, HA X31, gp-160 and VSV-G in all assays, except where indicated otherwise. Co-transfections were done at a 1:1 plasmid ratio keeping the total amount of plasmid used in transfections according to the manufactures protocol.

Analysis of Induced HA.

Cells are transfected and selected in a T-25. After selection cells are grown in t-25 flasks to ~ 90% confluency. All adherent cells were detached using 0.05% trypsin-EDTA (Hyclone) and aliquoted into 1.5mL microcentrifuge tubes and placed on ice. Cells were washed twice with PBSA and pelleted at 800xg using a benchtop microcentrifuge. The cells were then exposed to a pH induction step, citrate buffer at appropriate pH for 5 min at room temperature or a FlAsH induction step by addition of FlAsH buffer, containing 2.5 µM FlAsH-EDT2 and 0.25 µM EDT in serum free 1:1 DMEM:F-12K media, for 15 min at room temperature. Negative FlAsH buffer contains no FlAsH-EDT2 and 0.25 µM EDT in serum free 1:1 DMEM:F-12K media. The TC-FlAsH in cell tetra-cysteine tag detection kit (Molecular Probes # T34561, Eugene, OR) was used and optimized according manufacture's recommendations. After induction step the cells were immunofluorescently stained and assayed by flow cytometry. Cell surface expression was determined by monoclonal antibody (mAb) HC2 and HA conformation was determined by pre-activation specific monoclonal antibody HC58 (Sugrue et. al, 1990). A previously shown mutant, HAcmyc, was used to monitor activated state by mAb 9e10 (Lee et al 2006). Bi-modal response allowed for the flow cytometry data to be gated based on controls to allow the calculation of

fraction of cells induced. A variable slope dose-response curve was fitted to data to calculate an EC50 value which characterized the transition pH.

Results

Bi-modal Transition of X31 HA.

The fusion peptide region is used as a detection flag due to the irreversibility of the conformational change and the fact that this region is exposed only in the activated state. CHO cells transfected and selected with the epitope tagged H3 subtype, X31-HAcmyc, were used to analyze the pH at which the protein goes through its conformational change via flow cytometry. After selection cells were exposed to a 5 min low pH pulse then immunofluorescently stained with mAb 9E10 to detect exposure of c-myc epitope tag. Flow cytometry data from a pH titration shows that the transition/activation pH at which 50% of the cells have gone through the conformational change is at pH 5.23 (Figure 4.1). Negative control, CHO cells that were not transfected, were used to determine a background fluorescence, and set gates to determine which population of cells were positive for c-myc. The number of cells that were positive for c-myc, activated HA on the surface, was divided by the number of cells expressing HA in order to calculate the fraction induced which was plotted against pH (Figure 4.1). A variable slope dose response curve was fitted to the data and the EC50 (the pH at which half the max response is observed), was used to characterize the transition/activation pH. The cells exposed to the pH pulses demonstrated a bimodal response at the cell population level. The samples that were exposed to pH in the transition

region, immunofluorescently stained, and analyzed via flow cytometry show two-state response (Figure 4.2). At a high pH 5.6 very few cells are activated and at a low pH 5.0 very few remain inactive. The intermediate states (pH 5.2 and pH 5.4) the activation is bimodal and included no cells with an intermediate level of c-myc exposure. These intermediate pH's had two distinct populations which indicates a mixture of cells that are fully in the pre-active state and another population that is fully in the active state. Flow cytometry data suggests that no cell has a fraction of it HA induced so there is no cell that have both pre-active and active state HA on the surface. This switch behavior of all or nothing, also seen in H7 subtype HA of influenza virus, indicates that each individual cell reaches a threshold at which it completely commits all the HA on the surface to refold to the active state.

Subtype Crosstalk: H3 HA and H7 HA.

The ability to crosstalk between the two subtypes of HA, H7 and H3, was assessed by co-expressing both proteins. CHO cells were transfected at a 1:1 plasmid ratio with both HA4xCys, which is the tetra-cysteine construct in the FPV H7 HA, and X31-HAcmyc. With the transition pH characterizing the two HA subtypes only being 0.2 pH units in difference we decided to use a non-acidic induction step. X31-HAcmyc showed a small amount of c-myc signal at pH 5.4 so the use of an acidic induction might result in false positives. In our co-expression model the HA4xCys is used as the sensing HA which will be induced by a ligand, FlAsH, while the X31-HAcmyc will be used as the reporter HA that will give a positive signal using the c-myc epitope flag for the active state. This model is similar to the previous experiments with crosstalk in the H7 subtype between different mutants. If the autocatalysis phenomenon applies to the H3 subtype, then ligand-induced

H7 HA should cause all HA on the surface of a cell to activate including the X31-HAcmyc HA. After transfection a selection for expressing CHO cells was applied in the same fashion as the other transfections. The cells were then incubated for 15 min in FlAsH buffer, neutralized, and resuspended in PBSA. The cells were immunofluorescently stained and analyzed via flow cytometry. The negative control, transfected cells incubated in negative FlAsH buffer, show no c-myc positive cells for both co-expressing and X31-HAcmyc samples (Figure 4.3). Cells incubated with the FlAsH buffer have a positive c-myc signal only for the co-expressing samples, while the cells expressing only X31-HAcmyc are negative for c-myc signal (Figure 4.3). The cells expressing only X31-HAcmyc and the co-expressing system were also pulsed at pH 5.0 to demonstrate the capability of activating all HA on surface directly (Figure 4.3). The flow cytometry data indicates that the phenomena of autocatalysis applies across subtypes. Cells expressing only the X31 HAcmyc, which has no tetra-cysteine tag, did not respond to the ligand. The co-expression system allows for a sensing HA, HA4xCys, to be activated by FlAsH and in turn activate X31 HAcmyc via autocatalysis. Crosstalk allows for the indirect activation of H3 HA subtype by a ligand. The ability to induce X31 HA indirectly with a ligand that only binds FPV HA could suggests the subtypes share a common self-activating mechanism.

Fusion Protein Crosstalk: VSV-G and H7 HA.

The autocatalytic phenomenon applying across different subtypes of HA supports our hypothesis for the role that the membrane plays in activation. If the disruption of the membrane environment can alter other subtypes we want to test if other viral fusion proteins that go through a similar conformational change. Vesicular stomatitis virus (VSV) has a viral fusion protein (G)

that undergoes a conformational change at pH ~ 6.1 (Kim et al., 2017; Libersou et al., 2010; Roche et al., 2008; Stanifer et al., 2011). This pH is significantly higher than the pH of transition for H7 HA (pH 5.4) and could be used in a co-expression model similar to the system with two subtypes. Cells co-expressing VSV-G (viral fusion protein of VSV) and HAcmyc can potentially indicate crosstalk between different viral fusion proteins in a modular system. The VSV-G protein would work as a pH sensor that would respond at pH's below 6.1 and HAcmyc would be a reporter protein that would give a positive c-myc signal if crosstalk observed. A pH titration would show a positive c-myc signal arising from the indirect induction of HAcmyc from VSV-G at a pH significantly higher than the transition pH. CHO cells were co-expressed with both VSV-G (which activate at 6.1) and HAcmyc (which should not activate until 5.4) plasmids and selected. The cells were induced at high pH (7.0), intermediate pH (5.8), and a low pH (5.2). After the induction step the cells where immunofluorescently stained and analyzed via flow cytometry. The flow cytometry data shows that at all pH inductions and even with no induction step we always had a positive c-myc signal (Figure 4.4). The induction at pH 5.2 has a lower mean fluorescence due to the loss of the second peak which are cells that have a higher expression level of HA (Figure 4.4). The second peak is believed to be lost due to the low pH being more stressful on the cells lysing some during the induction and subsequent spin cycles. There was no sample of cells that resembled our negative controls (non-transfected CHO cells). The VSV-G protein differs from HA due to the viral fusion protein conformational change to catalyze fusion is reversible (Kim et al., 2017; Stanifer et al., 2011; Albertini et al., 2012; Roche et al., 2002). The pH shifts the equilibrium of the proteins on the cell surface being either in its active or pre-active state. With some VSV-G proteins always

switching from one state to the other we believe that this is the cause for the HA on the surface of the cell to also go through its conformational change.

Fusion Protein Crosstalk: gp-160 and H7 HA.

In order to further test if the autocatalysis applies to other viral fusion proteins we tested gp-160 of human immunodeficiency virus type 1 (HIV-1). This viral fusion protein shares similarities to HA including being synthesized as a single polypeptide, gp-160, which is proteolytically cleaved into a mature gp-120/gp-41 complex (Checkley et al., 2012; Krell et al., 2004; Blumenthal et al., 2012). The complex exists on the surface of the virus as a heterotrimer with gp-120 being the receptor binding domain and gp-41 being the transmembrane fusion active domain carrying the fusion peptide region (Checkley et al., 2012; Krell et al., 2004; Blumenthal et al., 2012). The receptor binding domain, gp-120, goes through an irreversible conformational change induced by the binding of CD4. The conformational change of the receptor binding domain leads to the gp-120/gp-41 complex coming apart as gp-120 is shed from the surface and gp-41, the fusion active domain, remaining tethered to the surface via its transmembrane domain (Moore et al., 1990). The shedding of gp-120 induced by receptor binding allows us to use mAb α-gp-120 (this reagent was obtained through the NIH AIDS Reagent Program, Division of AIDS, NIAID, NIH: Anti-HIV-1 gp120 Monoclonal (F105) from Dr. Marshall Posner and Dr. Lisa Cavacini) in immunostaining to monitor for the conformational refolding reagent. (Posner et al., 1993). CHO cells were transfected with gp-160 plasmid and selected using geneticin, like in previous experiments. The cells were then induced by a CD4 (obtained through the NIH AIDS Reagent Program, Division of AIDS, NIAID, NIH: Human Soluble CD4 Recombinant Protein (sCD4) from

Progenics) incubation for 2 h at 37˚C. A titration of CD4 concentrations, ranging from 0 – 1000 µM, was used to determine the amount of CD4 required to cause the refolding and shedding of gp-120. After the CD4 incubation the cells were extensively washed to remove any gp-120 left in solution. The cells were then labeled with α-gp-120 and appropriate secondary anti-body before being analyzed via flow cytometry. Flow cytometry data indicates that 100 and 1000 µM CD4 generates the largest response of gp-120 shedding (Figure 4.5). The decrease in α-gp-120 binding indicates that gp-160 has refolded. The response to refolding is not bimodal like the conformational change seen in HA. A mock incubation with buffer containing no CD4 was is shown as our maximum fluorescence. Concentrations 100 and 1000 µM CD4 overlap and a maximum shedding of CD4 response was observed.

CHO cells transfected with gp-160 plasmid were used to test the stability of the protein at a pH that would induce HA. Cells were induced at pH 5.0 for 5 min at room temperature then stained with both α-gp-120 and α-c-myc. The fusion protein of HIV, gp-160, is stable at low pH's and shows no evidence of gp-120 shedding linked to the conformational change at pH 5.0 which would activate HA (Figure 4.6D). Cells that were incubated in a mock induction with 0 µM CD4 in serum free medium (Figure 4.6A) show a similar stain to cells incubated at pH 5.0 (Figure 4.6D). This indicates that low pH does not cause the conformational change seen when incubated with soluble CD4. Shedding of the receptor domain is seen only when incubating the cells with soluble CD4 at 10 µM and 100 µM (Figure 4.6B & 4.6C). Cells incubated with 100 µM CD4 showed the maximum amount of CD4 shedding with 24.3% of the cells analyzed still positive for mAb α-gp-120. None of the cells expressing only gp-160 had any significant α-c-myc stain (Figure 4.6).

Co-expressing the HA reporter protein, HAcmyc, with gp-160 allows us to test modular systems by inducing with either low pH or with CD4 incubation. With anti-bodies, α-gp-120 and α-c-myc, that are conformational specific for the two fusion proteins the modular systems expressing both gp-160 and HAcmyc were tested for crosstalk. CHO cells were co-transfected with the two fusion proteins and selected using geneticin. The plasmid containing gp-160 has the same promotor and geneticin resistance as the pLNCX2 plasmid used with all of our HA transfections. The cells expressing the modular system were then induced with either 0 μM (Figure 4.7A) or 100 μM (Figure 4.7B) CD4 at 37˚C for 2 h or a room temperature 5 min incubation at indicated pH. The range of pH's tested, pH 5.4 – 5.0 (Figure 4.7 C-D), correspond to the transition range of HA. The expression levels of both HAcmyc and gp-160 were not as high as we normally see following selection. Both proteins appear to have an expression level ~ 65% when probing with mAb gp-120 and HC2. The modular system, similar to cells expressing only gp-160, shows shedding of the receptor domain gp-120 after incubation with CD4 which indicates a refolding of the HIV fusion protein. This refolding does not show any significant c-myc stain meaning that the HA on the surface of the cell is still in its inactive state. The refolding of gp-160 does not cause any change in the conformational state of HA. However, when induced by low pH the activated HAcmyc does show the ability to cause gp-120 shedding seen by the decrease in α-gp-120 stain (Figure 4.7 C-D). In the transition pH's, 5.4 and 5.2, the cells become positive for α-c-myc stain and negative for α-gp-120 stain (Figure 4.7 C & D). At 5.0 pH, which was seen in Figure 4.6 not to reduce gp-120 staining, all of the cells are negative for gp-120 probe. This indicates that HA activation is sufficient enough to crosstalk, presumably through the membrane, and cause refolding of gp-160 seen by the decrease in gp-120 stain.

Discussion

The crosstalk of different subtypes of HA and between different enveloped viral fusion proteins was tested in this chapter. Taking advantage of the communication between H7 HA mutants, we examined the ability to activate other viral fusion proteins (VSV-G and gp-160) and other subtypes of HA via the same pathway. Activating fusion proteins from other enveloped viruses would suggest that these proteins can communicate through modulations of the local membrane properties. The need to better understand autocatalysis would facilitate our modular systems that can benefit more efficient therapy and delivery to target cells.

We first tested the ability to communicate through autocatalysis with other subtypes of HA. Human influenza virus (A/Aichi/68/X31) HA was first exposed to a pH titration pulse to determine the pH of transition. The transition pH was demonstrated to be at pH 5.2, which is 0.2 pH units lower than the H7 FPV-HA. The transition of activation has the same bimodal response as the FPV-HA. Flow cytometry data showed that no cell exists in a state in which only a fraction of its HA trimers have undergone the irreversible conformational change. Indicating that H7 and H3 subtypes share the autocatalytic response where the cell reaches a critical point and all HA trimers on the cell are committed to refolding.

Sharing a common bimodal response to activation allowed us to test modular systems where different subtypes of HA could be co-expressed similar to the systems shown in Chapter 2. In this chapter we continued with the H7 sensing mutant, HA4xCys, triggered by ligand binding to induce the conformational change co-expressed with a signal HA H3 X31-HAcmyc. The bimodal response of X31-HA leads us to expect the modular system to work if the communication

results solely from modulation of local membrane properties. Similar to previous modular systems the different subtype system also gave a positive signal which indicates a shared autocatalytic mechanism for activation.

The fusion protein of vesicular stomatitis virus (VSV-G) goes through a conformational refolding induced by pH 6.1 but unlike all other enveloped viral fusion proteins it is reversible (Kim et al., 2016; Libersou et al., 2010; Roche et al., 2008). The higher pH of activation was tested in our modular system with the VSV-G acting as the sensing protein that would then communicate with HAcmyc (reporter trimer). All of our pH pulses, ranging from 7.2 – 5.2, indicated that the HAcmyc had refolded even in the absence of any pulse. Negative controls, CHO cells transfected with only HAcmyc, showed no refolding. The equilibrium of the state of VSV-G is shifted depending on the pH. At high pH's there are still some G protein that might be undergoing the refolding. The reversibility of VSV-G suggests that the refolding of these proteins is enough to cause the HA to refold via modulations in the membrane. There is a possibility that the refolding caused by co-expression of these two proteins might arise from protein-protein interactions. At this point we only have the membrane being a common link as to one possible reason for crosstalk.

We continued to test other viral fusion proteins that are not reversible and share a similar conformational change to HA. The fusion protein of HIV (gp-160) is proteolytically processed to generate two subunits, gp-120 (receptor binding) and gp-41 (contains N-terminal fusion peptide), which then are induced into a conformational change to catalyze fusion via CD4 binding (Falcigno et al., 2004; Welman et al., 2007; Eckert and Kim, 2001). We assessed that gp-120/gp-41 complex does not demonstrate autocatalytic activation when induced by purified soluble CD4 via conformational sensitive antibodies. Co-expression of gp-160 and HA was used to determine the

ability to trigger gp-160 activation by pH pulse and HA activation by CD4 binding. This indicates that different membrane fusion proteins can communicate during activation through modulation of local membrane properties. Modular systems expressing both gp-120 and HA show the ability to crosstalk only when using the pH induction. CD4 induction did not show any crosstalk and this might be due to the gp-160 not causing enough of a disturbance in the cell membrane. Complete viral fusion protein rearrangement of gp-120/gp-41 complex has been linked to a co-receptor that might be needed in this case. The CD4 binding might only cause shedding of gp-120 but the complete extended trimer discussed in the background section could require another binding event. Future experiments of expression levels might help conclude if enough gp-160 is going through the conformational change to elicit a change in HA. The crosstalk between the two fusion proteins, observed only after low pH induction, might be due to HA causing a more substantial disruption in the lipid membrane. Expression levels for of both proteins when co-expressed were ~ 65% even after selection. This suggests that there might be a density dependence for complete activation.

These studies elucidate similarities of fusion mechanisms among different classes of fusion proteins and subtypes of influenza HA. The triggering caused by communication of different viral fusion proteins suggests a common mechanism mediated through the membrane.

Appendix

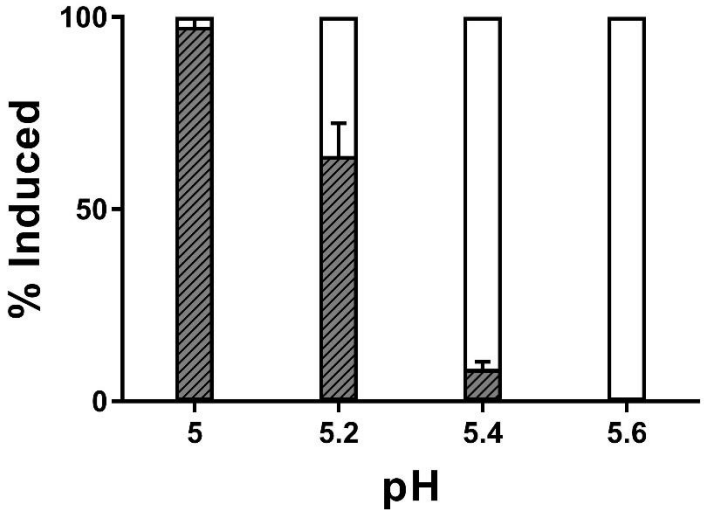

Figure 4.1. pH induction of X31 HA. CHO cells expressing X31-HAcmyc were induced at indicated pH. The cells were stained with mAb 9E10 which is specific for the activated state. The fraction induced are the number of cells that are positive for c-myc (active HA) divided by number of cells expressing HA. An average of 3 independent experiments with the standard deviation as error bars is shown.

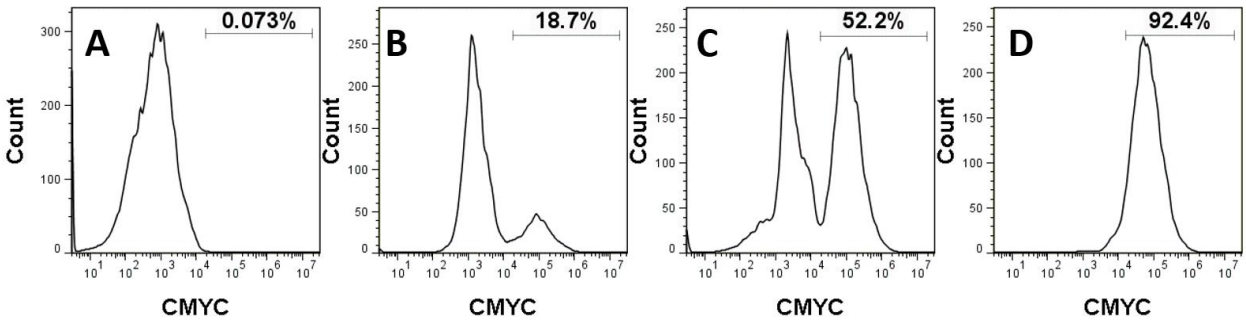

Figure 4.2. Bi-modal activation of X31 HA. CHO cells expressing X31-HAcmyc were induced at pH 5.6 (A), pH 5.4 (B), pH 5.2 (C), and pH 5.0 (D). The cells were stained with mAb 9E10 which is specific for the activated state. The fraction induced were cells that observed a higher c-myc stain than the negative control as described in the chapter. The gate shows the fraction that is in the refolded active state. The activation of X31 HA is bimodal, which is covered in the results section, similar to that of FPV HA.

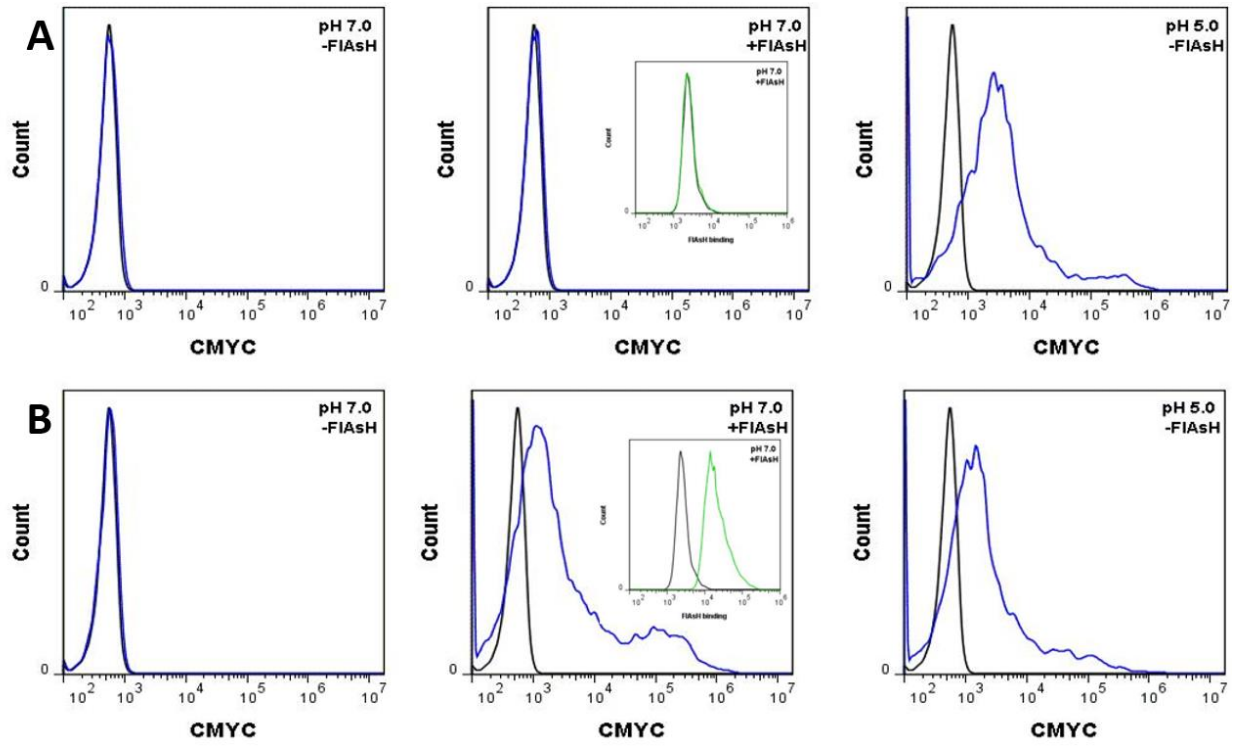

Figure 4.3. H3 and H7 HA crosstalk. CHO cells expressing X31-HAcmyc (row A) and co-expressing X31-HAcmyc and HA4xCys were induced as indicated in the top right corner of each graph. Column 1 induced at pH 7.0 with no FlAsH, column 2 induced at pH 7.0 with FlAsH buffer, and column 3 induced at pH 5.0 with no FlAsH. The cells were stained with mAb 9E10 (blue curve) which is specific for the activated state of the X31-HAcmyc. Non-transfected CHO cells (black curve) were also subject to the same treatment and used as negative controls. Insert in column 2 shows the FlAsH binding (green).

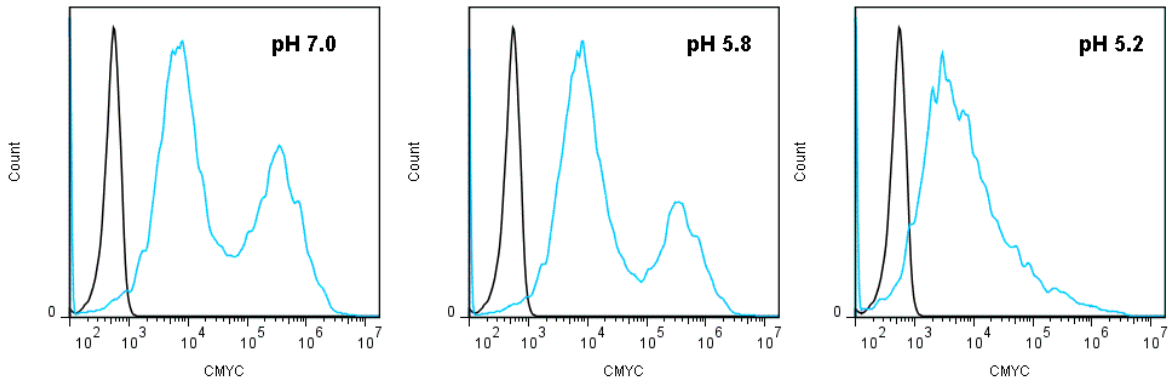

Figure 4.4. HA and VSV-G crosstalk. CHO cells were co-transfected with HAcmyc (reporter trimer) and VSV-G (sensing trimer) plasmids. After selection cells were induced as indicated in the top right corner of each graph (pH 7.0, pH 5.8, or pH 5.2). The equilibrium of the reversible conformational change of VSV-G protein shifts to the active state below pH 6.1. The cells were stained with mAb 9E10 (blue curve) which is specific for the active state of the HAcmyc. Non-transfected CHO cells (black curve) were used as negative control.

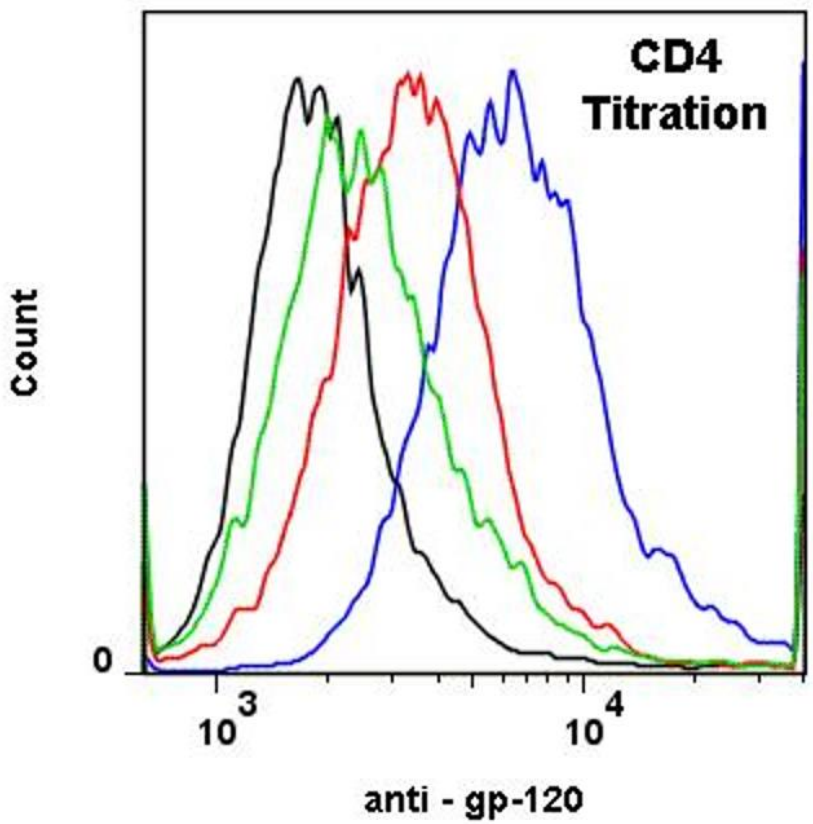

Figure 4.5. CD-4 induction of gp-160. CHO cells were transfected with gp-160 plasmid and selected with geneticin. The cells were incubated for 2 h at 37˚C with 0 µM CD4 (blue), 10 µM CD4 (red), 100 µM CD4 (green), and 1000 µM CD4 (not shown because it overlaps with 100 µM). Non-transfected CHO cells (black) were used as negative control. After CD4 incubation the cells were stain with anti-gp-120. The reduced stain of gp-120 correlates with the conformational change of gp-120/gp-41 complex due to CD4 binding.

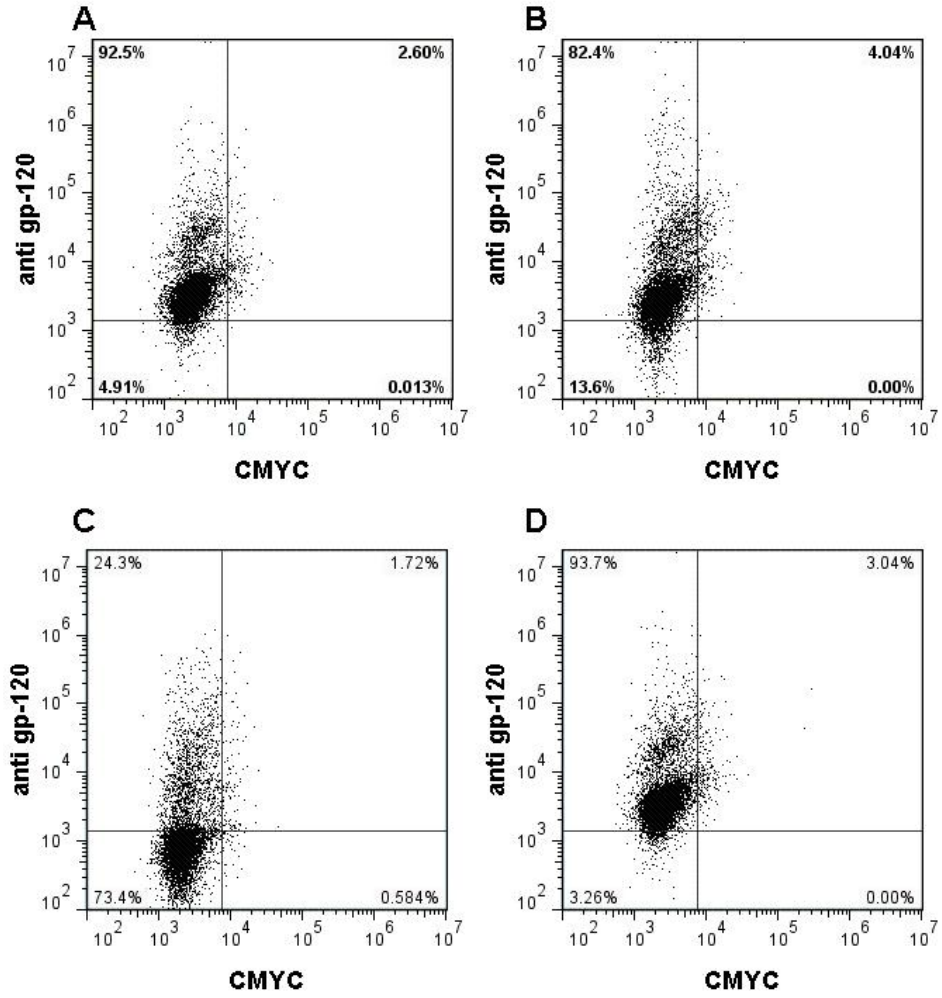

Figure 4.6. Dual stain of gp-160. CHO cells were transfected with gp-160 plasmid and selected with geneticin. The cells were incubated for 2 h at 37˚C with 0 μM CD4 (A), 10 μM CD4 (B), 100 μM CD4 (C), or 5 min room temperature at pH 5.0 (D). Non-transfected CHO cells were used as negative control to set the gates. After incubation the cells were stain with α-gp-120 and α-c-myc. The reduced stain of gp-120 correlates with the conformational change of gp-120/gp-41 complex due to CD4 binding and shedding gp-120 domain. In all sample no significant population was positive for c-myc stain.

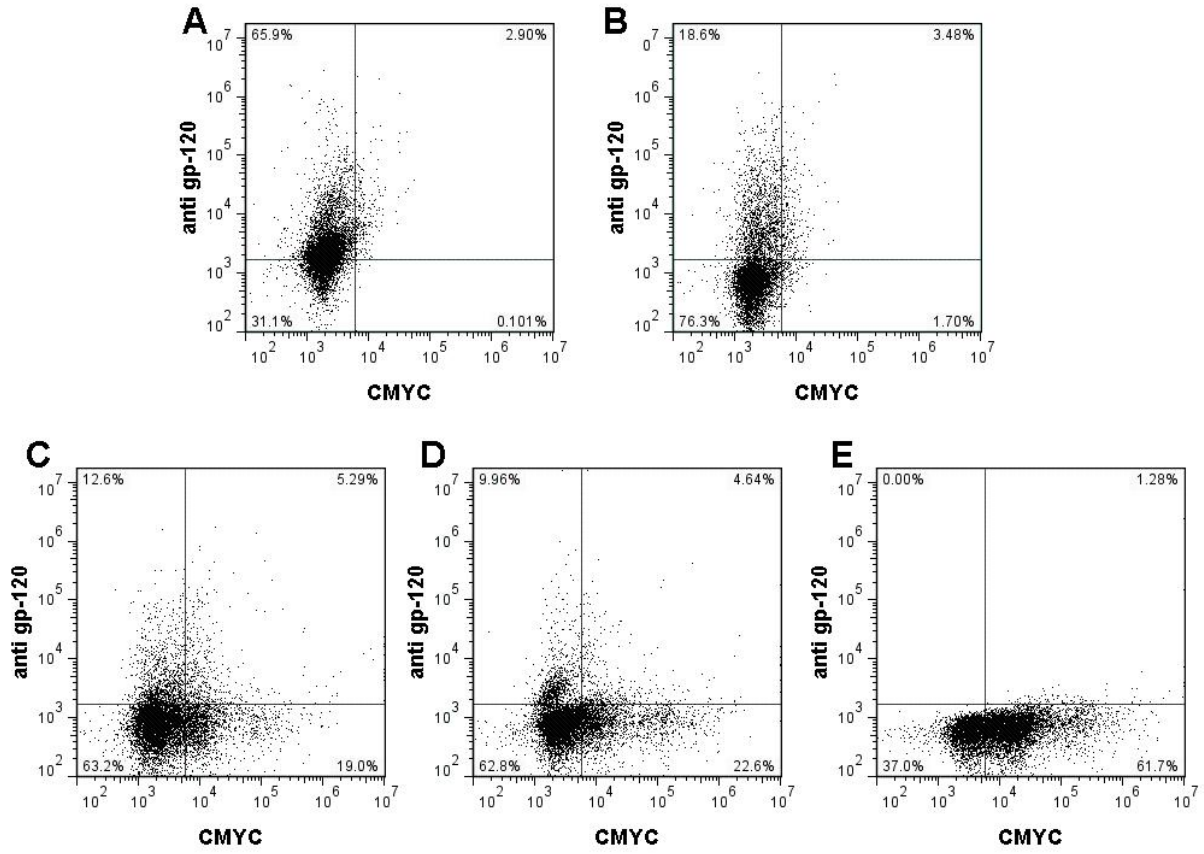

Figure 4.7. HA and gp-160 crosstalk. CHO cells were co-transfected with both gp-160 and HAcmyc plasmid and selected with geneticin. The cells were incubated for 2 h at 37˚C with 0 µM CD4 (A), 100 µM CD4 (B) or 5 min room temperature at pH 5.4 (C), pH 5.2 (D), and pH 5.0 (E). Non-transfected CHO cells were used as negative control to set the gates. After the induction incubations the cells were stain with α-gp-120 and α-c-myc. The reduced stain of gp-120 correlates with the conformational change of gp-120/gp-41 complex due to CD4 binding and shedding gp-120 domain. The populations positive for c-myc stain indicate HA that has gone through the refolding to its active state.

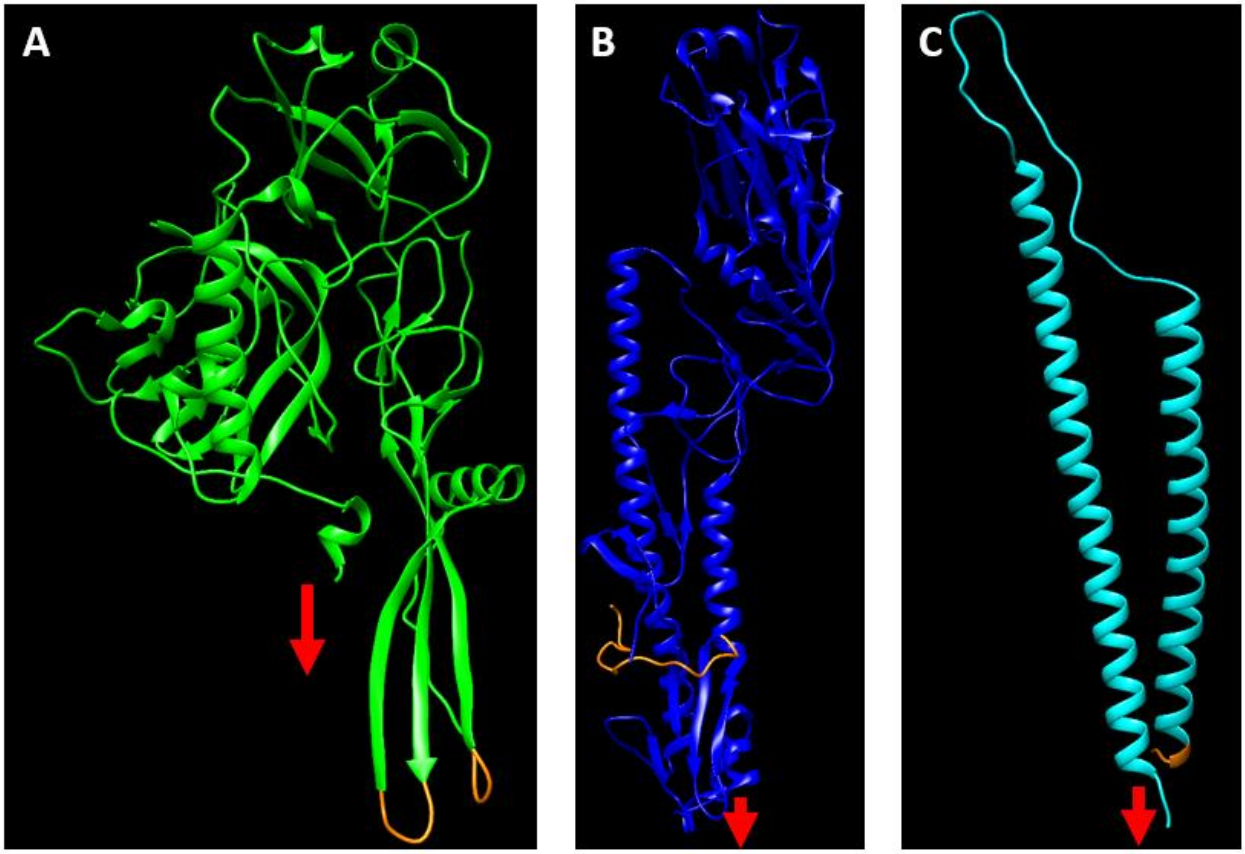

Figure 4.8. Structural comparison of viral fusion proteins. All images were generated using UCSF Chimera and structures downloaded from PDB. Orange section indicates the fusion peptide/loop section and red arrows indicate the direction of the transmembrane region embedded into viral membrane. (A) VSV-G (PDB 2J6J) has a .32% sequence identity with the HA1 subunit of HA shown in (B). (C) Fusion domain, gp41, of gp160 has a 18.92% sequence identity with the fusion domain of HA shown in (B).

CHAPTER 5
HA LANDSCAPE

Abstract

To engineer the HA protein for novel properties it is essential to understand the structure-function relationship. Directed evolution allows us to create large libraries of HA mutants with altered phenotypes due to sequence mutations. Mutations are introduced by random genetic mutagenesis. These large libraries also allow us to gather information on the sequence-function relationship which is often hard to predict. Using the reporter HA, HAcmyc, we can screen for mutants with desired phenotypes, such mutant that are positive for expression and the ability to undergo the conformational change after a pH pulse. Directed evolution was used in the lab previously to study key residues that control pH activation. We used random mutagenesis and screening combined with next generation sequencing (NGS; Mi-Seq Ilumina high-throughput sequencing) to comprehensively assess amino acid sites that can tolerate mutations without compromising correct folding or the ability to be activated (Figure 5.1). This allowed us to map out potential sites for mutagenesis of desired phenotypes. Landscapes of potential mutation sites for several antibodies or antibody fragments have been produced as well as other proteins (Traxlmayr et. al., 2012; Doolan et. al., 2015; Roscoe et. al., 2013; Wrenbeck et al., 2017; Rosenfeld et al., 2016; Whitehead et al., 2012), enabling efficient design of combinatorial libraries for engineering new protein functions.

Methods and Materials

Cell Culture.

CHO-K1 cells (ATCC CCL-61) were cultured in Dulbecco's Modified Eagles Medium: Kaighn's Modification of Ham's F-12 (DMEM:F-12K). Medium was supplemented with 10% fetal bovine serum (FBS) (Hyclone, Logan, UT), 100 µg/ml penicillin and 100 µg/ml streptomycin (Life Technologies, Grand Island, NY) to generate full growth medium. CHO-K1 cells were cultured at 37 ˚C and 5% CO_2.

Plasmids and Transfections.

The retroviral expression vector pLNCX2 (Clontech, Mountain View, CA) was used with the fowl plague virus (A/FPV/Rostock/34) HA gene (Lin et al. 2001) ligated in-between a XhoI and NotI site. Overlap extension PCR was used to replace the second half of the fusion peptide region, residues 11-20, with a c-myc epitope tag (EQKLISEEDL), herein referred to as HAcmyc. This allowed for specific staining with anti-c-myc antibody for the activated conformation. All DNA manipulations were performed in E. Coli DH5α and cultured in Luria broth and supplemented with ampicillin at 50 µg/mL unless otherwise stated. Transfection using Lipofectamine 2000 reagent (Invitrogen, Carlsbad, CA) of CHO-K1 cells were used in all experiments to surface display HA libraries following the manufacturer's recommended procedure. Transfected CHO cells were cultured in selective full growth medium, 0.85 mg/ml geneticin (Hyclone, Logan, UT), 16 h post-transfection and selected for 48 h before any assay.

After first 48 h selection 0.25 mg/ml geneticin was used to grow cells and maintains ~100% expression for 1 week.

DNA Library Construction and Expression.

A library was generated using random error-prone PCR using nucleoside analogs dPTP and 8-oxo-dGTP to induce single point mutants (Zaccolo et al., 1993; Zaccolo et al., 1993). The error-prone PCR was ran for 10 cycles with the analogs at 2 µM concentration in order to create a library with single point mutations (Colby et al., 2004). PCR products were ran on an agarose gel then purified via electro-elution, digested with XhoI and NotI, and ligated into retroviral expression vector pLNCX2 (Clontech). Library size was determined by serial dilution plating onto ampicillin agar plates. CHO cells were transfected with the library and selected with geneticin as described above.

Analysis of pH-induced Libraries and Recovery of Plasmids.

After selection of CHO cells transfected with library cells were subjected to a pH activation step. Adherent cells were detached using 0.05% trypsin-EDTA (Hyclone) and aliquoted into Eppendorf tubes and placed on ice. Cells were washed twice with PBSA and pelleted in between washes at 800xg. Citrate buffer at pH 5.0 was then used to activate CHO cells expressing the library of mutants for 5 min at room temperature. After activation step cells were immunofluorescently stained with monoclonal antibody (mAb) HC2 for expression and anti-c-myc for active state conformation. Cell sorting was done with FACS Aria II to isolate double

negative, single positive, and double positive populations as described in Figure 5.1. Quick-DNA universal kit (Zymo, Irvine, CA) was used on the sorted cells to recover the DNA plasmids.

Sequencing and Analysis of Mutations.

The recovered plasmids were PCR amplified with primers specific to the pLNCX2 vector and used for high-throughput sequencing. Ilumina Mi-Seq with NextEra XT DNA library preparation kit was used to evaluate the starting and sorted libraries. The St. Petersburg genome assembler (SPAdes) pipeline read error correction tool, BayesHammer, was used to remove potential errors and rare k-mers (Bankevich et al., 2012). Analysis of sequencing data was done on CLC genomics workbench.

Results

Library Creation and Expression.

Error-prone PCR was applied to generate the library of mutants. The HAcmyc plasmid was mutated, which is used as a detection flag for activation, using nucleoside analogs dPTP and 8-oxo-dGTP and ligated back into the pLNCX2 retroviral plasmid (Clontech). Highly competent cells were transformed, grown, and maxi prepped to recover plasmids. The size of the library was calculated to be $> 10^6$ mutants via serial dilution plating onto ampicillin plates. CHO cells were transfected with the library and selected as described in the methods. The mutated HAcmyc library

allowed for the screening of both expression and activation simultaneously. A plasmid recovery kit (Zymo) was used to harvest plasmids from cells.

Screening for Expression and Activation.

After the selection of CHO cells transfected with the HAcmyc mutant library, the cells were incubated in a pH 5.2 pulse for 5 min. We have shown that wild type FPV HA shows activation at pH 5.2 for 5 min so this pulse should activate any HA mutants that retain the ability to be activated similar to the wild type. After the pulse cells were immunofluorescently double-stained with mAb HC2, which screens for expression, and mAb 9E10, which screens for the activated state. Flow cytometry data of the library shows distinct populations that are double negative for both antibodies, positive for only HC2, and double positive for both HC2 and 9E10 (Figure 5.2). Gates were drawn based on negative and positive controls. Non-transfected CHO cells, that did not go through any selection, were used as the negative control. CHO cells that were transfected with un-mutated HAcmyc plasmid was used as a positive control. This double stain allowed for us to sort the three separated populations. Immediately after the sort a plasmid recovery kit (Zymo) was used to harvest plasmids from the cells to keep a physical link between genotype and phenotype.

Isolation of Sorted Populations.

The plasmids were recovered from the three sorted cell populations: double negative, HC2 single positive, and double positive. These plasmids were used as the template for PCR amplification in the following sequencing steps. Due to the transient transfection there was a

possibility of a cell taken up more than one plasmid and expressing multiple mutant trimers or even a mixed trimer where the trimer is made up of different monomer mutants. If this were the case, then we can potentially get false positives in each population due to an average effect from multiple mutants rather than screen for individual mutants. To test our sorting efficiency, we PCR amplified using the harvested plasmids as our templates, digested, and ligated back into pLNCX2. These plasmids were then used to transfect and select CHO cells expressing the sorted library populations. The cells were treated and induced using the same protocol from before the sort. The three cell samples were induced with pH 5.2 for 5 min and double stained with mAb HC2 and mAb 9E10 and analyzed via flow cytometry. The flow cytometry data shows that each population has ≥ 82.6 % of the cells in the quadrant in which it was selected for using the same negative and positive controls to determine the gates (Figure 5.3). The double negative cells have 82.6 %, the single HC2 positive cells have 96.0 %, and the double positive cells have 84.0% of the cells within the quadrant that it was sorted for (Figure 5.3). Mutants that do not resemble what they were screened for, double negative cells having a 17.4% population in the single positive quadrant, may arise from cells that take up more than one mutant with different phenotypes.

Sequencing and Analysis.

The harvested plasmids from the sorted cells were then used as the template in a PCR amplification for the MiSeq sequencing using NextEra XT DNA library preparation kit. The three sorted libraries along with the original library were prepared according to the manufactures protocol and sequenced. The raw data from the sequencing results were first filtered through BayesHammer read error correction tool to remove potential errors. After the initial error filtering,

only high-quality reads with a Phred quality score ≥ 35 were kept corresponding to a probability of 3.0×10^{-4} of an incorrect base call. The stringent quality control was enforced in order to rule out sequencing errors which in the analysis could be considered mutations from the original library. After filtering each sample (single positive, double positive, and original library) produced $\geq 10^6$ high quality reads that were used for the analysis.

The sequencing analysis was done with CLC genomics workbench (Qiagen, Hilden, Germany). The reads from all four samples were treated in the same manner. The reads, which had an average length of 204 bp after the quality trim, were aligned to the reference HAcmyc sequence to create larger contigs. A minimum of half of the total read length had to match the reference sequence and a similarity fraction of 0.8 between the aligned region and reference was implemented. Non-specific reads, where a read aligns at more than one position with an equal score, were ignored in the final mapping. A low frequency variant caller was used to determine the amount of times a base call differed from the reference gene. The filtering out of low quality reads allows for more relaxed parameters in the variant calling algorithm. Only positions with a coverage ≥ 100 were considered. Coverage is the amount of reads that line up to the reference at that particular position. The reading frame of the HAcmyc sequence was used to determine the variants that caused mutations in the amino acid sequence. Variants that caused silent mutations, deletions, or frame shifts were filtered out.

The variant caller output the mutations at each position and at what frequency they appeared. The frequency of the original library was used to compare and determine the change in mutational rate seen after the selection for expression (HC2) and after the double selection for both expression and activation (HC2 and c-myc). The frequency of the mutation after the expression

selection ,f_{HC2}, was divided by the frequency of mutation of the original library, f_{Lib}, for each mutation and summed up for every position. A summation of all the frequency ratios was determined for each position to evaluate the change in mutational rate after the selection. The change in mutational rate for each amino acid position is shown in Figure 5.4 after the expression (HC2) selection. Change in mutation rates (f_{HC2} / f_{Lib}) that drop below 1 represent amino acid positions that did not tolerate mutations. Low mutation rate ration indicates that the frequency at which a mutation appears in the library is significantly larger than the frequency that it appears in the selected cells. After the expression selection we observed a few positions where the frequency ratio was below 0.25. This indicates that point mutants don't disrupt the expression of HA and were only observed in the first position, last position, and the presumed binding site of the HC2 antibody (Figure 5.4, indicated in red). A heat map of the mutational rate data was rendered onto the known sequence of H7 hemagglutinin (Protein Data Base ID: 1TI8) and positions within the loop region of HA1 head group shown in red can potentially be involved in mAb HCs binding (Figure 5.5). Positions G142, T144, S145, C147, R148, and R149 all have a change in mutational rate frequency ratio lower than .01 which strongly indicates that these residues have a role in HC2 binding (Figure 5.3). The actual binding site the antibody has not been defined but the point mutation, G144E, has been shown to disrupt the binding of HC2 (Sugrue et. al., 1990). The lack of mutations tolerated at the binding site of antibodies used in the selection work as an internal control.

The library was simultaneously screened for both expression and activation (using mAb HC2 and mAb c-myc) and analyzed in the same way. The frequencies of the mutation found in the original library were used to compare to the frequencies found after the double selection. The

frequency of the mutation after the double selection, f_{cmyc}, was divided by the frequency of mutation of the original library, f_{Lib}, for each mutation and summed up for every position. The change in mutational rate (f_{cmyc} / f_{Lib}) was again defined as the ratio of the sum of single mutations at every position and graphed against the amino acid position (Figure 5.6). The residues in the mAb HC2 binding site again were selected against and shown in red. The mAb c-myc epitope site, which we cloned into the positions 353 – 362, also had a change in mutation rate below .01 for every position indicating the lack of mutations tolerable at that residue. The average mutational change rate was significantly observed when comparing the two selections and could be seen in the heat map of the double selection rendering (Figure 5.7). The heat map indicates a more significant selection when compared to just the single HC2 selection due to the protein having more intolerable mutation residues. This data gives us sites that do not tolerate mutations when trying to keep both expression and the ability to activate. The majority of the mutation intolerable positions have residues which are titratable.

One region with low mutational tolerance is the second alpha helix in the coiled coil and the β-loop which previously has been shown by our lab to effect fusion capability and the stability of fusion activation. Residues E406, D409, E411, E416, E417, S429, and D445 are all found in the β-loop or the following larger α-helix and all have a change in mutational rate below .25 (Figure 5.7, residues shown in red). Further down that same α-helix we find another region of low mutational tolerance, which is the fusion peptide and the surrounding residues that are potentially in the fusion peptide pocket (Figure 5.8). Focusing on the fusion peptide region we observe mutational conserved residues (N17, L323, D451, D454, and N458) which all are within 5 Å of

one or multiple fusion peptide residues. Possible interactions with the fusion peptide might hinder the ability for the HA to undergo its conformational change.

Discussion

The phenotypic characteristics of the conformational change plays an important role in host infection. Studying the residues that contribute to the stability of HA allow for a better understanding of what mutations in nature can cause potential pandemics. Previous work of residues contributing to the stability of HA has focused on subtypes H3 and more recently H5 (Daniels et at., 1985; Steinhauer et al., 1996; Thoennes et al., 2008; Cross et al., 2001; Bryd-Leotis et al., 2015; Reed et al., 2010; Reed et al., 2009). We used error-prone PCR to introduce mutations in an unbiased way to the entire gene. Our assay to monitor conformational change isn't constrained by having to retain fusion so it allows us to explore mutations that wouldn't appear in fusion assays. The CHO cells were transfected with the library of mutants and induced at pH 5.2.

Expression selection identified positions G142, T144, S145, C147, R148, and R149 all have a change in mutational rate frequency ratio lower than .01 which strongly indicates that these residues have a role in HC2 binding (Figure 5.3). The actual binding site the antibody has not been defined but the point mutation, G144E, has been shown to disrupt the binding of HC2 (Sugrue et. al., 1990). Previous studies have shown the ability mapping binding interfaces using

directed evolution and deep sequencing (Whitehead et al., 2012; Fowler et al., 2010; Araya et al., 2011)

The double selection for expression as well as activation identified regions of interest that did not tolerate the mutations found in the original library. The positions that did not tolerate mutations also identified mutants that were more stable than the wild-type which would have been induced at that pH. The B-helix, β-loop, and fusion peptide pocket were identified as having residues that play a role in the stability of HA. The β-loop residues that did not tolerate mutations are Glu406, Asp409, Glu411, and Glu414. None of these residues have previously been identified as key contributors to the conformational change. In the B-helix we identify Glu416, Lys417, Ser429, Glu445, and Thr449 as being positions that did not tolerate mutations. Previous studies have identified residues in the B-helix of HA2 that stabilize HA. Mutation Ser429Pro in sub-type H7 has been identified by previous graduate students in the lab to stabilize HA which agrees with our sequencing data. Another position is in the B-helix that has been identified is Glu105 (numbering based on HA2 subunit of H5 subtype) which resembles the positioning of our Glu445. The mutation Glu105Lys has been found to stabilize HA which would agree with our results (Reed et al., 2009).

In the fusion pocket we identify the largest cluster of mutational intolerant positions. There has been literature that suggests the stability of HA is influenced by the residues in the fusion peptide and fusion peptide pocket (Cross et al., 2001; Ilushina et al., 2007; Thoennes et al., 2008; White et al., 2006). We identify Gly343, Gly346, and Gly350 in the fusion peptide as being positions that don't tolerate mutations. These Glycine residues have been identified as crucial residues contributing to the interaction with the target membrane (Li et al., 2005). Our

data indicates that Glycine residues stabilize the peptide in the fusion pocket. Mutations at these positions can potentially disrupt the spacing needed for the other residues in the pocket to create proper contact with the cavity. In the fusion peptide pocket, which is a cavity where the peptide forms extensive contacts in the pre-active state, we identify Asn17, Asp451, Asp454, Asn458, and Leu323 as residues that did not tolerate the mutations found in the original library. Position Asp112 (numbering based on HA2 subunit of H5 subtype) has been shown to destabilize HA when mutated to Lys and resembles our Asp454 position (Byrd-Leotis et al., 2015; Reed et al., 2010). This aspartic acid is highly conserved among all HA sub-types and has been shown to form several H-bonds with residues in the fusion peptide. The Asp to Lys mutation did not appear in our original mutation library. Another mutation that was been found to destabilize HA is Asn114Lys. This Asn114 resembles Asn458 that we identified in our sequencing data. The destabilization discrepancies might arise from sequence differences between H5 and H7 or from different assays used (refolding versus fusion) to determine the pH of transition.

Appendix

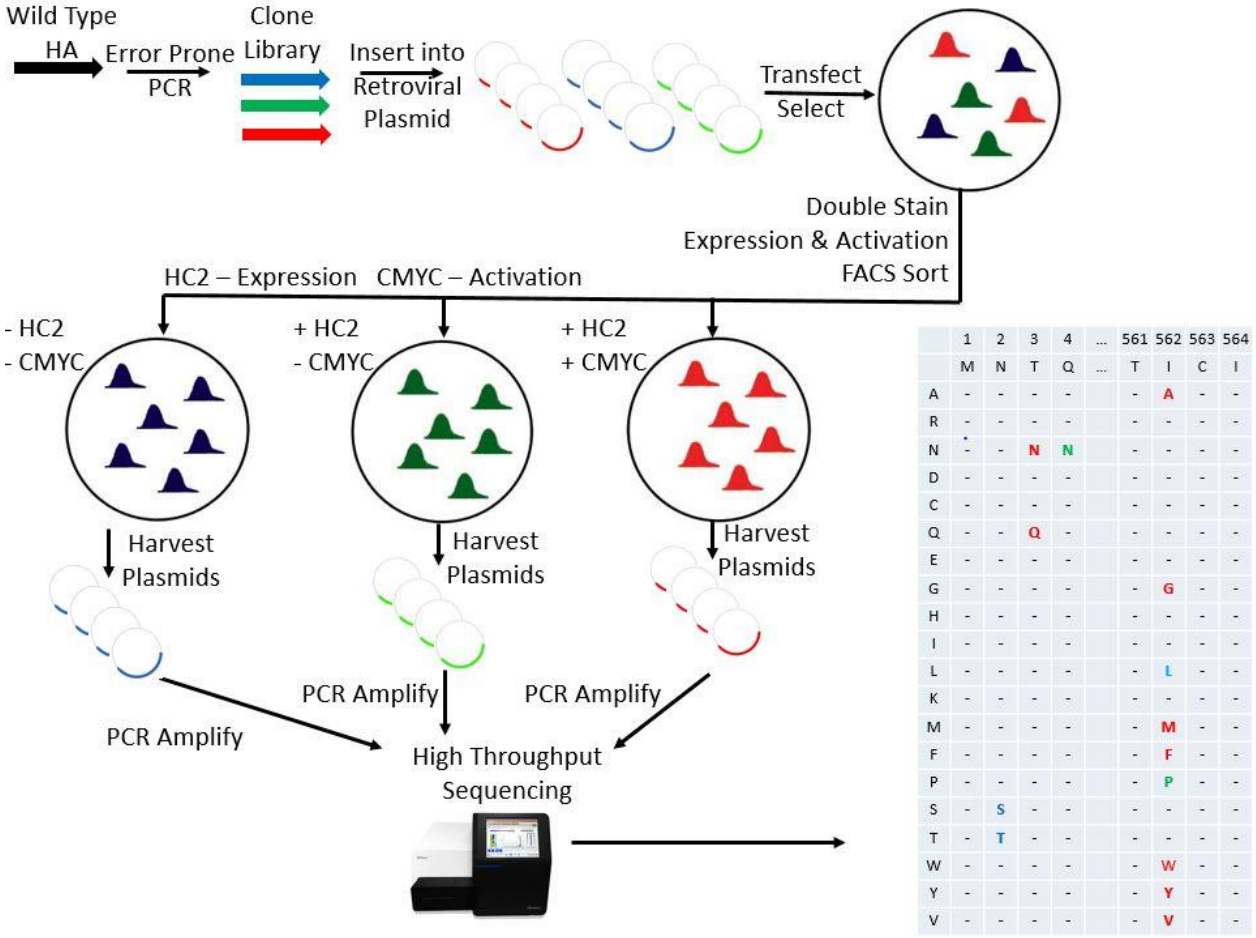

	1	2	3	4	...	561	562	563	564
	M	N	T	Q	...	T	I	C	I
A	-	-	-	-		-	A	-	-
R	-	-	-	-		-	-	-	-
N	-	-	N	N		-	-	-	-
D	-	-	-	-		-	-	-	-
C	-	-	-	-		-	-	-	-
Q	-	-	Q	-		-	-	-	-
E	-	-	-	-		-	-	-	-
G	-	-	-	-		-	G	-	-
H	-	-	-	-		-	-	-	-
I	-	-	-	-		-	-	-	-
L	-	-	-	-		-	L	-	-
K	-	-	-	-		-	-	-	-
M	-	-	-	-		-	M	-	-
F	-	-	-	-		-	F	-	-
P	-	-	-	-		-	P	-	-
S	-	S	-	-		-	-	-	-
T	-	T	-	-		-	-	-	-
W	-	-	-	-		-	W	-	-
Y	-	-	-	-		-	Y	-	-
V	-	-	-	-		-	V	-	-

Figure 5.1. Identification of mutation tolerant sites. A mutant clone library was generated and ligated into retroviral plasmids. After selection for transformants, cells were sorted into three groups by FACS based on expression and activation. Clones negative for both expression and activation (blue), clones positive for expression but not activation (red), and clones positive for both expression and activation (green). Plasmids from the three populations will be recovered and sequenced along with the presort library to identify all mutations at all HA positions.

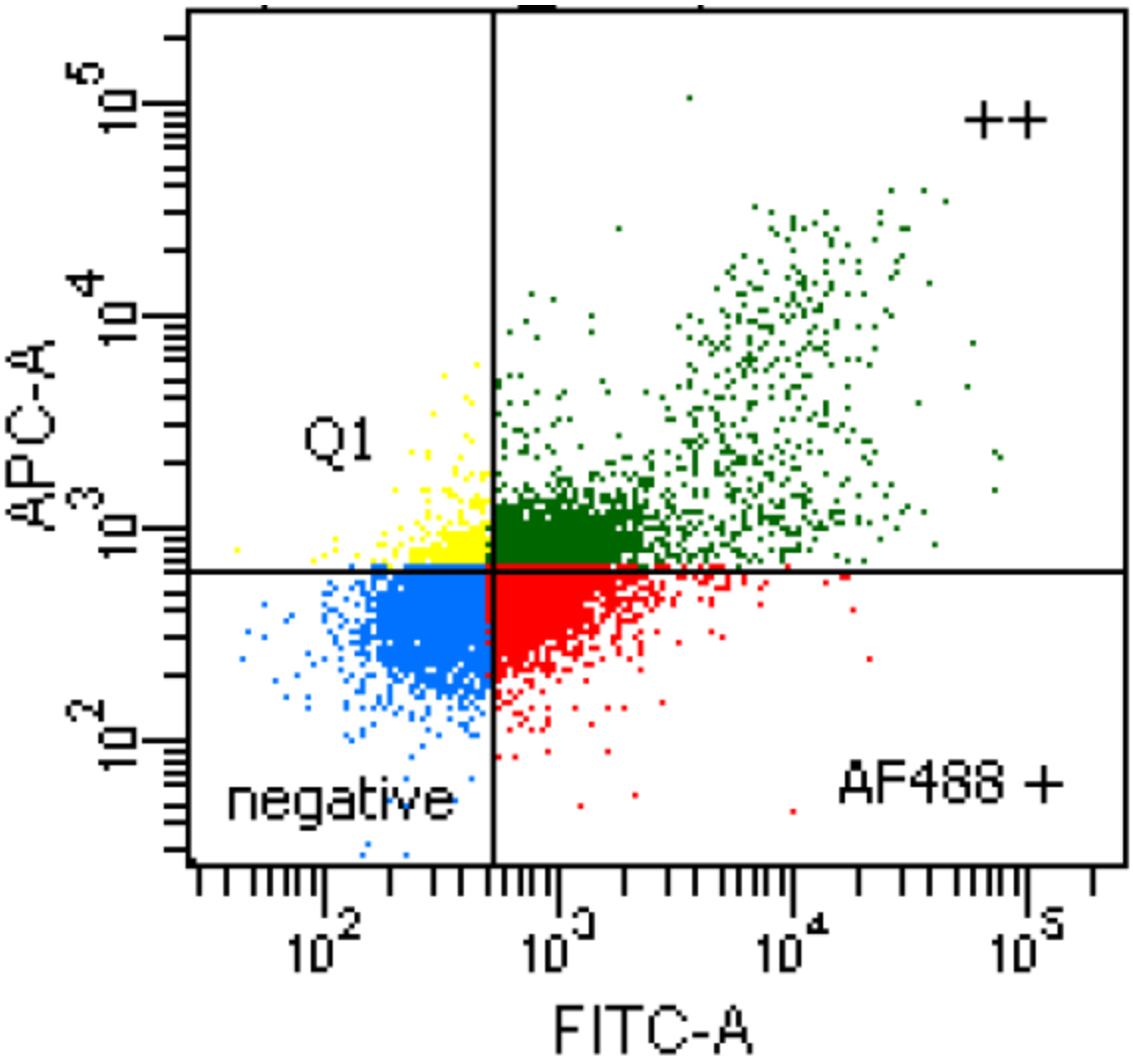

Figure 5.2. Pre-sort library. CHO cells were transfected with the mutant library and selected with geneticin. The cells were induced by pH 5.2 for 5 min and double stained with mAb HC2 and mAb 9E10 and analyzed via flow cytometry. Non-transfected CHO cells (negative) and CHO cells transfected with HAcmyc (positive) were used to determine the gates. The cells were sorted by quadrants: double negative (blue), single HC2 positive (red), and double positive (green).

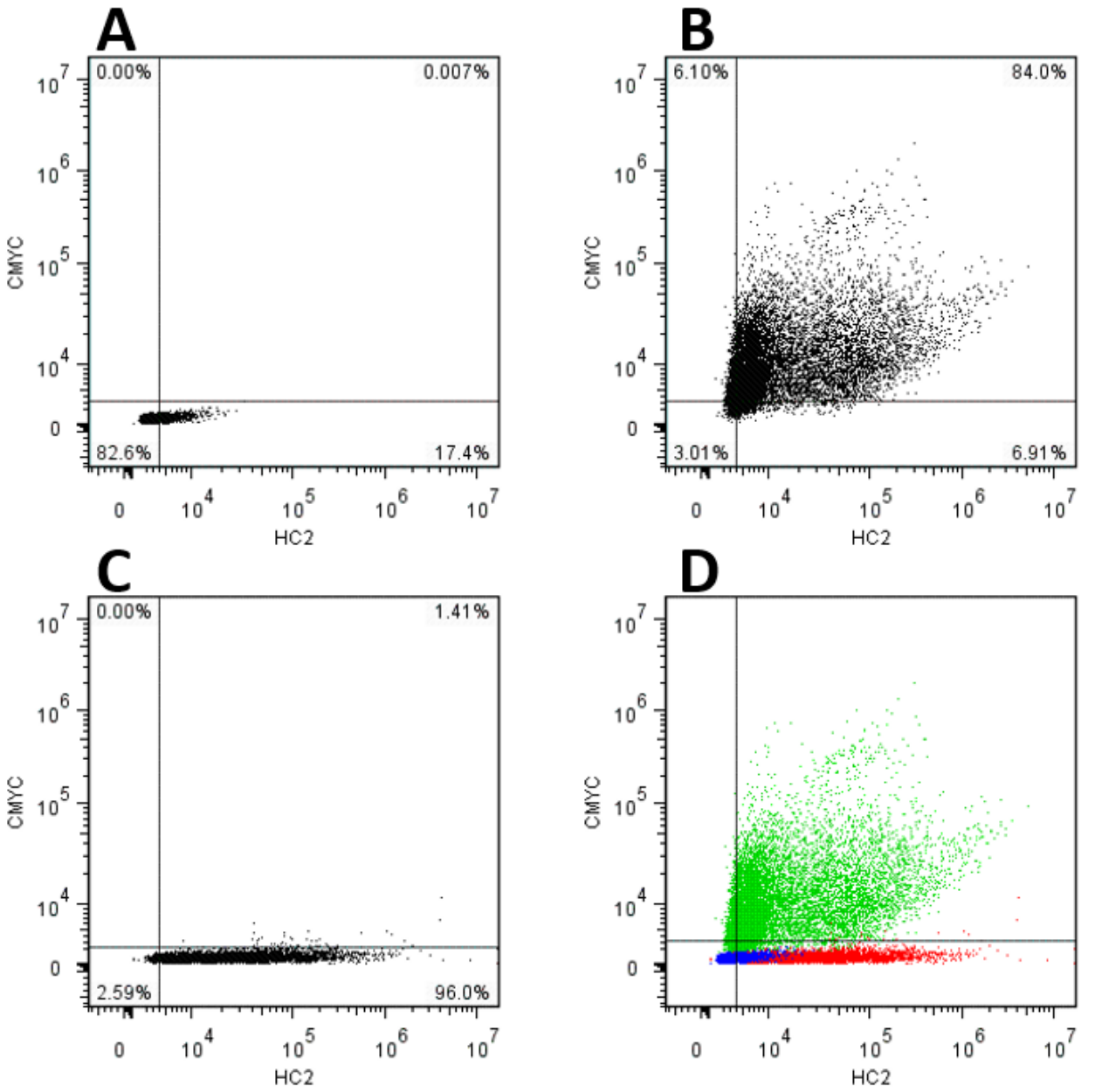

Figure 5.3. Post-sort isolated populations. CHO cells were transfected with plasmids recovered from the sorted cells. The cells were induced by pH 5.2 for 5 min and doubled stained with mAb HC2 and mAb 9E10 and analyzed via flow cytometry. Non-transfected CHO cells (negative) and CHO cells transfected with HAcmyc (positive) were used to determine the gates. Double negative stain (A-blue), double positive stain (B-green), single positive HC2 (C-red), and an overlay of the three populations (D) are shown.

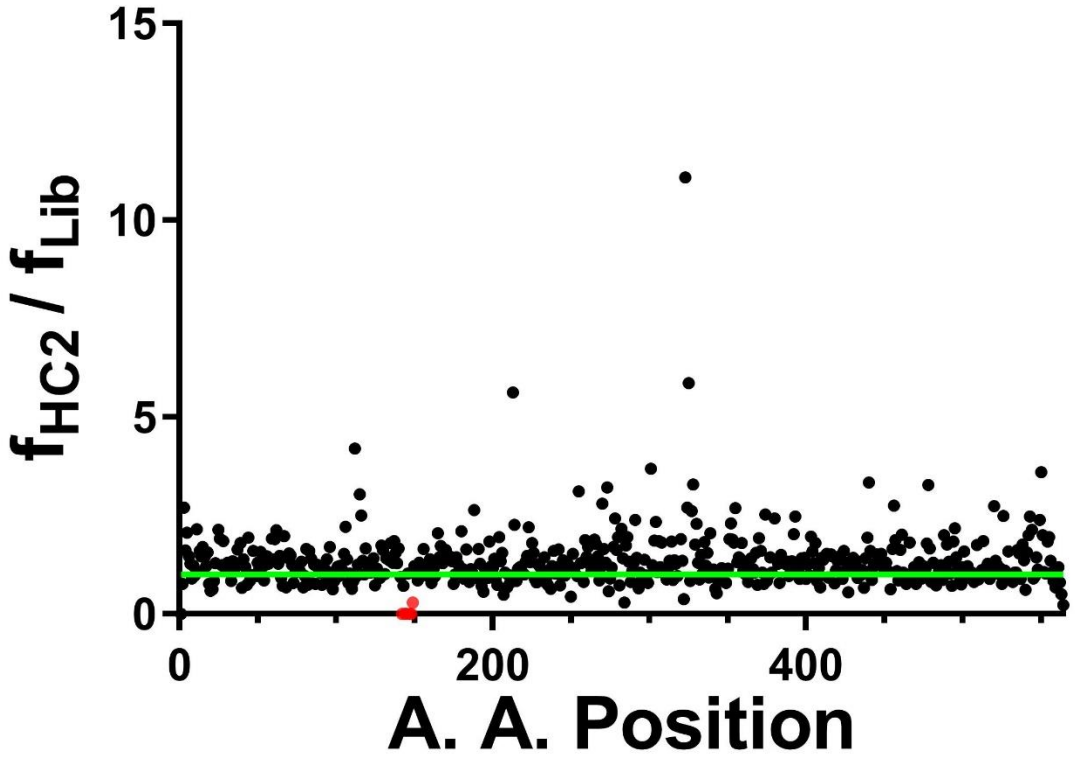

Figure 5.4. Change in mutation rate after HC2 selection. The change in mutational rate (described in the chapter) was plotted against the amino acid position for the sequencing data recovered from the expression selection (HC2). Positions that were highly intolerable to mutations are shown in red and are believed to be implicated in HC2 binding. The green line represents mutation rate change of 1.

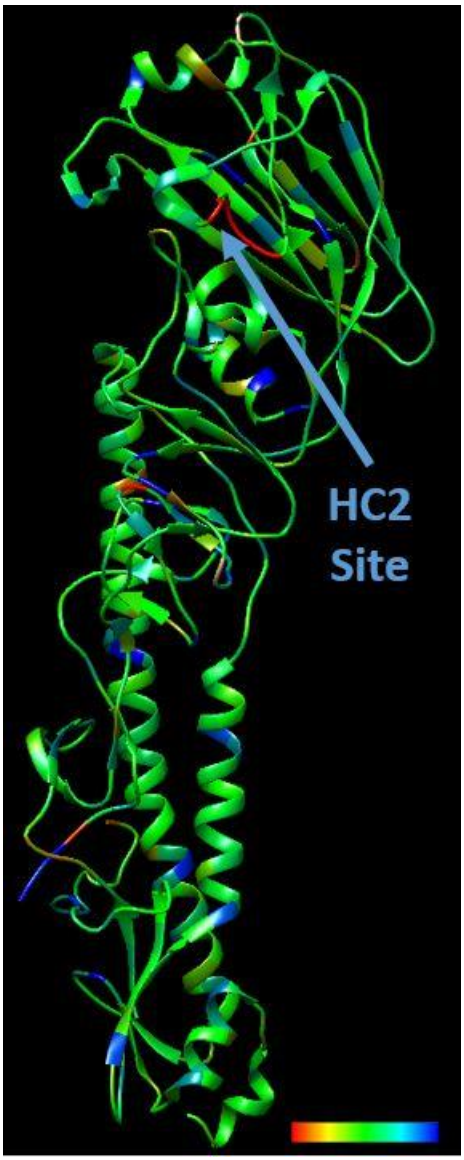

Figure 5.5. Heat map of mutation rate after HC2 selection. The mutational rate change attribute from the expression selection was rendered onto the H7 HA structure (1TI8) that was downloaded from the Protein Data Bank. The figure was prepared using Chimera. The potential residues implicated in binding HC2 are shown in red.

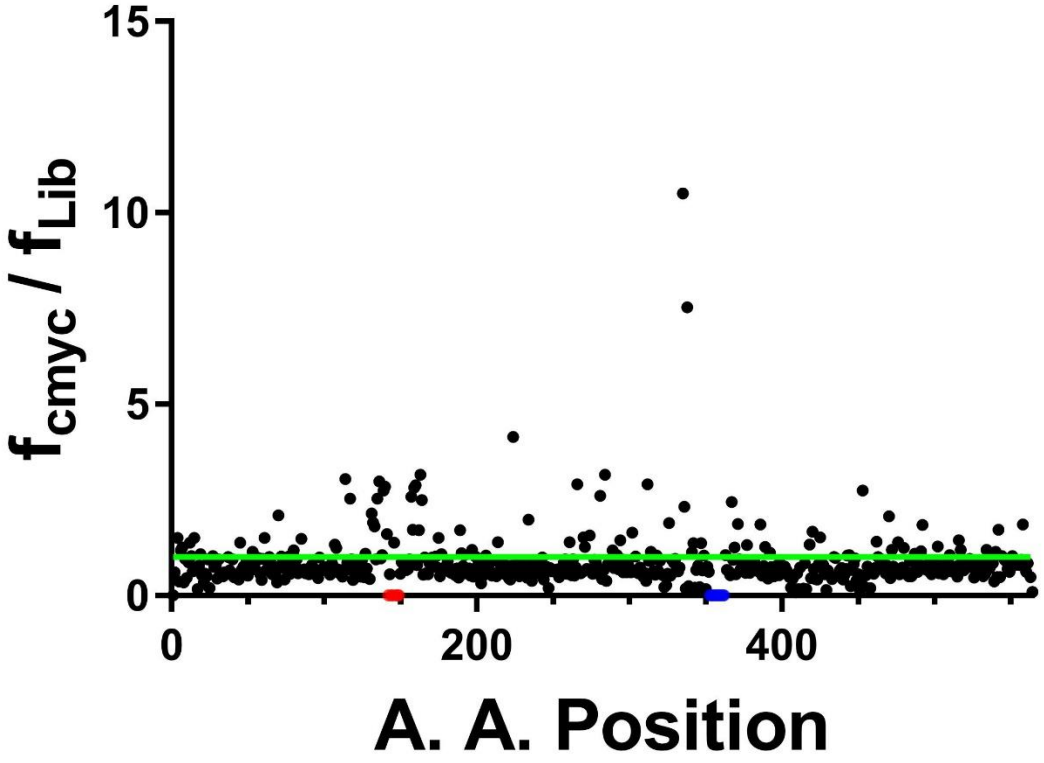

Figure 5.6. Change in mutation rate after double selection. The change in mutational rate (described in the chapter) was plotted against the amino acid position for the sequencing data recovered from the double selection (HC2 and c-myc). Positions that were highly intolerable to mutations are shown in red and blue and are believed to be implicated in HC2 and c-myc binding respectively. The green line represents mutation rate change of 1.

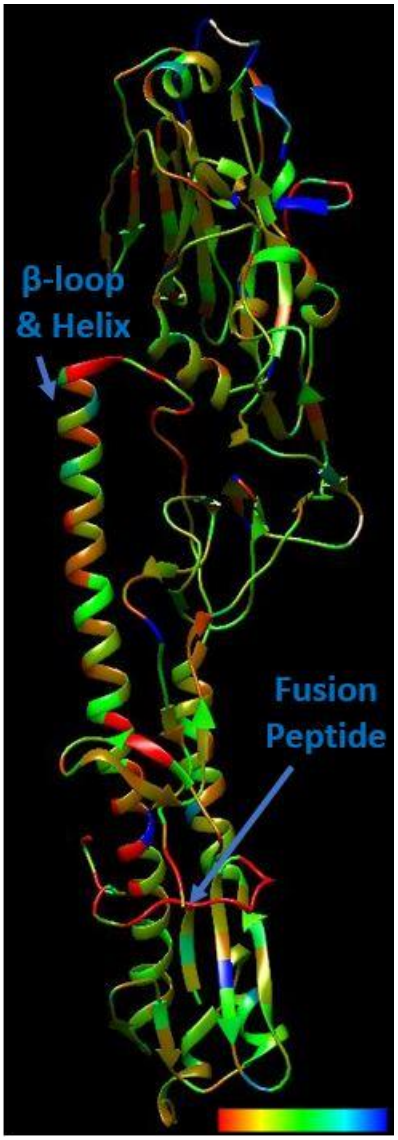

Figure 5.7. Heat map of mutation rate after double selection. The mutational rate change attribute from the double selection was rendered onto the H7 HA structure (1TI8) that was downloaded from the Protein Data Bank. The figure was prepared using Chimera.

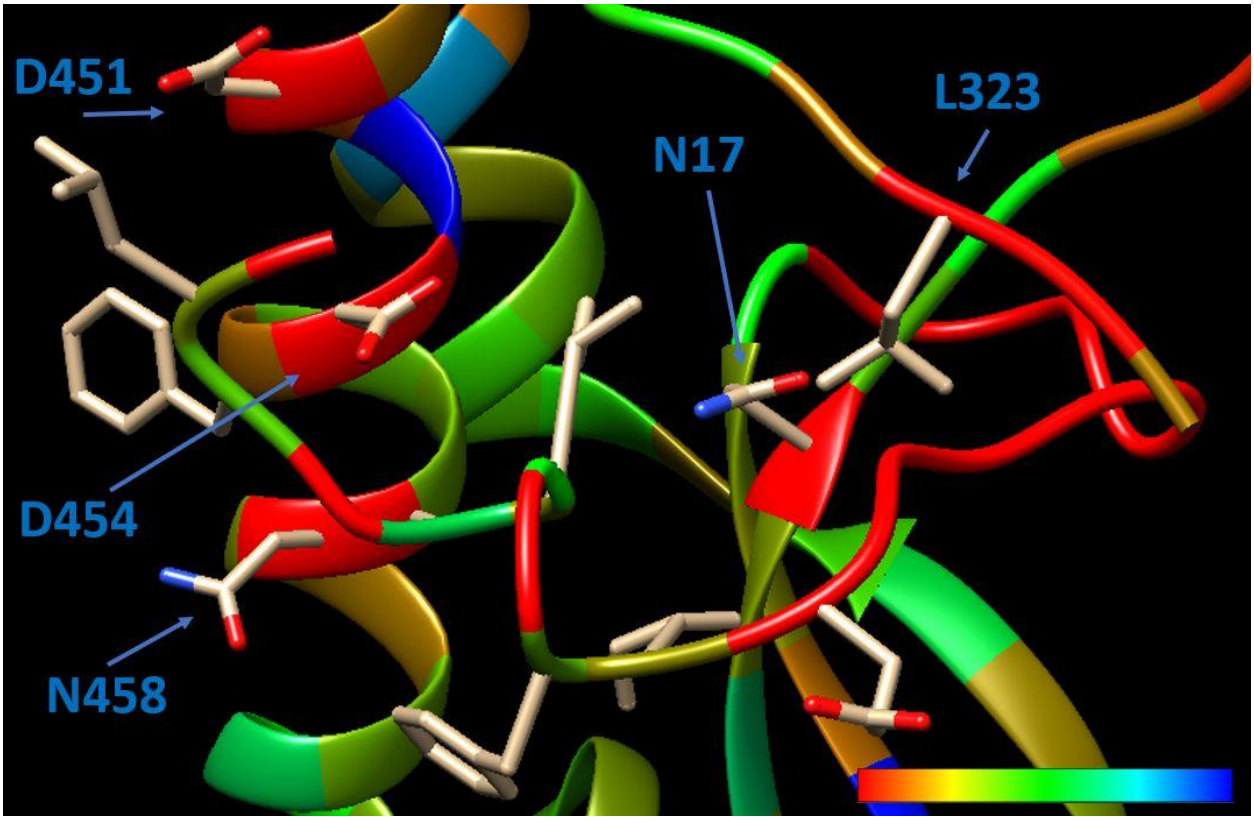

Figure 5.8. Heat map of mutation rate in fusion peptide vicinity. The mutational rate change attribute from the double selection was rendered onto the H7 HA structure (1TI8) that was downloaded from the Protein Data Bank. The figure was prepared using Chimera. This image shows the residues that did not tolerate mutations that are within 5 angstroms of the fusion peptide.

CHAPTER 6
SUMMARY AND RECOMMENDATIONS

Summary

The ability for viral fusion proteins to catalyze fusion with the target cell facilitates the delivery of the viral contents for infection. The ability for these proteins to undergo a conformational change in response to a stimulus allows them to drive fusion. Hemagglutinin (HA) refolds to an active state induced by a low pH. The refolding exposes a fusion peptide region that likely inserts into the target membrane leading to disruption of the lipid packing and eventually fusion. The need to understand the mechanism of refolding that leads to fusion would benefit future engineering of fusogenic machines responding to specific environments. An understanding of the mechanism of fusion, which has shared similarities among all enveloped viruses, could lead to potential therapies targeting novel contributors of the process.

The results indicate a novel alternative pathway of activation for influenza hemagglutinin through binding the fusion peptide region which we presume destabilizes it in the pre-activation pocket. Ligand induction of enveloped viral fusion proteins, such as HA, with small molecules that have high affinity for the fusion peptide region can benefit future therapies. Furthermore, trimers activated by ligand can activate non-ligand binding trimers through autocatalysis. Taken advantage of the autocatalysis found in the activation of HA we can create modular systems where sensing HA can refold due to a novel stimulus which would in turn trigger an HA with an actuating component. Controlling the conformational change which leads to fusion allows for future application varying from biosensing, molecular imaging, or drug delivery. Our modular systems activated by ligand showed not only the ability to refold non-ligand bind trimers but also drive fusion when the actuating trimer retains that phenotype.

The mechanism of autocatalysis was further characterized in Chapter 3. The kinetics of refolding as well as the role of the membrane environment were tested to better understand the phenomenon of autocatalysis. Previous work had proposed a model of autocatalysis that potentially arose from effects mediated by locally altered membrane structure and tension (Lee et. al., 2006). The cell-wide communication of HA's suggested the protein's interaction with the membrane to be a key contributor. Using methyl-β-cyclodextrin (MβC) to extract cholesterol we showed that these cells had slower kinetics and a lower extent of fusion overall when compared to cells not treated with anything. The dependence of HA and possibly other viral fusion proteins on cholesterol for more efficient fusion could impact future therapies. Exogenous fusion peptide, which has been shown to embed into and disrupt lipid packing, was used to determine its effects on refolding. Altering the local membrane environment with peptide showed the ability to induce the conformational refolding in wild type HA as well as two other mutants. Previous work has shown and suggested the interaction of the fusion peptide with the membrane in order to disrupt lipid structure and induce lipid mixing and vesicle leakage (Lau et al., 2004; Harrison 2015; Lorieau et al., 2010; Baquero et al., 2015; White, 2016; Lorieau et al., 2012). We can't rule out that the fusion peptide interacts directly with the HA to cause the conformational change by competing for the pocket. These results taken together indicate that the membrane plays a role in autocatalysis and will further our understanding for future engineered modular systems.

Whether the phenomenon of autocatalysis extends to other subtypes of HA and other viral fusion proteins was examined in Chapter 4. Human influenza virus (A/Aichi/69/X31) HA was seen to have a bimodal response to activation similar to the FPV HA. Indicating that no cell has a fraction of the HA's on the surface in a refolded state much like the other subtype the cell shares

a common mechanism for activation. The similar bimodal response was promising for the modular system when co-expressing two different subtypes. A modular system expressing ligand induced H7 HA, HA4xCys, and signal H3 HA, X31-HAcmyc, showed the capability to induce other subtypes.

Fusion proteins (VSV-G and gp-160) from other viruses were also tested for crosstalk communication. Fusion protein G, of vesicular stomatitis virus, appeared to activate all the HA co-expressed on the cell. VSV-G, which has a reversible conformational change, co-expressed with a signal HA, HAcmyc, had a positive c-myc stain even in the absence of a pulse. The reversibility of VSV-G suggests that the refolding of these proteins is enough to cause the HA to refold. The refolding of the fusion protein of HIV (gp-160) did not indicate any crosstalk when expressed with HAcmyc. However, the refolding of HAcmyc due to low pH did indicate crosstalk and the ability to cause gp-160 to refold and shed the receptor binding domain.

The HA landscape was examined through directed evolution techniques coupled with deep sequencing analysis revealed key areas of the protein. The expression selection allowed for the identification of residues that bind the anti-body used in screening. The double selection of expression as well as activation identified key areas that do not tolerate mutations and contribute to HA stability. The large number of residues that don’t tolerate mutations clustered around the fusion peptide region suggests the stability of HA is influenced by the residues in the pocket.

Recommendations

Crystal Structure of Ligand Inducible HA Mutant.

Determining the crystal structure of the ligand induced mutant would benefit this and future work. A structure of HA4xCys would greatly benefit the model proposed here of FlAsH binding the fusion peptide region in its pre-active state and destabilizing it. Structures of both the ligand bound and unbound sates would provide details and a complete understanding of what causes the HA to refold. The unbound structure could guide future engineered fusion proteins that could potentially be induced by more interesting ligands. Maintaining the metastable state after altering the sequence would provide a better understanding to the refolding mechanism. The structures and its details would give insight to the dynamics of refolding induced by a ligand.

Directed Evolution for New Stimulus.

Engineering of the fusion peptide region to bind a variety of stimuli could provide novel sensing functions while not having to retain the fusion capability. The sensing HA co-expressed with a fusion capable HA, such as wild-type, would create a fusogenic systems that would be induced in specific environments.

Directed evolution of HA guided by the high throughput sequencing data identifies key places that tolerate mutations that would be a potential place to engineer ligand binding sites. Novel ligand-binding sites mutated into regions of HA that will not destabilize the metastable structure and can promote refolding to the active state upon binding a ligand could be used in the modular systems. This region must also be accessible for the ligand binding to disrupt the conformation

allowing the trimer to refold upon binding the ligand. Phage display libraries have been used to identify peptides capable of binding small ligands (Rozinov and Nolan, 1998), and mapping data allows us to find potential sites for these peptides. Expression of cloned HA with peptides capable of binding ligands can be expressed in CHO cells followed by selection of properly folded metastable states can be done through the mammalian expression assay.

Our tetra-cysteine data suggest an alternative pathway to activation by engineering the fusion peptide region, this could be a potential site where new peptides can be inserted. Tumor homing motifs, RGD and NGR, have shown the ability to selectively bind markers in tumor vasculature (Allen, 2002; Pasqualini et. al., 2000). Both linear and cyclic NGR motifs, such as GNGRG, CNGRC, and KNGRE, coupled with fluorescent probes have been used to image tumors (Arap et. al., 2008; Colombo et. al., 2002; Negussie et. al., 2010). Using phage display libraries, NGR motifs have been found to bind a selectively overexpressed tumor marker, aminopeptidase N (CD13) (Pasqualini et. al., 2000). Directed evolution can be used randomly mutagenize the surface of the HA1 region opposed to where the peptide has been inserted and screen for stable mutants.

Protein Reconstitution in Liposome.

The role of the membrane in activation and extent of fusion was shown in Chapter 3. Further experiments exploring the role the membrane structure or tension play in the refolding of HA can be continued. Fusion proteins from transfected CHO can be reconstituted into liposomes of varying lipid composition and size. The use of different lipids in order to create large unilamellar vesicles and short unilamellar vesicles to determine the effect of curvature on HA refolding

(Riqaud and Levy, 2003). Kinetic and refolding data could be monitored with the HA4xCys mutant. Mixtures of palmitoyloleoyl- and dioleoyl-sn-glycero-3-phosphatidylcholine (POPC and DOPC), -phosphatidylethanolamine (POPE and DOPE), and cholesterol can be used to form liposome of varying size and curvature. Previous work has shown that an increase in activation energies of fusion intermediates is seen when including higher amounts of phosphatidylcholine (Kasson 2007). The reconstitution of protein in a liposome would be an arduous process but the result would allow for a very promising application using the modular systems presented in this project. This data could also be coupled with collaborations with computational groups with expertise in membrane biophysics.

Vesicles carrying a payload and having reconstituted engineered HA on the surface could add selectivity to the delivery. An assay similar to the luciferase assay could be applied to monitor gene transfer to target cells overexpressing markers of human breast carcinoma cells (SK-BR-3 and AU565). The ability to control HA refolding in response to a marker would benefit the fusogenic modular systems. Selectivity of the delivery system could further be investigated with mixtures of target and non-target cells to assess the feasibility of using vesicles for future efforts of drug and gene delivery.

REFERENCES

Adams, Stephen R. et al. 2002. “New Biarsenical Ligands and Tetracysteine Motifs for Protein Labeling in Vitro and in Vivo: Synthesis and Biological Applications.” *Journal of the American Chemical Society* 124(21): 6063–76.

Aeffner, Sebastian, Tobias Reusch, Britta Weinhausen, and Tim Salditt. 2012. “Energetics of Stalk Intermediates in Membrane Fusion Are Controlled by Lipid Composition.” *Proc Natl Acad Sci U S A* 109(25): 9678–79.

Albertini, A et al. 2012. “Characterization of Monomeric Intermediates during VSV Glycoprotein Structural Transition.” *PLoS Pathogens* 8(2).

Allen, Theresa M. 2002. “Ligand-Targeted Therapeutics in Anticancer Therapy.” *Nature Reviews. Cancer* 2(10): 750–63.

Arap, Wadih, Renata Pasqualini, and Erkki Ruoslahti. 1998. “Cancer Treatment by Targeted Drug Delivery to Tumor Vasculature in a Mouse Model.” *Science* 279: 377–80.

Araya, Carlos L, and Douglas M Fowler. 2011. “Deep Mutational Scanning : Assessing Protein Function on a Massive Scale.” *Cell* 29(9): 435–42. http://dx.doi.org/10.1016/j.tibtech.2011.04.003.

Bankevich, Anton et al. 2012. “SPAdes: A New Genome Assembly Algorithm and Its Applications to Single Cell Sequencing.” *Journal of Computational Biology* 19(5): 455–77.

Baquero, Eduard, Aurélie A V Albertini, and Yves Gaudin. 2015. “Recent Mechanistic and Structural Insights on Class III Viral Fusion Glycoproteins.” *Current Opinion in Structural Biology* 33: 52–60.

Blumenthal, Robert, Stewart Durell, and Mathias Viard. 2012. “HIV Entry and Envelope Glycoprotein-Mediated Fusion *.” *Journal of Biological Chemistry* 287(49): 40841–49.

Böttcher, Christoph et al. 1999. “Structure of Influenza Haemagglutinin at Neutral and at Fusogenic pH by Electron Cryo-Microscopy.” *FEBS Letters* 463(3): 255–59.

Byrd-Leotis, Lauren, Summer E. Galloway, Evangeline Agbogu, and David A. Steinhauer. 2015. “Influenza Hemagglutinin (HA) Stem Region Mutations That Stabilize or Destabilize the Structure of Multiple HA Subtypes.” *Journal of Virology* 89(8): 4504–16. http://jvi.asm.org/lookup/doi/10.1128/JVI.00057-15.

Carr, Chavela M., and Peter S. Kim. 1993. “A Spring-Loaded Mechanism for the Conformational Change of Influenza Hemagglutinin.” *Cell* 73(4): 823–32.

Chang, T et al. 2013. “Cholesterol-Rich Lipid Rafts Are Required for Release of Infectious Human Respiratory Syncytial Virus Particles.” *Virology* 422(2): 205–13.

Chao, Luke H. et al. 2014. “Sequential Conformational Rearrangements in Flavivirus Membrane Fusion.” *eLife* 3: e04389.

Checkley, Mary Ann, Benjamin G Luttge, and Eric O Freed. 2012. “HIV-1 Envelope Glycoprotein Biosynthesis, Trafficking, and Incorporation.” *Journal of molecular biology* 410(4): 582–608.

Chen, J, J J Skehel, and D C Wiley. 1999. “N- and C-Terminal Residues Combine in the Fusion-pH Influenza Hemagglutinin HA(2) Subunit to Form an N Cap That Terminates the Triple-Stranded Coiled Coil.” *Proceedings of the National Academy of Sciences of the United States of America* 96(16): 8967–72. http://www.pubmedcentral.nih.gov/articlerender.fcgi?artid=17716&tool=pmcentrez&rendertype=abstract.

Chen, J et al. 1995. “A Soluble Domain of the Membrane-Anchoring Chain of Influenza Virus Hemagglutinin (HA2) Folds in Escherichia Coli into the Low-pH-Induced Conformation.” *Proceedings of the National Academy of Sciences of the United States of America* 92(26): 12205–9.

Chernomordik, Leonid V, and Michael M Kozlov. 2003. “Protein-Lipid Interplay in Fusion and Fission of Biological Membranes.” *Annual review of biochemistry* 72: 175–207. http://www.ncbi.nlm.nih.gov/pubmed/14527322 (July 13, 2012).

Chernomordik, Leonid V, and Michael M Kozlov. 2008. “Mechanics of Membrane Fusion.” *Nature structural & molecular biology* 15(7): 675–83. http://www.pubmedcentral.nih.gov/articlerender.fcgi?artid=2548310&tool=pmcentrez&rendertype=abstract.

Colby, D W et al. 2004. “Engineering Antibody Affinity by Yeast Surface Display.” *Methods in enzymology* 388(2000): 348–58.

Colman, Peter M, and Michael C Lawrence. 2003. “The Structural Biology of Type I Viral Membrane Fusion.” *Nature reviews. Molecular cell biology* 4(4): 309–19.

Colombo, Giorgio et al. 2002. “Structure-Activity Relationships of Linear and Cyclic Peptides Containing the NGR Tumor-Homing Motif.” *Journal of Biological Chemistry* 277(49): 47891–97.

Cross, Karen J. et al. 2001. “Studies on Influenza Haemagglutinin Fusion Peptide Mutants Generated by Reverse Genetics.” *EMBO Journal* 20(16): 4432–42.

Cross, Karen J et al. 2009. “Composition and Functions of the Influenza Fusion Peptide.” *Protein and peptide letters* 16(7): 766–78. http://www.ncbi.nlm.nih.gov/pubmed/19601906.

Daniels, P S et al. 1987. “The Receptor-Binding and Membrane-Fusion Properties of Influenza Virus Variants Selected Using Anti-Haemagglutinin Monoclonal Antibodies.” *The EMBO journal* 6(5): 1459–65.

Daniels, R. S. et al. 1985. “Fusion Mutants of the Influenza Virus Hemagglutinin Glycoprotein.” *Cell* 40(2): 431–39.

Diao, Jiajie et al. 2012. “Synaptic Proteins Promote Calcium-Triggered Fast Transition from Point Contact to Full Fusion.” *eLife* 2012(1): 1–21.

Doolan, Kyle M, and David W Colby. 2015. “Conformation-Dependent Epitopes Recognized by Prion Protein Antibodies Probed Using Mutational Scanning and Deep Sequencing.” *Journal of Molecular Biology* 427(2): 328–40. http://dx.doi.org/10.1016/j.jmb.2014.10.024.

Dou, Xiujing et al. 2018. “Cholesterol of Lipid Rafts Is a Key Determinant for Entry and Post-Entry Control of Porcine Rotavirus Infection.” *BMC Veterinary Research* 14(45): 1–12.

E. I. Pecheur, J. Sainte-Marie, A. Bienvenue, D. Hoekstra. 1999. “Membrane Biology Peptides and Membrane Fusion : Towards an Understanding of the Molecular Mechanism.” *The Journal of Membrane Biology* 17(167): 1–17.

Eckert, Debra M, and Peter S Kim. 2001. “Mechanisms of Viral Membrane Fusion and Its Inhibition.” *Annual review of biochemistry* 70: 777–810.

Erster, Oran, Miriam Eisenstein, and Mordechai Liscovitch. 2007. “Ligand Interaction Scan : A General Method for Engineering Ligand- Sensitive Protein Alleles.” *Nature Methods* 4(5): 393–96.

Falcigno, Lucia et al. 2004. “Structural Investigation of the HIV-1 Envelope Glycoprotein gp160 Cleavage Site 3: Role of Site-Specific Mutations.” *Chembiochem : a European journal of chemical biology* 5(12): 1653–61. http://www.ncbi.nlm.nih.gov/pubmed/15526330 (October 12, 2012).

Feigenson, Gerald W. 2006. “Phase Behavior of Lipid Mixtures.” *Nature Chemical Biology* 2(11): 560–63.

Floyd, D. L. et al. 2008. “Single-Particle Kinetics of Influenza Virus Membrane Fusion.” *Proceedings of the National Academy of Sciences* 105(40): 15382–87. http://www.pnas.org/cgi/doi/10.1073/pnas.0807771105.

Fowler, Douglas M et al. 2010. “High-Resolution Mapping of Protein Sequence- Function Relationships.” *Nature Publishing Group* 7(9): 741–46. http://dx.doi.org/10.1038/nmeth.1492.

Freed, Eric O. 2015. “REVIEWS HIV - 1 Assembly , Release and Maturation.” *Nature Publishing Group* 13(8): 484–96. http://dx.doi.org/10.1038/nrmicro3490.

Gallo, Stephen A et al. 2003. “The HIV Env-Mediated Fusion Reaction.” *Biochimica et biophysica acta* 1614: 36–50.

Galloway, Summer E., Mark L. Reed, Charles J. Russell, and David A. Steinhauer. 2013. “Influenza HA Subtypes Demonstrate Divergent Phenotypes for Cleavage Activation and pH of Fusion: Implications for Host Range and Adaptation.” *PLoS Pathogens* 9(2).

Godley, L et al. 1992. “Introduction of Intersubunit Disulfide Bonds in the Membrane Distal-Region of the Influenza Hemagglutinin Abolishes Membrane Fusion Activity.” *Cell* 68: 635–45.

Griffin, B. A. 1998. “Specific Covalent Labeling of Recombinant Protein Molecules Inside Live Cells.” *Science* 281(5374): 269–72. http://www.sciencemag.org/cgi/doi/10.1126/science.281.5374.269 (August 6, 2013).

Gutman, O, T Danieli, J M White, and Y I Henis. 1993. “Effects of Exposure to Low pH on the Lateral Mobility of Influenza Hemagglutinin Expressed at the Cell Surface: Correlation between Mobility Inhibition and Inactivation.” *Biochemistry* 32(1): 101–6. http://www.ncbi.nlm.nih.gov/pubmed/8418830.

Han, X, J H Bushweller, D S Cafiso, and L K Tamm. 2001. “Membrane Structure and Fusion-Triggering Conformational Change of the Fusion Domain from Influenza Hemagglutinin.” *Nature structural biology* 8(8): 715–20. http://www.ncbi.nlm.nih.gov/pubmed/11473264.

Harrison, Stephen C. 2008. “Viral Membrane Fusion.” *Nature Structural Biology* 15(7): 690–98.

Harrison, Stephen C. 2015. “Viral Membrane Fusion.” *Virology* 479–480: 498–507. http://dx.doi.org/10.1016/j.virol.2015.03.043.

Heftberger, Peter et al. 2015. “In Situ Determination of Structure and Fluctuations of Coexisting Fluid Membrane Domains.” *Biophysical Journal* 108(4): 854–62. http://dx.doi.org/10.1016/j.bpj.2014.11.3488.

Hong, H., and L. K. Tamm. 2004. “Elastic Coupling of Integral Membrane Protein Stability to Lipid Bilayer Forces.” *Proceedings of the National Academy of Sciences* 101(12): 4065–70. http://www.pnas.org/cgi/doi/10.1073/pnas.0400358101.

Huang, Qiang, Cheng-Lung Chen, and Andreas Herrmann. 2004. “Bilayer Conformation of Fusion Peptide of Influenza Virus Hemagglutinin: A Molecular Dynamics Simulation Study.” *Biophysical journal* 87(1): 14–22.

http://www.pubmedcentral.nih.gov/articlerender.fcgi?artid=1304337&tool=pmcentrez&rendertype=abstract (July 24, 2012).

Huang, Qiang et al. 2002. “Protonation and Stability of the Globular Domain of Influenza Virus Hemagglutinin.” *Biophysical Journal* 82(66): 1050–58. http://dx.doi.org/10.1016/S0006-3495(02)75464-7.

Huerta, Leonor et al. 2009. “HIV-Envelope–Dependent Cell-Cell Fusion: Quantitative Studies.” *The Scientific World JOURNAL* 9: 746–63. http://www.hindawi.com/journals/tswj/2009/618273/abs/.

Hughson, Frederick M. 1997. “Enveloped Viruses: A Common Mode of Membrane Fusion?” *Current Biology* 7(9): R565–69. http://linkinghub.elsevier.com/retrieve/pii/S0960982206002831.

Ilyushina, Natalia A. et al. 2007. “Contribution of H7 Haemagglutinin to Amantadine Resistance and Infectivity of Influenza Virus.” *Journal of General Virology* 88(4): 1266–74.

Ivanovic, Tijana et al. 2013. “Influenza-Virus Membrane Fusion by Cooperative Fold-Back of Stochastically Induced Hemagglutinin Intermediates.” *eLife* 2013(2): 1–20.

Jahn, Reinhard, Thorsten Lang, and Thomas C Su. 2003. “Membrane Fusion.” *Cell* 112(3): 519–33.

Jahn, Reinhard, and Richard H Scheller. 2006. “SNAREs - Engines for Membrane Fusion.” *Nature reviews. Molecular cell biology* 7: 631–43.

Ju, William et al. 2004. “Activity-Dependent Regulation of Dendritic Synthesis and Trafficking of AMPA Receptors.” *Nature Neuroscience* 7(3): 244–53.

Kasson, Peter M, and Vijay S Pande. 2007. “Control of Membrane Fusion Mechanism by Lipid Composition: Predictions from Ensemble Molecular Dynamics.” *PLoS computational biology* 3(11): e220. http://www.pubmedcentral.nih.gov/articlerender.fcgi?artid=2077900&tool=pmcentrez&rendertype=abstract (October 12, 2012).

Kemble, G W et al. 1992. “Intermonomer Disulfide Bonds Impair the Fusion Activity of Influenza Virus Hemagglutinin.” *Journal of virology* 66(8): 4940–50. http://www.pubmedcentral.nih.gov/articlerender.fcgi?artid=241339&tool=pmcentrez&rendertype=abstract.

Kim, Irene S et al. 2016. “Mechanism of Membrane Fusion Induced by Vesicular Stomatitis Virus G Protein.” *Proceedings of the National Academy of Sciences* Online.

Krautkra, Ellen et al. 2004. “Human Immunodeficiency Virus Type 1 Nef Activates p21-Activated Kinase via Recruitment into Lipid Rafts.” *Journal of Virology* 78(8): 4085–97.

Krell, Tino, and El Habib. 2004. “HIV-1 gp41 and gp160 Are Hyperthermostable Proteins in a Mesophilic Environment.” *Journal of Biochemistry* 1579: 1566–79.

Lau, Wai Leung et al. 2004. “Oligomerization of Fusogenic Peptides Promotes Membrane Fusion by Enhancing Membrane Destabilization.” *Biophysical journal* 86(1 Pt 1): 272–84. http://www.pubmedcentral.nih.gov/articlerender.fcgi?artid=1303790&tool=pmcentrez&rendertype=abstract.

Lee, J H, M Goulian, and E T Boder. 2006. “Autocatalytic Activation of Influenza Hemagglutinin.” *Journal of molecular biology* 364(3): 275–82.

Lee, Kelly K. 2010. “Architecture of a Nascent Viral Fusion Pore.” *EMBO Journal* 29(7): 1299–1311. http://dx.doi.org/10.1038/emboj.2010.13.

Leikina, Eugenia et al. 2002. “Reversible Stages of the Low-pH-Triggered Conformational Change in Influenza Virus Hemagglutinin.” *The EMBO journal* 21(21): 5701–10.

Leung, Horasis S Y et al. 2012. “Entry of Influenza A Virus with a 2 , 6-Linked Sialic Acid Binding Preference Requires Host Fibronectin.” *Journal of Virology* 86(19): 10704–13.

Li, Y. et al. 2010. “Genetically Engineered, Biarsenically Labeled Influenza Virus Allows Visualization of Viral NS1 Protein in Living Cells.” *Journal of Virology* 84(14): 7204–13. http://jvi.asm.org/cgi/doi/10.1128/JVI.00203-10.

Li, Y et al. 2005. “Membrane Structures of the Hemifusion-Inducing Fusion Peptide Mutant G1S and the Fusion-Blocking Mutant G1V of Influenza Virus Hemagglutinin Suggest a Mechanism for Pore Opening in Membrane Fusion.” *J Virol* 79(18): 12065–76. http://www.ncbi.nlm.nih.gov/entrez/query.fcgi?cmd=Retrieve&db=PubMed&dopt=Citation&list_uids=16140782.

Libersou, Sonia et al. 2010. “Distinct Structural Rearrangements of the VSV Glycoprotein Drive Membrane Fusion.” *Journal of Cell Biology* 191(1): 199–210.

Lin, Yi Pu et al. 1997. “Adaptation of Egg-Grown and Transfectant Influenza Viruses for Growth in Mammalian Cells: Selection of Hemagglutinin Mutants with Elevated pH of Membrane Fusion.” *Virology* 233(2): 402–10.

Lingwood, Daniel, and Kai Simons. 2010. “Lipid Rafts As a Membrane- Organizing Principle.” *Science* 327: 46–51.

Lorieau, Justin L, John M Louis, Charles D Schwieters, and Adriaan Bax. 2012. “pH-Triggered, Activated-State Conformations of the.” *Proceedings of the National Academy of Sciences of the United States of America* 109(49): 19994–99.

Lu, Dongmei et al. 2012. “Phosphatidylinositol 4-Kinase IIα Is Palmitoylated by Golgi-Localized Palmitoyltransferases in Cholesterol-Dependent Manner.” *The Journal of biological chemistry* 287(26): 21856–65. http://www.ncbi.nlm.nih.gov/pubmed/22535966 (October 12, 2012).

Madani, Fatemeh et al. 2009. “Sup Inf Hairpin Structure of a Biarsenal –tetracysteine Motif Determined by NMR.” *J. Am. Chem. Soc.* 131: 4613–15.

Mañes, Santos, Gustavo Real, and Carlos Martínez-a. 2003. “PATHOGENS : RAFT HIJACKERS.” *Nature Reviews Immunology* 3(557).

Marek, Kurt W., and Graeme W. Davis. 2002. “Transgenically Encoded Protein Photoinactivation (FlAsH-FALI): Acute Inactivation of Synaptotagmin I.” *Neuron* 36(5): 805–13.

Markovic, I et al. 2001. “Synchronized Activation and Refolding of Influenza Hemagglutinin in Multimeric Fusion Machines.” *The Journal of cell biology* 155(5): 833–44. http://www.pubmedcentral.nih.gov/articlerender.fcgi?artid=2150858&tool=pmcentrez&rendertype=abstract (March 15, 2012).

Maurer, Ulrike E. et al. 2013. “The Structure of Herpesvirus Fusion Glycoprotein B-Bilayer Complex Reveals the Protein-Membrane and Lateral Protein-Protein Interaction.” *Structure* 21(8): 1396–1405.

Mkrtchyan, Samvel R et al. 2005. “Ternary Complex Formation of Human Immunodeficiency Virus Type 1 Env , CD4 , and Chemokine Receptor Captured as an Intermediate of Membrane Fusion.” *Journal of Virology* 79(17): 11161–69.

Molotkovsky, Rodion J et al. 2018. “Lateral Membrane Heterogeneity Regulates Viral-Induced Membrane Fusion during HIV Entry.” *Inernational Journal of Molecular Sciences* 19(1483): 1–15.

Moore, John P, and Robert W Doms. 2003. “The Entry of Entry Inhibitors : A Fusion of Science and Medicine.” *Proceedings of the National Academy of Sciences* 100(19): 10598–602.

Moore, John P, Jane A Mckeating, Robin A Weiss, and Quentin J Sattentau. 1990. “Dissociation of gp120 from HIV-1 Virions Induced by Soluble CD4.” *Science* 250(4984): 1139–42.

Negussie, Ayele H. et al. 2010. “Synthesis and in Vitro Evaluation of Cyclic NGR Peptide Targeted Thermally Sensitive Liposome.” *Journal of Controlled Release* 143(2): 265–73. http://dx.doi.org/10.1016/j.jconrel.2009.12.031.

Ohkura, Takashi, Fumitaka Momose, Reiko Ichikawa, and Kaoru Takeuchi. 2014. “Influenza A Virus Hemagglutinin and Neuraminidase Mutually Accelerate Their Apical Targeting through Clustering of Lipid Rafts.” *Journal of virology* 88(17): 10039–55.

Pan, Jianjun, Thalia T Mills, Stephanie Tristram-nagle, and John F Nagle. 2008. “Cholesterol Perturbs Lipid Bilayers Nonuniversally (B).” *Physical Review Letters* 10(9): 1–4.

Panchal, Rekha G et al. 2003. “In Vivo Oligomerization and Raft Localization of Ebola Virus Protein VP40 during Vesicular Budding.” *Proceedings of the National Academy of Sciences of the United States of America* 100(26): 15936–41. http://www.pubmedcentral.nih.gov/articlerender.fcgi?artid=307671&tool=pmcentrez&rendertype=abstract.

Pasqualini, Renata et al. 2000. “Aminopeptidase N Is a Receptor for Tumor-Homing Peptides and a Target for Inhibiting Angiogenesis.” *Cancer Research* 60(3): 722–27.

Perlman, Mira, and Marilyn D. Resh. 2006. “Identification of an Intracellular Trafficking and Assembly Pathway for HIV-1 Gag.” *Traffic* 7(6): 731–45.

Platt, Emily J, James P Durnin, Ujwal Shinde, and David Kabat. 2007. “An Allosteric Rheostat in HIV-1 gp120 Reduces CCR5 Stoichiometry Required for Membrane Fusion and Overcomes Diverse Entry Limitations.” *Journal of Molecular Biology* 347: 64–79.

Podbilewicz, Benjamin et al. 2006. “The C . Elegans Developmental Fusogen EFF-1 Mediates Homotypic Fusion in Heterologous Cells and In Vivo.” *Developmental Cell* 11: 471–81.

Pomorski, A, and A Krezel. 2011. “Exploration of Biarsenical Chemistry — Challenges in Protein Research.” *Chembiochem : a European journal of chemical biology* 12: 1152–67.

Poskanzer, K. E., Kurt W. Marek, S. T. Sweeney, and G. W. Davis. 2003. “Synaptotagmin I Is Necessary for Compensatory Synaptic Vesicle Endocytosis in Vivo.” *Letters to Nature* 426(December): 559–63.

Qiao, Hui et al. 1999. “A Specific Point Mutant at Position 1 of the Influenza Hemagglutinin Fusion Peptide Displays a Hemifusion Phenotype.” *Molecular Biology of the Cell* 10(August): 2759–69.

Qiao, Hui et al. 1998. “Specific Single or Double Proline Substitutions in the ‘Spring-Loaded’ Coiled-Coil Region of the Influenza Hemagglutinin Impair or Abolish Membrane Fusion Activity.” *The Journal of Cell Biology* 141(6): 1335–47.

Reed, Mark L et al. 2010. “The pH of Activation of the Hemagglutinin Protein Regulates H5N1 Influenza Virus Pathogenicity and Transmissibility in Ducks □.” *Journal of Virology* 84(3): 1527–35.

Reed, Mark L et al. 2009. “Amino Acid Residues in the Fusion Peptide Pocket Regulate the pH of Activation of the H5N1 Influenza Virus Hemagglutinin Protein □.” *Journal of virology* 83(8): 3568–80.

Rigaud, Jean-Louis, and Daniel Lévy. 2003. “Reconstitution of Membrane Proteins into Liposomes.” *Methods in enzymology* 372(2000): 65–86. http://www.ncbi.nlm.nih.gov/pubmed/14610807.

Roche, S et al. 2008. “Review Structures of Vesicular Stomatitis Virus Glycoprotein : Membrane Fusion Revisited.” *Cellular and Molecular Life Sciences* 65: 1716–28.

Roche, S, S Bressanelli, F A Rey, and Y Gaudin. 2006. “Crystal Structure of the Low-pH.” *Science* 313(July): 187–92.

Roche, S, and Yves Gaudin. 2002. “Characterization of the Equilibrium between the Native and Fusion-Inactive Conformation of Rabies Virus Glycoprotein Indicates That the Fusion Complex Is Made of Several Trimers.” *Virology* 297: 128–35.

Roche, S, F A Rey, Y Gaudin, and S Bressanelli. 2007. “Structure of the Prefusion Form.” *Science* 315(February): 843–49.

Romantsov, Tatyana, Leanne Stalker, Doreen E. Culham, and Janet M. Wood. 2008. “Cardiolipin Controls the Osmotic Stress Response and the Subcellular Location of Transporter ProP in Escherichia Coli.” *Journal of Biological Chemistry* 283(18): 12314–23.

Roscoe, Benjamin P et al. 2013. “Analyses of the Effects of All Ubiquitin Point Mutants on Yeast Growth Rate.” *Journal of Molecular Biology* 425(8): 1363–77. http://dx.doi.org/10.1016/j.jmb.2013.01.032.

Rosenfeld, Lior, Michael Heyne, Julia M Shifman, and Niv Papo. 2016. “Protein Engineering by Combined Computational and In Vitro Evolution Approaches.” *Trends in Biochemical Sciences* 41(5): 421–33. http://dx.doi.org/10.1016/j.tibs.2016.03.002.

Rozinov, M N, and G P Nolan. 1998. “Evolution of Peptides That Modulate the Spectral Qualities of Bound, Small-Molecule Fluorophores.” *Chemistry & biology* 5(12): 713–28. http://www.ncbi.nlm.nih.gov/pubmed/9862799.

Rudner, Lynnie et al. 2005. “Dynamic Fluorescent Imaging of Human Immunodeficiency Virus Type 1 Gag in Live Cells by Biarsenical Labeling.” *Society* 79(7): 4055–65.

Russell, C J, T S Jardetzky, and R A Lamb. 2004. “Conserved Glycine Residues in the Fusion Peptide of the Paramyxovirus Fusion Protein Regulate Activation of the Native State.” *Journal of Virology* 78(24): 13727–42.

Russell, R J et al. 2004. “H1 and H7 Influenza Haemagglutinin Structures Extend a Structural Classification of Haemagglutinin Subtypes.” *Virology* 325(2): 287–96. http://www.ncbi.nlm.nih.gov/pubmed/15246268 (October 12, 2012).

Russier, Marion et al. 2016. “Molecular Requirements for a Pandemic Influenza Virus: An Acid-Stable Hemagglutinin Protein.” *Proceedings of the National Academy of Sciences* 113(6): 1636–41. http://www.pnas.org/lookup/doi/10.1073/pnas.1524384113.

Scheiffele, Peter, Anton Rietveld, Thomas Wilk, and Kai Simons. 1999. “Influenza Viruses Select Ordered Lipid Domains during Budding from the Plasma Membrane *.” *The Journal of biological chemistry* 274(4): 2038–44.

Schwegmann-, Christel, Ben Peeters, and Pascale Que. 2014. “Characterization of the Sialic Acid Binding Activity of Influenza A Viruses Using Soluble Variants of the H7 and H9 Hemagglutinins.” *PloS one* 9(2): 1–9.

Shangguan, T et al. 1998. “Morphological Changes and Fusogenic Activity of Influenza Virus Hemagglutinin.” *Biophysical journal* 74(1): 54–62. http://www.pubmedcentral.nih.gov/articlerender.fcgi?artid=1299361&tool=pmcentrez&rendertype=abstract.

Skehel, John J., and D. C. Wiley. 2000. “Receptor Binding and Membrane Fusion in Virus Entry: The Influenza Hemagglutinin.” *Annual Reviews in Biochemistry* 69: 531–69. http://arjournals.annualreviews.org/doi/abs/10.1146/annurev.biochem.68.1.863%5Cnpapers3://publication/uuid/37777FFE-E284-4B0C-9648-9DF205012ADD.

Songalia, A et al. 1994. “Structure of Influenza Haemagglutinin at the pH of Membrane Fusion.” *Nature* 371: 37–43.

Stanifer, Megan L, David K Cureton, and Sean P J Whelan. 2011. “A Recombinant Vesicular Stomatitis Virus Bearing a Lethal Mutation in the Glycoprotein Gene Uncovers a Second Site Suppressor That Restores Fusion □.” *Journal of Virological Methods* 85(16): 8105–15.

Steinhauer, D a et al. 1996. “Studies Using Double Mutants of the Conformational Transitions in Influenza Hemagglutinin Required for Its Membrane Fusion Activity.” *Proceedings of the National Academy of Sciences of the United States of America* 93(23): 12873–78. http://www.pubmedcentral.nih.gov/articlerender.fcgi?artid=24013&tool=pmcentrez&rendertype=abstract.

Sugrue, R J et al. 1990. “Specific Structural Alteration of the Influenza Haemagglutinin by Amantadine.” *The EMBO journal* 9(11): 3469–76. http://www.pubmedcentral.nih.gov/articlerender.fcgi?artid=552095&tool=pmcentrez&rendertype=abstract.

Takeda, Makoto, George P Leser, Charles J Russell, and Robert A Lamb. 2003. “Influenza Virus Hemagglutinin Concentrates in Lipid Raft Microdomains for Efficient Viral Fusion.” *Proceedings of the National Academy of Sciences* 100(25): 14610–17.

Thoennes, Sudha et al. 2008. “Analysis of Residues near the Fusion Peptide in the Influenza Hemagglutinin Structure for Roles in Triggering Membrane Fusion.” *Virology* 370(2): 403–14.

Traxlmayr, Michael W et al. 2012. “Construction of a Stability Landscape of the CH3 Domain of Human IgG1 by Combining Directed Evolution with High Throughput Sequencing.” *Journal of Molecular Biology* 423(3): 397–412. http://dx.doi.org/10.1016/j.jmb.2012.07.017.

Turville, Stuart G. et al. 2008. “Resolution of de Novo HIV Production and Trafficking in Immature Dendritic Cells.” *Nature Methods* 5(1): 75–85.

Vaccaro, Loredana et al. 2005. “Plasticity of Influenza Haemagglutinin Fusion Peptides and Their Interaction with Lipid Bilayers.” *Biophysical journal* 88(1): 25–36. http://www.pubmedcentral.nih.gov/articlerender.fcgi?artid=1305003&tool=pmcentrez&rendertype=abstract (July 24, 2012).

Welman, Mélanie, Guy Lemay, and Eric a Cohen. 2007. “Role of Envelope Processing and gp41 Membrane Spanning Domain in the Formation of Human Immunodeficiency Virus Type 1 (HIV-1) Fusion-Competent Envelope Glycoprotein Complex.” *Virus research* 124(1–2): 103–12. http://www.ncbi.nlm.nih.gov/pubmed/17129629 (October 12, 2012).

White, Judith M. 1990. “Viral and Cellular Membrane Fusion Proteins.” *annual review of Physiology*: 675–97.

White, Judith M., Sue E. Delos, Matthew Brecher, and Kathryn Schornberg. 2008. “Structures and Mechanisms of Viral Membrane Fusion Proteins: Multiple Variations on a Common Theme.” *Critical Reviews in Biochemistry and Molecular Biology* 43(3): 189–219.

White, Judith M., and Gary R. Whittaker. 2016. “Fusion of Enveloped Viruses in Endosomes.” *Traffic* 17(6): 593–614.

White, Mitchell R. et al. 2014. “Alzheimer’s Associated B-Amyloid Protein Inhibits Influenza a Virus and Modulates Viral Interactions with Phagocytes.” *PLoS ONE* 9(7): 1–9.

Whitehead, Timothy A et al. 2012. “Optimization of Affinity , Specificity and Function of Designed Influenza Inhibitors Using Deep Sequencing.” *Nature Biotechnology* 30(6): 543–48. http://dx.doi.org/10.1038/nbt.2214.

Wilks, Sam, Miranda de Graaf, Derek J Smith, and David F Burke. 2012. “A Review of Influenza Haemagglutinin Receptor Binding as It Relates to Pandemic Properties.” *Vaccine* 30(29): 4369–76. http://www.ncbi.nlm.nih.gov/pubmed/22682293 (June 14, 2012).

Wilson, I. A., J. J. Skehel, and D. C. Wiley. 1981. “Structure of the Haemagglutinin Membrane Glycoprotein of Influenza Virus at 3 Å Resolution.” *Nature* 289(5796): 366–73.

Wilson, Kirilee A et al. 2005. “The Conserved Glycine-Rich Segment Linking the N-Terminal Fusion Peptide to the Coiled Coil of Human T-Cell Leukemia Virus Type 1 Transmembrane Glycoprotein gp21 Is a Determinant of Membrane Fusion Function.” *Journal of virology* 79(7): 4533–39. http://www.pubmedcentral.nih.gov/articlerender.fcgi?artid=1061562&tool=pmcentrez&rendertype=abstract.

Wrenbeck, Emily E, Matthew S Faber, and Timothy A Whitehead. 2017. “Deep Sequencing Methods for Protein Engineering and Design.” *Current Opinion in Structural Biology* 45: 36–44. http://dx.doi.org/10.1016/j.sbi.2016.11.001.

Xu, Kai et al. 2015. “Crystal Structure of the Pre-Fusion Nipah Virus Fusion Glycoprotein Reveals a Novel Hexamer-of-Trimers Assembly.” *PLoS Pathogens* 11(12): 1–17.

Yang, Sung-tae et al. 2017. “The Role of Cholesterol in Membrane Fusion.” *Chem Phys Lipids* 199: 136–43.

Zaccolo, Manuela, and Ermanno Gherardi. 1999. “The Effect of High-Frequency Random Mutagenesis on in Vitro Protein Evolution : A Study on TEM-1 B -Lactamase.” *Journal of molecular biology* (285): 775–83.

Zaccolo, Manuela, David M Williams, Daniel M Brown, and Ermanno Gherardi. 1996. “An Approach to Random Mutagenesis of DNA Using Mixtures of Triphosphate Derivatives of Nucleoside Analogues.” *Journal of molecular biology* (255): 589–603.

Zaraket, H. et al. 2013. “Increased Acid Stability of the Hemagglutinin Protein Enhances H5N1 Influenza Virus Growth in the Upper Respiratory Tract but Is Insufficient for Transmission in Ferrets.” *Journal of Virology* 87(17): 9911–22. http://jvi.asm.org/cgi/doi/10.1128/JVI.01175-13.

Zaraket, H., O. A. Bridges, and C. J. Russell. 2013. “The pH of Activation of the Hemagglutinin Protein Regulates H5N1 Influenza Virus Replication and Pathogenesis in Mice.” *Journal of Virology* 87(9): 4826–34. http://jvi.asm.org/cgi/doi/10.1128/JVI.03110-12.

Zhang, Xin Yu, and Anthony C. Bishop. 2007. “Site-Specific Incorporation of Allosteric-Inhibition Sites in a Protein Tyrosine Phosphatase.” *Journal of the American Chemical Society* 129(13): 3812–13.

VITA

Mauricio Valverde was born March 12, 1986 in Popayan, Colombia to Mauricio and Nidia Valverde. His father immigrated to the United States in 1985 in search of a better life for his family where he ultimately settled in Ft. Lauderdale, FL. His mom arrived to the United States with Mauricio two years later in 1988. Mauricio has a younger sister, Nicolle, born in 1990. He attended Hollywood Hills High School where he excelled in science and math. Mauricio then attended the University of Florida, Gainesville on a full academic scholarship. He participated in undergraduate research in Dr. Tony Ladd's computational lab. He graduated in 4 years with a bachelor's in chemical engineering. Mauricio then attended the University of Tennessee to earn his Ph.D. working in the protein engineering group of Eric T. Boder.